

Dissertation  
submitted to the  
Combined Faculty of Natural Sciences and Mathematics  
of the Ruperto Carola University Heidelberg, Germany  
for the degree of  
Doctor of Natural Sciences

Presented by

M.Sc. Anja Barbara Hoffmann  
born in: Darmstadt, Germany  
Oral examination: 14<sup>th</sup> May, 2019



Early phlebovirus host cell interactions:  
The small GTPase Rab11 and the  
autophagic factor Atg7 promote Uukuniemi virus entry

Referees: Prof. Dr. Ralf Bartenschlager

Dr. Pierre-Yves Lozach



# 1 Acknowledgement

The present work was carried out under the supervision of Dr. Pierre-Yves Lozach in the Department of Infectious Diseases, Virology, at the University Hospital Heidelberg and supported by the Cluster of Excellence Cellular Networks.

I warmly thank Pierre-Yves, for giving me the opportunity to work on such a fascinating and multifaceted project in his lab. It was and is a pleasure to be part of your research team. Thank you for numerous interesting, very helpful and fruitful discussions. I appreciate your motivating and joyful way of managing your group with a constantly open door for scientific and non-scientific conversations.

I am grateful to Prof. Dr. Ralf Bartenschlager for taking time to accompany my project throughout my time as a PhD student and for agreeing on being the first examiner of this work. Thank you for valuable discussions during our TAC meetings.

I would like to thank Prof. Dr. Stefan Kunz for coming all the way from Lausanne to my TAC meetings. The stimulating and very lively discussions were very valuable for me and my project.

I am grateful to Dr. Alessia Ruggieri and Prof. Dr. Thomas Söllner who kindly agreed on being part of my PhD Defense Committee.

There is no good research without constant discussions, mutual support and good relationships. I thank all my colleagues from various research groups for creating such a good and friendly research environment. I would like to thank Dr. Keisuke Tabata for providing me with very useful cell lines and Dr. Vibor Laketa for comprehensive support at the microscope.

Four years have passed since I came to Heidelberg and the Lozach team has changed a lot. But there is one honest and lovely person who was always there. Psylvia, it is a pleasure to be there with you since such a long time. Your motivation is infectious! Thank you for all your support since the beginning in research-related questions, your advice during mock-presentations and not least for integrating me into the group. This expression of thanks is also addressed to Magalie. I am grateful for the happy coffee breaks and deep conversations we had together. Zina, your laugh makes me smile, and Shawon, thank you for your sympathetic ear and warm words while I was writing. And what would the Lozach lab be without students? I am grateful

to all my talented students, Hannah, Malte, Sven, Jana, Michelle and Ann-Kathrin for their contribution to my project.

I would like to thank Nele, Nicole, Juliane, Janina, Rene, Frauke, David, Laurence, Anke, Vojtech, Rebecka and Susann for creating a nice working atmosphere, having a smile and warm words for me. Thank you Thorsten for your scientific and bouldering advice. Thank you Annica, for being my friend and being there for me.

I am grateful to have friends from high school and bachelor studies Desi, Svenja, Anni, Clarissa, Darina, Maggi und Meli who showed sympathy for me and distracted me during many happy evenings and weekends.

There is someone who deserves more than 10 000 in cash. Thank you Herr Spätzle for encouraging and believing in me incessantly, for cooking delicious meals, making me smile and a very happy person.

Last but not least I want to thank my parents, Lara and Flo for encouraging me and believing in me ever since.

## 2 Summary

Phleboviruses, in the *Phenuiviridae* family within the *Bunyavirales* order, are important pathogenic arthropod-borne viruses (arboviruses), causing severe diseases in humans and domestic animals. Outbreaks are no longer limited to tropical and developing countries. Global trade, deforestation and global warming are reasons for the expansion of arthropod vectors, and the viruses they carry. The mosquito-borne phlebovirus Rift Valley fever (RVFV) spread from sub-Saharan parts of Africa over the entire continent and to the Arabic peninsula during the last two decades. As it already happened for other arboviruses (e.g. dengue virus), RVFV is now at risk of introduction into Southern Europe. Phleboviruses represent a risk to public health and agricultural productivity and must be taken seriously as potential emerging and reemerging pathogens. For humans, neither specific antiviral treatments nor vaccines are currently approved.

Ideally, treating phlebovirus infection in humans, would target early virus-host cell interactions, preventing the release of the virus genome into the cytosol. Yet, the details of the entry pathways exploited by phleboviruses are mostly elusive, awaiting to be uncovered. For my PhD project, I used Uukuniemi virus (UUKV). UUKV is a validated biosafety level (BSL)-2 model for phleboviruses of higher biosafety classification such as RVFV.

Our lab previously reported that UUKV enters human host cells by receptor-mediated endocytosis, transits Rab5-positive early endosomes and penetrates the cytosol from late endosomal compartments with a pH value around 5.4. With the aim to identify additional host factors involved in UUKV entry, two genome-wide siRNA screens were performed. In those screens, VAMP3 was identified to facilitate late endosomal penetration of UUKV. The v-SNARE protein VAMP3 plays an important role in recycling endosome trafficking and the initiation of autophagy. In addition to VAMP3, several other autophagy-associated host factors were found as potential host factors in the siRNA screens for UUKV entry. The overall goal of my PhD project was to clarify the role of autophagy in phlebovirus entry and decipher the molecular mechanisms subverted by phleboviruses to penetrate human host cells. Therefore, I analyzed UUKV infection by flow cytometry and confocal microscopy approaches.

Within my PhD project, I assessed numerous autophagy-associated proteins for their role in UUKV infection. I identified the autophagic factor Atg7 and the small GTPase Rab11a as important host factors for UUKV infection. Atg7 is known mainly for its function in autophagosome maturation. Rab11a regulates recycling endosome trafficking and is involved

in the initiation of autophagy. Addressing single steps of the virus entry process, I found that Atg7 and Rab11 specifically promote UUKV intracellular trafficking, while no effects were observed on other steps during early virus host cell interactions, i.e. binding or replication. Interestingly however, my results also indicate that Atg7 and Rab11 participate in UUKV infection in an autophagy-independent manner.

In conclusion, this thesis expands our knowledge about entry of UUKV particles into human cells with a role of two more host factors, Rab11a and Atg7. Both proteins facilitate the transport of endocytosed viral particles from the plasma membrane to acidic endosomal compartments. Reaching these compartments is a critical step for acid-activated fusion and the subsequent release of the viral genome into the cytosol. Additionally, this work provides an indication of autophagy-independent functions of Atg7 in endosomal trafficking. The importance of Rab11a and VAMP3 in UUKV infection points towards a potential involvement of recycling endosomes in UUKV intracellular trafficking. UUKV represents a tool of choice to better understand the role of recycling endosomes in late endosomal trafficking, a function that remains elusive and is potentially exploited by other related and unrelated viruses.

### 3 Zusammenfassung

Phleboviren aus der *Phenuiviridae* Familie in der Ordnung *Bunyavirales* sind wichtige durch Arthropoden übertragene Viren (Arboviren), die schwerwiegende Krankheiten in Menschen und Nutztieren verursachen. Krankheitsausbrüche sind nicht mehr auf tropische - und Entwicklungsländer begrenzt. Globaler Handel, Abforstung und Klimaerwärmung sind Gründe für die Ausbreitung von Arthropodenvektoren, und deren Viren. Das durch Zecken übertragene Phlebovirus Rift Valley fever virus (RVFV) breitete sich innerhalb der letzten zwei Jahrzehnte von Teilen Subsahara-Afrikas über den gesamten Kontinent und die Arabische Halbinsel aus. Es besteht nun das Risiko, dass RVFV, wie bereits andere Arboviren (beispielsweise Dengue virus), in Südeuropa heimisch wird. Phleboviren stellen eine Bedrohung für die öffentliche Gesundheit und die landwirtschaftliche Produktivität dar und sollten als potentielle neu- oder wiederaufkommende Pathogene ernst genommen werden. Momentan sind für Menschen weder spezifische antivirale Medikamente noch Impfstoffe zugelassen.

Idealerweise würde die Behandlung von Phlebovirusinfektionen in Menschen das Freisetzen des viralen Genoms in das Zytosol verhindern. Bislang bleiben die Details über die Transportwege, die von Phleboviren genutzt werden, unbekannt und warten darauf entdeckt zu werden. Für mein Promotionsprojekt arbeitete ich mit Uukuniemi Virus (UUKV). UUKV ist ein in Laboren der biologischen Sicherheitsstufe 2 validiertes Modell für Phleboviren einer höheren Sicherheitsstufe, beispielsweise RVFV.

Unsere Labor hat zuvor gezeigt, dass UUKV humane Zellen durch Rezeptoren-vermittelte Endozytose betritt, über Rab5-positive, frühe Endosomen in späte Endosomen gelangt, von wo aus es bei einem pH-Wert von etwa 5.4 in das Zytosol eintritt. Mit dem Ziel weitere Wirtsfaktoren zu identifizieren, die am Zelleintritt von UUKV beteiligt sind, wurden zwei genomabdeckende siRNA-Screens durchgeführt. In diesen Screens wurde VAMP3 identifiziert, welches den Eintritt von UUKV von späten Endosomen erleichtert. Das v-SNARE Protein VAMP3 ist wichtig für den Transport von Recycling-Endosomen und die Einleitung von Autophagie. Neben VAMP3 wurden im siRNA-Screen weitere Autophagie-assoziierte Wirtsfaktoren als potentielle Wirtsfaktoren für den Zelleintritt von UUKV gefunden. Das übergreifende Ziel meines Promotionsprojekts war es, die Rolle von Autophagie im Phleboviruszelleintritt aufzuklären und molekulare Mechanismen, die von Phleboviren zum Eintritt in humane Zellen genutzt werden, zu entschlüsseln. Dazu habe ich UUKV-Infektion mit Durchflusszytometrie und konfokaler Mikroskopie analysiert.

Während meines Promotionsprojekts habe ich die Rolle zahlreicher Autophagie-assoziiierter Proteine in Bezug auf UUKV-Infektion untersucht. Ich habe den Autophagiefaktor Atg7 und die kleine GTPase Rab11 als wichtige Wirtsfaktoren identifiziert. Atg7 ist hauptsächlich bekannt für seine Funktion zur Reifung von Autophagosomen. Rab11a reguliert den Transport von Recycling-Endosomen und ist an der Initiation der Autophagie involviert. Durch das Analysieren einzelner Schritte des Viruszeintritts habe ich herausgefunden, dass Atg7 und Rab11 den intrazellulären Transport von UUKV-Partikeln begünstigen, während kein Effekt auf weitere Schritte während früher Viruswirtsinteraktionen festgestellt wurden, zum Beispiel Bindung und Replikation. Interessanterweise jedoch, deuten meine Ergebnisse darauf hin, dass Atg7 und Rab11 in einer Autophagie-unabhängigen Funktion an der UUKV-Infektion teilhaben.

Zusammenfassend erweitert diese Dissertation unser Wissen über den Zelleintritt von UUKV-Partikeln in humane Zellen um eine Rolle der beiden Wirtsfaktoren Rab11a und Atg7. Beide Proteine begünstigen den Transport endozytierter Viruspartikel von der Plasmamembran zu angesäuerten Endosomen. Das Erreichen von diesen Kompartimenten ist entscheidend für die durch niedrigen pH Wert aktivierte Membranfusion und die darauf folgende Freisetzung des viralen Genoms ins Zytosol. Zusätzlich weist diese Arbeit auf eine Autophagie-unabhängige Funktion von Atg7 im Endosomentransport hin. Die Relevanz von Rab11a und VAMP3 für UUKV-Infektion weist auf eine Beteiligung von Recycling-Endosomen am Transport von UUKV-Partikeln hin. UUKV stellt ein Werkzeug zum besseren Verständnis der Rolle von Recycling-Endosomen für den Transport von späten Endosomen dar, eine bislang unbekannte Funktion, die möglicherweise von anderen verwandten und nicht verwandten Viren genutzt wird.

## 4 Table of Contents

1	Acknowledgement.....	i
2	Summary .....	iii
3	Zusammenfassung.....	v
4	Table of Contents .....	vii
5	List of Figures .....	x
6	List of Abbreviations.....	xii
7	Introduction .....	1
7.1	Arboviruses – emerging agents of disease .....	1
7.2	<i>Phlebovirus</i> genus.....	3
7.2.1	Taxonomy.....	3
7.2.2	Epidemiology of phleboviruses.....	3
7.2.3	The model virus UUKV .....	4
7.2.4	Virion structure & genome organization of phleboviruses .....	5
7.2.5	Phlebovirus entry into mammalian cells .....	7
7.2.6	From replication to the release of infectious viral particles .....	15
7.3	siRNA based screen for UUKV host factors .....	16
7.4	Autophagy .....	17
7.4.1	Historic cornerstones of autophagy research in short .....	17
7.4.2	Functions of autophagy .....	17
7.4.3	Autophagy processes in mammalian cells.....	18
7.4.4	The macroautophagy process on a molecular level.....	19
7.4.5	Autophagy in viral infection .....	23
7.5	Rab GTPases: Regulators of cellular trafficking.....	26
7.5.1	Rab1b .....	27
7.5.2	Rab11 .....	28
7.6	Relationship between autophagy and endocytosis .....	30
8	Objectives of the study .....	32
9	Materials and Methods .....	33
9.1	Materials .....	33
9.1.1	Devices and Instruments .....	33
9.1.2	Consumables .....	34
9.1.3	Commercial kits .....	35
9.1.4	Chemicals and Reagents.....	35
9.1.5	Buffers and Solutions .....	37
9.1.6	Media used for cell culture and infection assays.....	39
9.1.7	Plasmids .....	40
9.1.8	siRNAs .....	40
9.1.9	Viruses.....	41
9.1.10	Bacteria.....	42
9.1.11	Mammalian cells .....	42

9.1.12	Primary antibodies.....	43
9.1.13	Secondary antibodies.....	44
9.1.14	Image Analysis Programs.....	44
9.1.15	Services .....	44
9.2	Cellular biology methods.....	45
9.2.1	Mammalian cell culture.....	45
9.2.2	Cell lysis .....	45
9.2.3	Heat shock transformation and plasmid preparation.....	45
9.2.4	Cell transfection with siRNAs and DNA plasmids using Lipofectamine.....	46
9.2.5	Flow cytometry-based infection assays.....	47
9.2.6	Cell fixation and immunostaining for flow cytometry.....	49
9.2.7	Imaging-based assays .....	49
9.2.8	Confocal fluorescence microscopy .....	51
9.3	Virology methods .....	51
9.3.1	Production of UUKV particles & SFV particles .....	51
9.3.2	UUKV & SFV semipurification.....	51
9.3.3	UUKV titration by focus-forming assay .....	52
9.3.4	SFV titration by plaque assay.....	52
9.3.5	UUKV labeling and purification .....	52
9.3.6	Generation of HeLa cells stably expressing shRNA against Atg3 or Beclin 1 by lentivirus transduction .....	53
9.4	Biochemistry methods .....	54
9.4.1	Viral protein analysis by SDS-PAGE & coomassie staining.....	54
9.4.2	Cellular protein analysis by SDS-PAGE & Western blot.....	54
9.5	Image analysis .....	55
9.5.1	LC3-puncta quantification with ImageJ.....	55
9.5.2	Colocalization analysis with Icy.....	55
9.6	Statistical analysis.....	55
10	Results .....	56
10.1	Autophagy-related proteins in UUKV infection.....	56
10.1.1	UUKV infection upon silencing autophagy-related proteins.....	56
10.1.2	Rab11a is involved in UUKV infection .....	60
10.1.3	UUKV infection in Huh7 cells knocked out for key autophagy proteins .....	61
10.2	Production of fluorescently labeled UUKV particles to study early virus-host cell interactions .....	62
10.3	The role of Rab11a in UUKV infection.....	66
10.3.1	Rab11a is involved in UUKV entry .....	66
10.3.2	Rab11a does not modify expression of the UUKV receptor DC-SIGN.....	68
10.3.3	Rab11a is not involved in UUKV binding to HeLa cells.....	68
10.3.4	Rab11a is not involved in internalization of UUKV particles into HeLa cells..	69
10.3.5	Rab11a silencing delays UUKV fusion .....	71
10.3.6	A minor fraction of UUKV-AF568 associates with eGFP-Rab11a positive vesicles	72
10.3.7	Rab11a – extending investigations to other cell lines, viruses and protein family members .....	75

10.4	The role of Atg7 in UUKV infection .....	79
10.4.1	Atg7 is involved in UUKV entry .....	79
10.4.2	Atg7 does not perturb expression of the UUKV receptor DC-SIGN.....	80
10.4.3	Atg7 does not play a major role in UUKV binding to Huh7 cells .....	81
10.4.4	Atg7 is not involved in internalization of UUKV particles into Huh7 cells .....	81
10.5	A cell line expressing blue fluorescent protein-tagged LC3 to study the role of autophagosomes in UUKV infection .....	82
10.5.1	Fluorescently labeled LC3 decorates autophagosomes in HeLa BFP-LC3 stable cell line	83
10.5.2	The impact of siATG7 on autophagosome formation .....	87
10.5.3	UUKV rarely enters autophagosomes 40 mpi.....	89
11	Discussion .....	92
11.1	A subset of autophagy-associated proteins is involved in UUKV infection .....	92
11.2	Rab11 facilitates intracellular trafficking of UUKV particles to acidic compartments for fusion .....	93
11.3	Atg7 promotes endosomal trafficking of UUKV.....	99
11.4	Perspectives.....	101
12	Publications and Contributions .....	103
12.1	Peer-reviewed publications .....	103
12.2	Conference Contributions .....	103
12.3	Contributions to this thesis.....	104
13	References .....	105

## 5 List of Figures

Figure 1: <b>Phlebovirus structure scheme</b> .....	6
Figure 2: <b>Phlebovirus replication cycle</b> .....	8
Figure 3: <b>Phlebovirus endocytosis into mammalian cells</b> .....	11
Figure 4: <b>Phlebovirus intracellular trafficking</b> .....	13
Figure 5: <b>RVFV fusion mechanisms</b> .....	15
Figure 6: <b>Autophagy processes in mammalian cells</b> .....	19
Figure 7: <b>Molecular basis for mammalian macroautophagy</b> .....	23
Figure 8: <b>Rab GTPases as molecular switches</b> .....	27
Figure 9: <b>Rab11-regulated processes</b> .....	29
Figure 10: <b>Rab11a positive membrane as a compartment for phagophore formation</b> ....	30
Figure 11: <b>Atg7, Rab1b and Rab11a were involved in UUKV infection in HeLa cells</b> ....	58
Figure 12: <b>Atg3 and Beclin 1 play a minor role in UUKV infection</b> .....	59
Figure 13: <b>Rab11a was involved in UUKV infection in HeLa cells</b> .....	60
Figure 14: <b>Atg7 was involved in UUKV infection in Huh7 cells</b> .....	61
Figure 15: <b>Semiquantification of UUKV G<sub>N</sub> and G<sub>C</sub></b> .....	63
Figure 16: <b>UUKV labeling with Alexa Fluor succinimidyl ester dyes</b> .....	65
Figure 17: <b>Rab11a plays a role during UUKV entry in HeLa cells</b> .....	67
Figure 18: <b>DC-SIGN expression was not modified on HeLa cells following Rab11a silencing</b> .....	68
Figure 19: <b>Silencing of Rab11a did not impair UUKV binding to HeLa cells</b> .....	69
Figure 20: <b>UUKV-AF488 internalization efficiency was not impacted by Rab11a silencing in HeLa cells</b> .....	70
Figure 21: <b>siRAB11A delays UUKV fusion</b> .....	71
Figure 22: <b>About 10 % UUKV-AF568 colocalize with eGFP-Rab11a</b> .....	75
Figure 23: <b>UUKV relies on the host factor Rab11a for the infection of multiple cell lines</b> .....	75
Figure 24: <b>Rab11a was not important for infection by IAV, SFV and RVFV</b> .....	76
Figure 25: <b>Rab11b was involved in UUKV infection and has no effect on DC-SIGN expression in HeLa cells</b> .....	77
Figure 26: <b>Atg7 played a role in UUKV entry into Huh7 cells</b> .....	79
Figure 27: <b>DC-SIGN expression was not modified by siATG7 in HeLa cells</b> .....	80
Figure 28: <b>Atg7 had no major impact on UUKV-AF488 binding to Huh7 cells</b> .....	81

Figure 29: <b>ATG7 knockout did not impact UUKV internalization into Huh7 cells</b> .....	82
Figure 30: <b>HeLa BFP-LC3 stable cell line heterogenously expressed LC3.</b> .....	83
Figure 31: <b>Sorting subpopulations of HeLa based on BFP-LC3 expression</b> .....	84
Figure 32: <b>BFP-LC3 expression and UUKV infection in two expresser clones of HeLa BFP-LC3 cells</b> .....	85
Figure 33: <b>BFP-LC3 puncta accumulate in HeLa BFP-LC3 C2 cells upon treatment with bafilomycin A1 or rapamycin, and are eliminated by wortmannin treatment</b> .....	86
Figure 34: <b>Atg7 was silenced by siRNA-mediated silencing in HeLa BFP-LC3 C2 cells.</b>	87
Figure 35: <b>BFP-LC3 puncta accumulation after Atg7-silencing in HeLa BFP-LC3 C2 cells</b> .....	89
Figure 36: <b>UUKV-AF568 rarely associated with BFP-LC3 puncta 40 mpi</b> .....	91

## 6 List of Abbreviations

Abbreviation	Written-out
μ	micro-
AF	Alexa Fluor
AMPK	AMP-activated protein kinase
AP	autophagosome
Atg	autophagy-related
ATP	adenosine triphosphate
BCL-2	B cell lymphoma-2
BFP	blue fluorescent protein
BG	background
BHK	baby hamster kidney
BiP	binding immunoglobulin protein
BMP	bis(monoacylglycerol)phosphate
BSA	bovine serum albumine
BSL	biosafety level
CaCl <sub>2</sub>	calcium chloride
Cas9	CRISPR-associated protein 9
CD	cluster of differentiation
CIE	clathrin-independent endocytic pathways
CMA	chaperone-mediated autophagy
CMC	carboxymethyl cellulose
CME	clathrin-mediated endocytosis
CNX	calnexin
COP	coat protein complex
CRD	cargo recognition domain
CRISPR	clustered regularly interspaced short palindromic repeats
cRNA	complementary RNA
cRNP	complementary RNP
CSFV	classical swine fever virus
C-type	calcium-dependent
Da	Dalton
DC	dendritic cell

DC-SIGN	dendritic cell-specific intercellular adhesion molecule 3-grabbing non-integrin
DENV	Dengue virus
dH <sub>2</sub> O	deionized water
DMEM	Dulbecco's Modified Eagle Medium
DMSO	dimethyl sulfoxide
dsRNA	double-stranded RNA
E2	envelope protein 2
EBOV	Ebola virus
EDTA	ethylenediaminetetraacetic acid
EE	early endosome
eGFP	enhanced green fluorescent protein
ER	endoplasmic reticulum
ERES	ER exit sites
ERGIC	ER-Golgi intermediate compartment
FACS	fluorescence activated cell sorting
FB	FACS buffer
FBS	fetal bovine serum
FCS	fetal calf serum
ffu	focus-forming units
FPB	FACS permeabilization buffer
g	gram
GAP	GTPase-activating protein
G <sub>C</sub>	glycoprotein C
GDI	guanine-nucleotide-dissociation inhibitor
GDP	guanosine diphosphate
GEF	guanine-nucleotide exchange factor
GMEM	Glasgow's Minimum Essential Medium
G <sub>N</sub>	glycoprotein N
gRNA	genomic RNA
GTP	guanosine triphosphate
h	hour
hCMV	human cytomegalovirus
HEK	human embryonic kidney

HeLa	Henrietta Lacks
HNE	HEPES - NaCl – EDTA
HOPS	homotypic fusion and protein sorting
hpi	hours post infection
HRTV	Heartland virus
HS	heparan sulfate
Hsc70	heat shock cognate protein of 70 kDa
HSV-1	herpes simplex virus type 1
Huh	human hepatoma
IAV	influenza A virus
IAV-N	influenza A virus nucleoprotein
IFITM	interferon-induced transmembrane protein
ILV	intraluminal vesicles
JEV	Japanese encephalitis virus
k	kilo-
KO	knockout
KSHV	Kaposi's sarcoma-associated herpesvirus
L	leucine
L	-liter
L segment	large segment
LAMP1	lysosome associated membrane protein type 1
LAMP2A	lysosome associated membrane protein type 2A
LAP	LC3-associated phagocytosis
LC3	microtubule-associated proteins 1A/1B light chain 3
LE	late endosome
LIR	LC3-interacting region
LL motif	dileucine motif
LSEC	lymph node sinusoidal endothelial cell
LSEctin	lymph node sinusoidal endothelial cell C-type lectin
L-SIGN	liver/lymph node cell-specific intercellular adhesion molecule 3-grabbing non-integrin
LYS	lysosome
m	milli-
M	molar

M segment	medium segment
MgCl <sub>2</sub>	magnesium chloride
MHCI/II	major histocompatibility complex I or II
MOI	multiplicity of infection
mpi	minutes post infection
MTORC1	mechanistic target of rapamycin complex 1
MVB	multivesicular body
Mφ	macrophage
N	asparagine
n	nano-
NaCl	sodium chloride
NH <sub>4</sub> Cl	ammonium chloride
NMMHC-IIA	nonmuscle myosin heavy chain IIA
ns	nonsignificant
NS <sub>M</sub>	nonstructural protein M
NS <sub>S</sub>	nonstructural protein S
nt	nucleotide
NT	nontreated
PAMP	pathogen-associated molecular pattern
PAS	preautophagosomal structure
PBMC	peripheral blood mononuclear cells
PBS	phosphate buffered saline
PDI	protein-disulfide-isomerase
PE	phosphatidylethanolamine
PI	phosphatidylinositol
PI3KC3-C1	class III phosphatidylinositol 3-kinase complex 1
PI3KC3-C2	class III phosphatidylinositol 3-kinase complex 2
PI3P	phosphatidylinositol-3-phosphate
PKR	protein kinase R
PLEKHM1	pleckstrin homology domain-containing protein family member 1
PP	phagophore
PRR	pattern recognition receptor
PTV	Punta Toro virus
Q	glutamine

RabGGTase	Rab geranylgeranyl transferase
RdRp	RNA-dependent RNA polymerase
RE	recycling endosome
rER	rough ER
RNA	ribonucleic acid
RNaseK	Ribonuclease kappa
RNP	ribonucleoprotein
RPMI	Rosewell Park Memorial Institute Medium
RU	relative units
RVFV	Rift Valley fever virus
rVSV-SFTSV	recombinant vesicular stomatitis Indiana virus pseudotyped with SFTSV glycoproteins G <sub>N</sub> and G <sub>C</sub>
S	serine
S segment	small segment
SD	standard deviation
SDS-PAGE	sodium dodecyl sulfate polyacrylamide gel electrophoresis
SFTSV	severe fever with thrombocytopenia syndrome virus
SFV	Semliki Forest virus
shRNA	small hairpin RNA
siATG7	siRNA targeting <i>ATG7</i>
siATP6V1A	siRNA targeting ATPase H <sup>+</sup> Transporting V1 Subunit A
siRAB11A	siRNA targeting <i>RAB11A</i>
siRNA	small interfering RNA
siVAMP3	siRNA targeting <i>VAMP3</i>
SNARE	soluble NSF attachment protein receptor
STX17	syntaxin 17
TB	trypan blue
TBST	TBS-Tween
TGN	trans-Golgi network
TLR	Toll-like receptor
TOSV	Toscana virus
TPB	tryptose phosphate broth
TPCK	N-tosyl-L-phenylalanine chloromethyl ketone
UGUC	glucosylceramide synthase

ULK1	Unc-51 like autophagy activating kinase 1
UUKV	Uukuniemi virus
UUKV-N	Uukuniemi virus nucleoprotein
UVRAG	UV-radiation resistance-associated gene protein
v	volume
VAMP3	vesicle-associated membrane protein 3
VCD	Vybrant Dye Cycle
VPS	vascular protein sorting
vRNA	viral RNA
vRNP	viral RNP
VSV	Vesicular stomatitis Indiana virus
VV	Vaccinia virus
VZV	Varicella zoster virus
v-SNARE	vesicle SNARE
w	weight
WB	Western blot
WT	wild type
x g	fold gravitational force

### 7 Introduction

#### 7.1 Arboviruses – emerging agents of disease

Out of the nineteen pandemic, epidemic diseases currently listed by the World Health Organization, a total of five are caused by arboviruses: chikungunya, Crimean-Congo hemorrhagic fever, Rift Valley fever, yellow fever and Zika virus. This emphasizes a high relevance with prevailing importance <sup>1</sup>.

Arthropod-borne viruses, abbreviated as arboviruses, share the common characteristic of a transmission cycle between vertebrate or plant hosts and arthropod vectors. Plant-specific viruses are transmitted by thrip vectors <sup>2</sup>, whereas vertebrate-specific viruses are transmitted by hematophagous arthropods such as ticks, mosquitoes, midges, or sand flies. These vectors acquire arboviruses while feeding on a viraemic host. After viral multiplication, the viruses are transmitted to the next vertebrate host during a blood meal. Typically, a sylvatic transmission cycle from the vector to the vertebrate host is required for amplification and to maintain viral reservoirs. In wild animals, such transmissions rarely cause symptomatic diseases, due to the long term of coevolution. Transmission to humans or domestic animals on the other hand occurred less frequently, and no balanced relationships could be established. Therefore, arbovirus infections in humans or domestic animals can result in significant morbidity and mortality. A low level of viraemia, typical for dead-end hosts, does not allow further arboviral transmission. Chikungunya, dengue, yellow fever and Zika virus however, have adapted to humans as vertebrate hosts. Viral replication in humans is efficient enough to sustain human-mosquito transmission <sup>3,4</sup>. This increases the danger for these viruses to become endemic. Importantly, arbovirus transmission is not limited to vector transmission. Crimean-Congo haemorrhagic fever virus was transmitted by direct contact with blood of a viraemic patient <sup>5</sup>. West Nile virus can be transmitted vertically <sup>6</sup>, by blood transfusions <sup>7</sup> and organ donations <sup>8</sup>. Rift Valley fever virus is stable as aerosol <sup>9</sup> and suggested to be transmitted via this route of exposure <sup>10</sup>.

A high population density accompanied with increasing exploitation of land disturbed the sylvatic arboviral transmission cycles and led to an increased exposure frequency of humans to arthropod vectors. Furthermore, globalization, including passenger traffic and trade, in combination with global warming, allowed vectors and viruses to spread easily and to broaden their geographic distribution. This results in geographic expansion of arboviral diseases and the establishment of arboviruses as endemic diseases, of which some cause severe pathology

## Introduction

including encephalitis (Rift Valley fever virus, La Crosse virus), severe hepatitis (dengue virus) and hemorrhagic fever (Crimean-Congo haemorrhagic fever virus) <sup>4,11</sup>.

Arboviruses are not a taxonomic classification, but rather define a super group including distinct viral families. Human-pathogenic members are comprised in the *Flaviviridae*, *Reoviridae* and *Togaviridae* families and the *Bunyavirales* order (more specifically in the *Peribunyaviridae*, *Nairoviridae* and *Phenuiviridae* families), and are responsible for a growing number of outbreaks worldwide <sup>12,13</sup>. The medically most relevant arbovirus is dengue virus (*Flaviviridae*). Dengue virus is present in most tropical or subtropical countries and was estimated to be responsible for 60 – 140 million cases annually, ranging from mild fever to partially fatal dengue shock syndrome <sup>14</sup>. Chikungunya virus (*Togaviridae*) and Zika virus (*Flaviviridae*) were both newly introduced into the Americas, followed by rapid expansion and outbreaks in 2013 and 2015 respectively <sup>15,16</sup>. Crimean-Congo haemorrhagic fever virus (*Nairoviridae*) is endemic in Africa, Middle East, Europe (the Balkans) and Asia and causes systematic haemorrhages with a mortality rate between 10 and 40 % <sup>17,18</sup>. Human-pathogenic isolates of the *Phlebovirus* genus within the *Phenuiviridae* family are described into more details in a separate chapter (chapter 7.2.2).

Efficient vaccines against Yellow fever virus and Japanese encephalitis virus (*Flaviviridae*) were successfully developed. But the absence of further vaccines or specific, effective drugs for the treatment of human pathogenic arbovirus infections in combination with their potential to cause a public health emergency <sup>19</sup>, urgently calls for comprehensive research and rapid development in the field of arboviruses. Ideally, drugs should target an early step in viral infection but unfortunately, little is known about arbovirus cell biology, the vector-to-human transmission and entry into mammalian cells.

The topic of my PhD project are phleboviruses, many isolates of which are highly pathogenic in both human and domestic animals. My thesis aimed to shed light on the productive pathways used by these viruses to enter host cells, with a specific emphasis on the tick-borne phlebovirus Uukuniemi (UUKV).

# Introduction

## 7.2 *Phlebovirus* genus

### 7.2.1 Taxonomy

Most of the time in my PhD I told interested researchers as well as my friends and family that I am working on bunyaviruses. Since March 2017 this is no longer true. The family *Bunyaviridae* was promoted to a new order: the *Bunyavirales*<sup>20</sup>. The rationale behind this was to create room to 1) correctly reflect the phylogenetic relationship to newly included members, e.g. previously unassigned genera *Emaravirus* and *Tenuivirus* and 2) be able to classify bunyavirus family members that could not be assigned to any genus due to established classification criteria<sup>21</sup>.

The *Bunyaviridae* family used to comprise five genera: *Hantavirus*, *Nairovirus*, *Orthobunyavirus*, *Phlebovirus* and *Tospovirus*. Except for the rodent-borne hantaviruses, the other four genera were arboviruses. Nairoviruses, orthobunyaviruses and phleboviruses are transmitted by the blood-feeding arthropods sand flies, mosquitos, midges or ticks, and the group of plant-infecting tospoviruses is transmitted by thrips. All are enveloped viruses with a trisegmented, single-stranded RNA genome<sup>22</sup>.

The new order *Bunyavirales* additionally comprises nonenveloped members i.e. members of the genus *Tenuivirus*, bisegmented members e.g. Wuhan millipede virus 2 and South Bay virus, and members with more than three segments i.e. *Emaravirus* and *Tenuivirus* (having 4 to 6 segments)<sup>21</sup>. *Bunyavirales* are currently comprised of twelve different families: *Arenaviridae*, *Cruliviridae*, *Fimoviridae*, *Hantaviridae*, *Leishbuviridae*, *Myopoviridae*, *Nairoviridae*, *Peribunyaviridae*, *Phasmaviridae*, *Tospoviridae*, *Wupedeviridae* and *Phenuiviridae*<sup>23</sup>. The latter includes the genus *Phlebovirus*, which is this project's focus.

The *Bunyavirales* order is currently under frequent rearrangement<sup>24,25</sup>. According to the latest taxonomy update the two former tick-borne phleboviruses severe fever with thrombocytopenia syndrome virus (SFTSV) and Heartland virus (HRTV) are now classified to the *Banyangvirus* genus<sup>23,24</sup>. For convenience with the project presented here and recent publications, I have chosen to keep the previous<sup>25</sup> taxonomy nomenclature.

### 7.2.2 Epidemiology of phleboviruses

The *Phlebovirus* genus comprises a variety of emerging pathogens of which some cause severe symptoms. The mosquito-borne Rift Valley fever virus (RVFV) is spread in Africa and Saudi Arabia and a major pathogen in domestic animals causing hepatitis and abortion in ruminants

## Introduction

as cattle, sheep, and goats, and also severe disease with fever, haemorrhages and sudden death in camels. Infection in humans is mostly asymptomatic. Some cases develop renal failure, acute hepatitis, neurologic dysfunction and haemorrhages. These symptoms are associated with 50 % lethality<sup>26,27</sup>. The tick-borne severe fever with thrombocytopenia syndrome virus (SFTSV) is another example. It was first reported in China 2009 and then also isolated in Japan, North Korea and South Korea. Infected humans suffer from thrombocytopenia, leukocytopenia and haemorrhages, these symptoms are associated with a lethality rate of 5-30 %<sup>28-30</sup>. The closely related Heartland virus (HRTV) is another tick-borne pathogen first isolated in the United States in 2012 with symptoms similar to SFTSV<sup>31,32</sup>. The sand fly-transmitted Toscana virus (TOSV) is endemic in North Africa and Europe, including Italy, Spain, and the south of France. Infection is generally asymptomatic but in some cases leads to meningoencephalitis<sup>33,34</sup>.

### 7.2.3 The model virus UUKV

This project is focused on Uukuniemi virus (UUKV; order *Bunyavirales*, family *Phenuiviridae*, genus *Phlebovirus*). UUKV is transmitted by ticks belonging to the species *Ixodes ricinus* and *Ixodes scapularis*, and infects a wide range of vertebrate hosts as birds, humans, cattle and reindeers<sup>35,36</sup>. To date UUKV is not associated with any disease in humans and therefore presents the advantage to be handled in biosafety level-2 (BSL-2) laboratories. Closely related, highly pathogenic phleboviruses such as the tick-borne SFTSV and HRTV have to be handled under BLS-3 or BLS-4 conditions. Due to easier handling conditions and the availability of established tools, UUKV is readily used as a model for the investigation of phleboviral host cell invasion.

UUKV strain 23, used in our laboratory, was originally isolated from *Ixodes ricinus* ticks, collected in 1959 in Finland, and was first amplified in chicken embryo fibroblasts and thereafter in BHK-21 cells<sup>35</sup>. UUKV infects a wide range of mammalian cells such as BHK-21, HEK 293T, HeLa and Huh7 cells as well as *Ixodes ricinus* and *Ixodes scapularis* tick cell lines<sup>37,38</sup>. In infected mammalian cells, UUKV replication is high, while there is little or no progeny release. An exception are BHK-21 cells that release high amounts of progeny and are therefore commonly used for UUKV particle production<sup>37</sup>. HeLa cells do not release viral progeny<sup>37</sup>. Hence they are useful to study viral entry because we are sure to assess only the first round of infection. While infected mammalian cells die after a couple of days, no cytopathogenic effect is detected in UUKV infected *Ixodes ricinus* tick cell lines<sup>37-39</sup>, reflecting the lack of pathology in arthropod vectors<sup>40</sup>.

## Introduction

### 7.2.4 Virion structure & genome organization of phleboviruses

Phlebovirus particles are enveloped, roughly spherical with a diameter of 80 – 160 nm and a tri-segmented single-stranded RNA genome, which exclusively replicates in the cytosol of host infected cells (**Figure 1a**). All three genomic RNA segments have highly conserved complementary nucleotides at the 3' and 5' end. A panhandle structure is formed by base pairing of the termini. The viral genomic RNA is thus present in a noncovalently closed circular form <sup>22</sup>.

A minimum of four structural proteins are encoded on the three genomic RNA segments in a negative-sense orientation (**Figure 1b**). An RNA-dependent RNA polymerase (RdRp), required for viral replication in the cytosol, is encoded on the largest segment (L). The lack of proofreading activity in the viral polymerase is accompanied by a high mutation rate (in the range of  $10^{-5}$ - $10^{-6}$  substitutions per nucleotide and replication) and thereby allows rapid adaptation to environmental changes – a feature that might enable phleboviruses to expand geographically and increase their host range. The medium segment (M) encodes a precursor polyprotein, which is processed into two envelope glycoproteins G<sub>N</sub> (amino-terminal) and G<sub>C</sub> (carboxy-terminal). Enzymatic processing is mediated by host cell proteases at the Golgi apparatus, where phleboviruses assemble and derive their lipid envelope from. The glycoproteins form spike-like protrusions on the lipid envelope, arranged in an icosahedral surface lattice in penton-hexon clusters and a T = 12 triangulation <sup>41</sup>. G<sub>N</sub> and G<sub>C</sub> are crucial for viral attachment to host cells and membrane fusion. The smallest segment (S) codes for the nucleoprotein N, coating the viral RNA to protect it from degradation. One RdRp molecule is bound per panhandle structure of the viral RNA. Altogether the viral RNA, coated by N proteins and bound to RdRp make up the ribonucleoprotein (RNP). A unique feature of *Bunyavirales* in comparison to other enveloped viruses is the lack of a rigid capsid or matrix <sup>22,42,43</sup>.

In addition to the four structural proteins, phleboviruses encode a nonstructural protein S (NS<sub>S</sub>) on the S segment in positive-sense orientation. NS<sub>S</sub> is an important virulence factor <sup>44</sup>. In the case of RVFV, NS<sub>S</sub> has been shown, for example, to inhibit general host cell transcription, interferon-β expression and protein kinase R (PKR) function, counteracting innate immune response and facilitating viral translation <sup>44</sup>. The M segment of phleboviruses transmitted by dipterans (sand flies and mosquitoes) encodes an additional nonstructural protein NS<sub>M</sub> that is part of the precursor polyprotein for G<sub>N</sub> and G<sub>C</sub>. NS<sub>M</sub> inhibits apoptotic cells death by inhibiting caspases <sup>45</sup> but is also proposed as the second factor of virulence in RVFV infection, after NS<sub>S</sub> <sup>46</sup>.

## Introduction

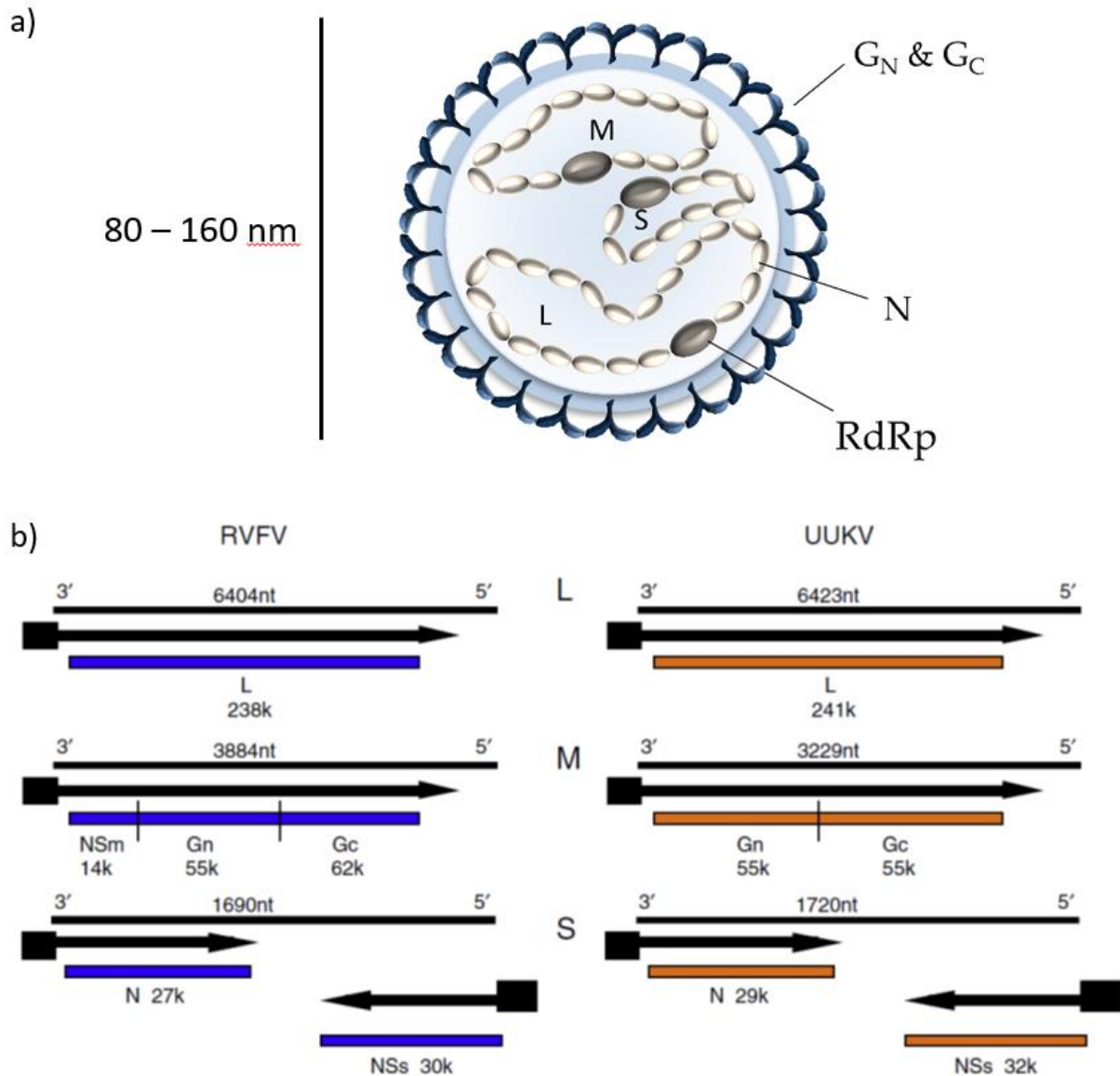


**Figure 1: Phlebovirus structure scheme**

**a)** Phlebovirus structure: Phlebovirus particles are enveloped, roughly spherical and have a diameter of 80 – 160 nm. The genomic RNA is trisegmented and the segments are termed according to their size, namely small (S), medium (M) and large (L) segment. They encode at least four structural proteins: the nucleoprotein N, the glycoproteins  $G_N$  and  $G_C$ , and the RNA-dependent RNA polymerase (RdRp)]. Adapted from <sup>43</sup>. **b)** Genomic organization of the mosquito-borne Rift Valley fever virus (RVFV) and the tick-borne Uukuniemi virus (UUKV): The three segments of the viral RNA genome and their respective length are shown. mRNAs are represented by arrows (boxes at the 5' end depict host cell-derived sequences) and gene products are indicated by colored boxes, including their molecular mass below. In addition to the structural proteins, the three genomic RNA segments code for up to two nonstructural protein, NS<sub>S</sub> and possibly NS<sub>M</sub>. The lack of NS<sub>M</sub> gene is a specificity of phleboviruses transmitted by ticks such as UUKV; all others encode the NS<sub>M</sub> protein. Nt = nucleotides. Adapted from <sup>43,47</sup>.

## Introduction

### 7.2.5 Phlebovirus entry into mammalian cells

Natural transmission of arboviruses to vertebrate hosts occurs during the arthropod's blood meal. Virions are injected into the host dermis, where dendritic cells (DCs) and macrophages (Mφs) are among the first encountered cells. As obligate intracellular parasites, viruses require entry into the target cell's intracellular environment to access the host cellular machinery for viral infection and replication. Viral entry can occur in a variety of mechanisms, depending on the host cell and virus. Viral fusion relies on numerous host cellular factors and processes, of which only a minor portion is identified and characterized. Phlebovirus entry into mammalian cells starts with binding to specific attachment factors or receptors and subsequent uptake via receptor-mediated endocytosis. Internalization is followed by endosomal trafficking to an acidified compartment for fusion of the viral envelope with the host endosome membrane, to release the viral genome into the cytosol (**Figure 2A-C**)<sup>40</sup>. UUKV is an excellent surrogate for the most highly pathogenic members in the *Phlebovirus* genus. Recent studies revealed important advances in the study of phlebovirus infection using UUKV as a model<sup>48</sup>. In the following chapter, the different entry steps of phleboviruses are introduced in more detail with a specific focus on UUKV entry.

## Introduction

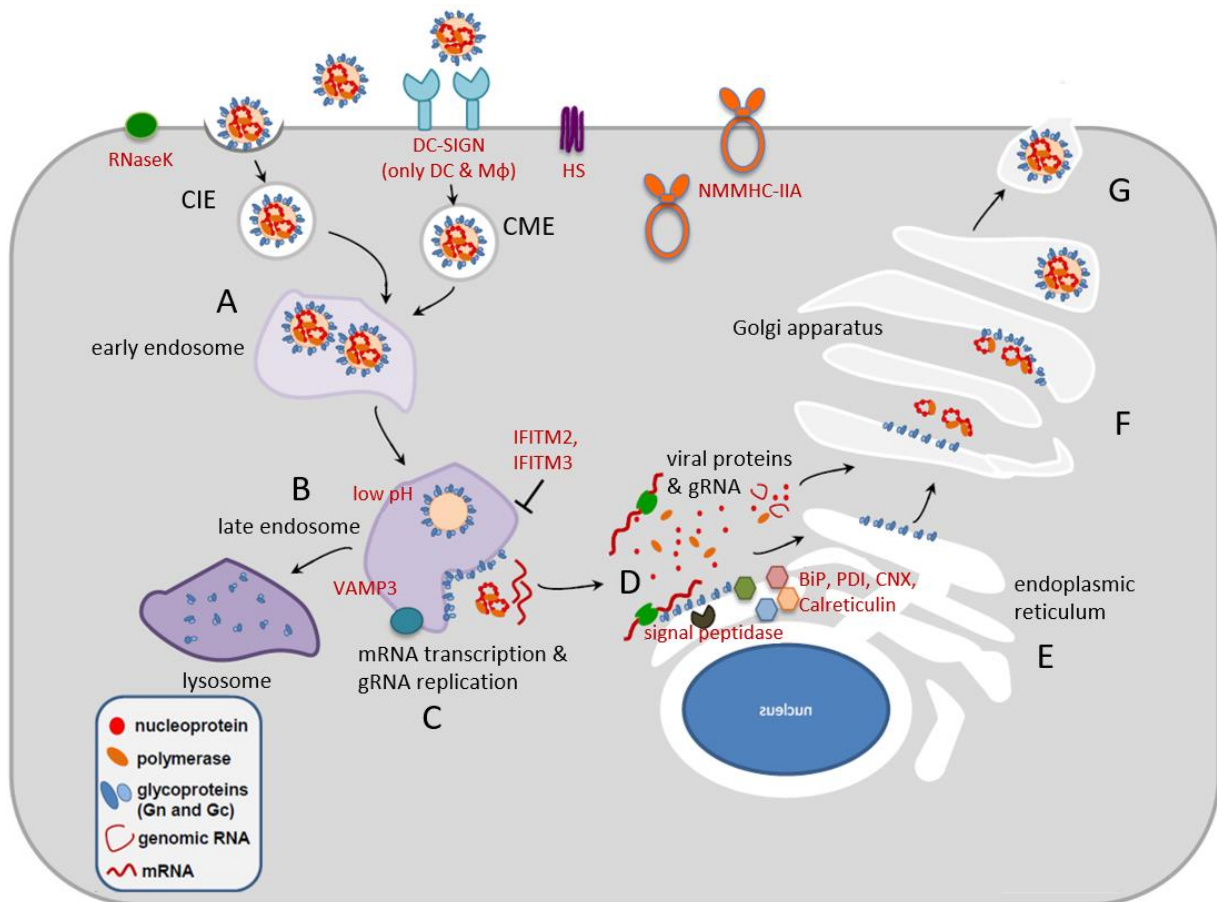


**Figure 2: Phlebovirus replication cycle**

**A)** Phlebovirus particles bind to the host cell membrane by interaction of the viral glycoproteins with different receptors, for example nonmuscle myosin heavy chain IIA (NMMHC-IIA), heparan sulfate (HS), dendritic cell-specific intracellular adhesion molecule-3-grabbing non-integrin (DC-SIGN) and liver/lymph node-SIGN (L-SIGN). Phleboviruses are taken up through clathrin-mediated endocytosis (CME) or clathrin-independent endocytic pathways (CIE). Internalization of virions is promoted by Ribonuclease kappa (RNaseK). **B)** Virions traffic to acidic late endosomal compartments. G<sub>C</sub> membrane fusion activity is induced by the low pH level. Fusion of UUKV is promoted by vesicle-associated membrane protein 3 (VAMP3) and fusion of RVFV is inhibited by interferon-induced transmembrane proteins 2 & 3 (IFITM2 & IFITM3). **C)** Upon fusion of the viral envelope with the host vesicular membrane, the viral RNPs are released into the cytosol, where transcription and replication take place. **D)** In the cytoplasm viral nucleoprotein, RdRp and genomic RNA (gRNA) are synthesized and associate to form the RNP. The glycoprotein precursor protein is translated at the rough endoplasmic reticulum (ER) and cleaved into G<sub>N</sub> & G<sub>C</sub> by a signal peptidase. **E)** ER chaperones, binding immunoglobulin protein (BiP) and calnexin (CNX) participate in the quality control of G<sub>N</sub> & G<sub>C</sub> maturation. The protein-disulfide-isomerase (PDI) supports proper folding by disulfide bond formation and calreticulin prevents the export of misfolded G<sub>N</sub> & G<sub>C</sub> from the ER. **F)** G<sub>N</sub>/G<sub>C</sub> heterodimers are transported to the Golgi apparatus. During budding of virions into the Golgi apparatus, the cytoplasmic tail of G<sub>N</sub> associates with RNPs. **G)** Vesicles containing virus particles are believed to be transported to the plasma membrane from where virions would be released by exocytosis. DC = dendritic cell, Mφ = macrophage. Adapted from <sup>48</sup>.

## Introduction

### 7.2.5.1 Phlebovirus receptors

Binding of phleboviruses to the host plasma membrane strictly relies on surface-exposed receptors including proteins and polysaccharides on glycoproteins<sup>49</sup>. The glycosaminoglycan heparan sulphate (HS) is a receptor for RVFV and TOSV<sup>50-52</sup>. Nonmuscle myosin heavy chain IIA (NMMHC-IIA), expressed on plasma membranes of Vero cells and human umbilical vein endothelial cells (HUVECs), is involved in infectious entry of SFTSV<sup>53</sup>.

A common receptor for the phleboviruses Punta Toro virus (PTV), RVFV, SFTSV, TOSV, UUKV is the DC-specific intracellular adhesion molecule-3-grabbing nonintegrin (DC-SIGN), also termed CD209<sup>54,55</sup>. In UUKV infection, DC-SIGN is not only employed for virus attachment but also for internalization, and thereby serves as an endocytic receptor<sup>54</sup>. DC-SIGN is specifically expressed on immature dermal DCs, specialized in capturing pathogens and antigen presentation<sup>56</sup>. The location of these DCs coincides with the anatomical site of arbovirus introduction into mammalian hosts, i.e. the skin dermis. Furthermore the calcium-dependent (C-type) lectin DC-SIGN binds high mannose and fucose *N*-glycans, typical insect-derived glycoproteins<sup>57</sup>, rendering DC-SIGN an interesting candidate receptor for phleboviruses. Indeed, human peripheral blood mononuclear cells (PBMC)-derived immature DCs are sensitive to RVFV and UUKV infection<sup>54</sup>.

The closely related liver/lymph node-specific intercellular adhesion molecule-3-grabbing nonintegrin (L-SIGN) is specifically expressed on human liver sinusoidal endothelial cells (LSECs). Like DC-SIGN, L-SIGN is a C-type lectin and recognizes high mannose *N*-glycans<sup>58</sup>. L-SIGN serves as a receptor for RVFV, SFTSV, TOSV and UUKV<sup>55,59</sup>. In contrast to the endocytic receptor DC-SIGN, L-SIGN has been shown to only serve as an attachment factor<sup>59</sup>. SFTSV infection depends on a third C-type lectin, the liver and lymph node sinusoidal endothelial cell C-type lectin (LSEctin)<sup>60</sup>. LSEctin is expressed on LSECs, dendritic cells and macrophages<sup>61,62</sup> and recognizes mannose, *N*-acetylglucosamine and fucose<sup>62</sup>. The three lectins DC-SIGN, L-SIGN and LSEctin play an important role in pathogen recognition and cell adhesion and, might be subverted by phleboviruses and other arboviruses to promote infection and facilitate virus spread<sup>63</sup>.

### 7.2.5.2 Uptake

To enter a target cell, phleboviruses rely on the uptake into an endocytic pathway (**Figure 2A**). Virion receptor-interactions are an important prerequisite for viral internalization. The use of fluorescently labeled UUKV particles in combination with enhanced green fluorescent protein (eGFP)-tagged DC-SIGN allowed the visualization of virus receptor interactions<sup>54</sup>. This was

## Introduction

the first time, that virus-receptor interactions were visualized live, making this system a useful model to study virus-receptor interactions in general. Cell-bound UUKV particles recruit DC-SIGN to their contact site and create a receptor-rich domain, important for membrane curvature and efficient receptor-mediated signal transduction, together resulting in virus internalization<sup>49,54</sup>.

Sequence motifs at the cytosolic tail of receptors serve as docking sites for specific adapter proteins and define the endocytic pathway, into which viral particles are taken up. One example is the dileucine (LL) motif at the cytosolic tail of the UUKV endocytic receptor DC-SIGN<sup>59</sup>. The LL motif is an internalization signal<sup>64</sup> and known to mediate uptake into clathrin-coated vesicles<sup>65</sup>. In addition to clathrin-mediated endocytosis, lipid raft-mediated endocytosis and phagocytosis have been proposed as internalization processes of DC-SIGN<sup>57,64,66,67</sup>. Furthermore, glycosylation patterns of cargo are important for receptor recognition and intracellular signaling. DC-SIGN is reported to activate different intracellular signaling pathways according to the recognized carbohydrates<sup>68,69</sup>. The differing glycosylation pattern of mammalian and arthropod cell-derived UUKV particles<sup>38</sup>, could hence influence the utilized endocytic route.

Electron microscopy-based studies show some UUKV particles in clathrin-coated vesicles and UUKV infection is not significantly reduced in absence of the clathrin heavy chain, indicating that the virus is mostly internalized through clathrin-independent mechanisms (**Figure 3**)<sup>37,54</sup>. The details of UUKV uptake mechanisms remain to be defined. SFTSV, and also vesicular stomatitis Indiana virus pseudotyped with SFTSV glycoproteins G<sub>N</sub> and G<sub>C</sub> (rVSV-SFTSV), are internalized in a clathrin-dependent manner (**Figure 3**)<sup>55,70</sup>. In the case of RVFV, three different internalization pathways have been proposed, each for different virus strains. While a nonspreading RVFV strain was shown to rely on clathrin for entry<sup>71</sup>, the vaccine strain MP12 was suggested to be internalized by macropinocytosis by a first study<sup>72</sup> and later through caveolin-dependent mechanisms by a second work (**Figure 3**)<sup>73</sup>. Harmon and colleagues additionally report an independence of MP12 on clathrin-mediated endocytosis and macropinocytosis<sup>73</sup>. Various outcomes could result from the use of different virus strains and cell models. Together these studies most likely reflect the ability of viral particles to use diverse internalization mechanisms. The use of certain viral receptors and uptake mechanisms influence in part the capacity of viruses to infect specific cell types and tissues. The ubiquitous transmembrane protein ribonuclease kappa is an additional factor involved in the internalization of RVFV MP12<sup>74</sup> but its specific function remains to be uncovered (**Figure 2**).

## Introduction

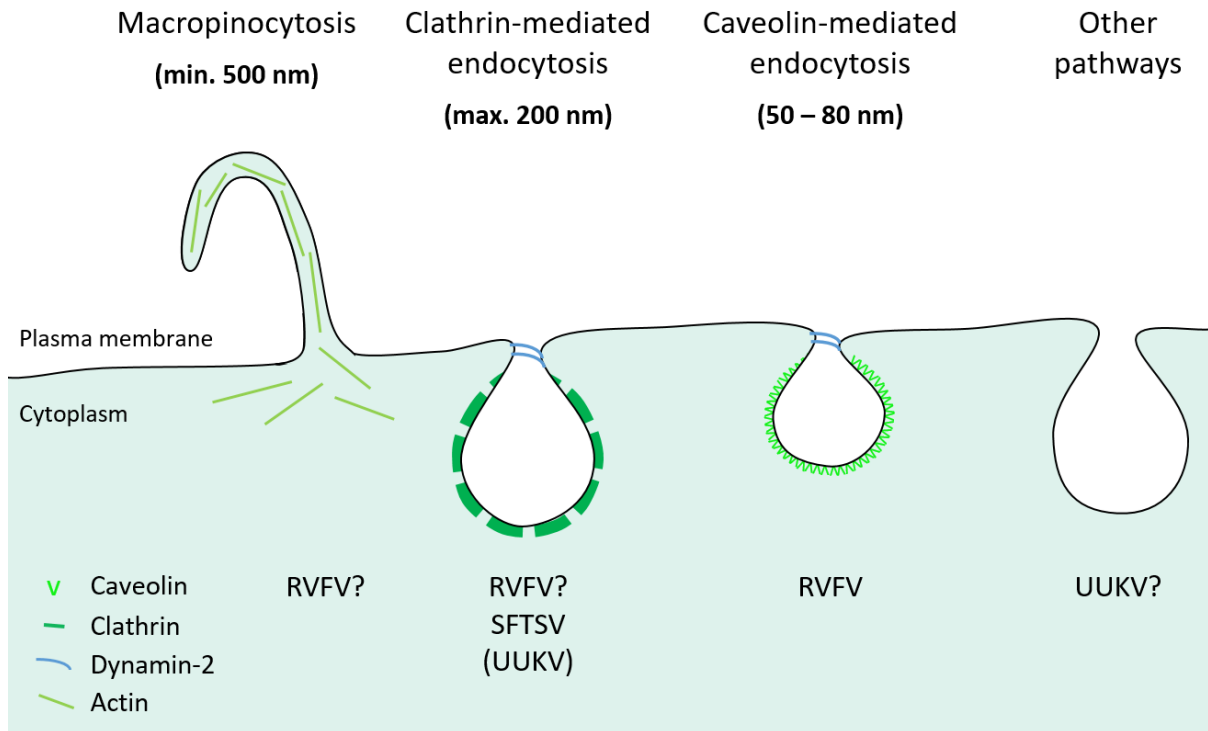


**Figure 3: Phlebovirus endocytosis into mammalian cells**

Phlebovirus internalization follows several endocytic pathways, involving many host cellular factors as adaptor and coat proteins. RVFV = Rift Valley fever virus, SFTSV = severe fever with thrombocytopenia syndrome virus, UUKV = Uukuniemi virus. Adapted from <sup>43</sup>.

### 7.2.5.3 Intracellular trafficking

Upon internalization, phleboviral particles are sorted into the endocytic system to traffic towards an acidic endosomal compartment for membrane fusion and subsequent viral genome release into the cytoplasm. Fusion of RVFV, SFTSV and UUKV envelope with the host endosome membrane strictly relies on a low pH (pH 5.7, 5.6 and 5.4 respectively), characteristically found in late endosomal compartments (**Figure 4**) <sup>37,70,71</sup>. In line with the low pH-dependence, phleboviruses are highly sensitive to drugs, neutralizing the endosomal pH including the lysosomotropic weak bases ammonium chloride and chloroquine as well as inhibitors of the vacuolar H<sup>+</sup> ATPases concanamycin B and bafilomycin A<sub>1</sub> <sup>37,54,55,71,73</sup>.

Cargo can access acidic endosomal compartments by following the classic endocytic pathway from early endosomes (EEs) to multivesicular bodies (MVBs) and then late endosomes (LEs) that fuse with lysosomes (LYs) to form endolysosomes. MVBs are formed by endosomal sequestration and formation of intraluminal vesicles (ILVs). Rab proteins (small GTPases) are important factors that regulate endosomal trafficking and maturation. Rab5-positive EEs undergo conversion to Rab7-positive LEs, which finally fuse with LAMP1-positive LYs. A

## Introduction

continuously decreasing pH value in the luminal environment of endosomes is reached by vacuolar H<sup>+</sup> ATPases concomitantly with endosomal maturation<sup>75</sup>. To assess how phleboviruses reach fusion-competent compartments, trafficking within this classic endocytic pathway was investigated. Phleboviruses are proposed to transit Rab5-positive early endosomes (**Figure 4**). Studies with constitutively active or dominant negative Rab5 mutants as well as confocal microscopy imaging clearly show that UUKV relies on entering Rab5-positive early endosomes<sup>37</sup>. Also rVSV-SFTSV and SFTSV were detected in Rab5-positive vesicles but functional studies with e.g. Rab5 mutants remain to be performed for this virus<sup>70,76</sup>.

A series of results indicates that phleboviruses can be classified as late-penetrating viruses, a group of viruses entering host cells through late endosomal compartments<sup>77</sup>. In accordance with the acidic pH-dependence described above, RVFV and UUKV penetrate host cells 20 – 40 minutes post infection (mpi), the time period required for late endosomal maturation (**Figure 4**)<sup>37,71</sup>. Also SFTSV fuses 15 – 60 mpi<sup>70</sup>. During late endosomal maturation, LEs traffic along microtubules<sup>78</sup>. UUKV and SFTSV are sensitive to the microtubule-depolymerizing agents colcemid and nocodazole, respectively, indicating an importance of late endosomal mobility along microtubules for viral infection<sup>37,70</sup>. Histone deacetylase 8, participating in endosome maturation and microtubule organization, is an additional host factor involved in UUKV entry<sup>79</sup>.

Even though phleboviruses are considered late penetrating viruses, the function of Rab7-positive late endosomes in infection remains elusive. Life-cell imaging and confocal microscopy studies demonstrate the presence of UUKV in Rab7-positive late endosomes and LAMP1-positive lysosomes. But while constitutively active Rab7 mutants increase UUKV infection, dominant negative Rab7 mutants do not modify UUKV infection<sup>37</sup>. Either there is no effect of the dominant negative Rab7 mutant or UUKV does not rely on Rab7-positive late endosomes to reach acidic compartments for fusion. Transmission electron microscopy and confocal microscopy-based studies identified SFTSV in late endosomal compartments and revealed an increase in colocalization with Rab7 in Vero E6 (African green monkey kidney) cells 30 – 60 mpi<sup>70</sup>. Drake and colleagues, however could detect no or only little colocalization between rVSV-SFTSV and Rab7 in A549 (human lung) and U-2 OS (human osteosarcoma) cells 20 mpi and 40 mpi, respectively<sup>76</sup>. Functional studies in Rab7-silenced cells for example remain to be performed to determine the importance of Rab7 in SFTSV infection. The vesicle associated membrane protein 3 (VAMP3) belongs to the family of v-SNARE fusion proteins and is an important host cellular factor required for late penetration of UUKV<sup>80</sup>. 20 minutes

## Introduction

post infection, when viral particles start to colocalize with Rab7-positive late endosomes<sup>37</sup>, colocalization of UUKV and VAMP3 also reaches a maximum<sup>80</sup>. 30 mpi UUKV and VAMP3 can be detected in LAMP1-positive late endosomes or endolysosomes in the nuclear periphery. Silencing of VAMP3 significantly reduces colocalization between UUKV and LAMP1, indicating that VAMP3 aids trafficking to late endosomal and lysosomal compartments. The endogenous function of VAMP3 in relation to its specific function in UUKV infection is further discussed in chapter 7.3.

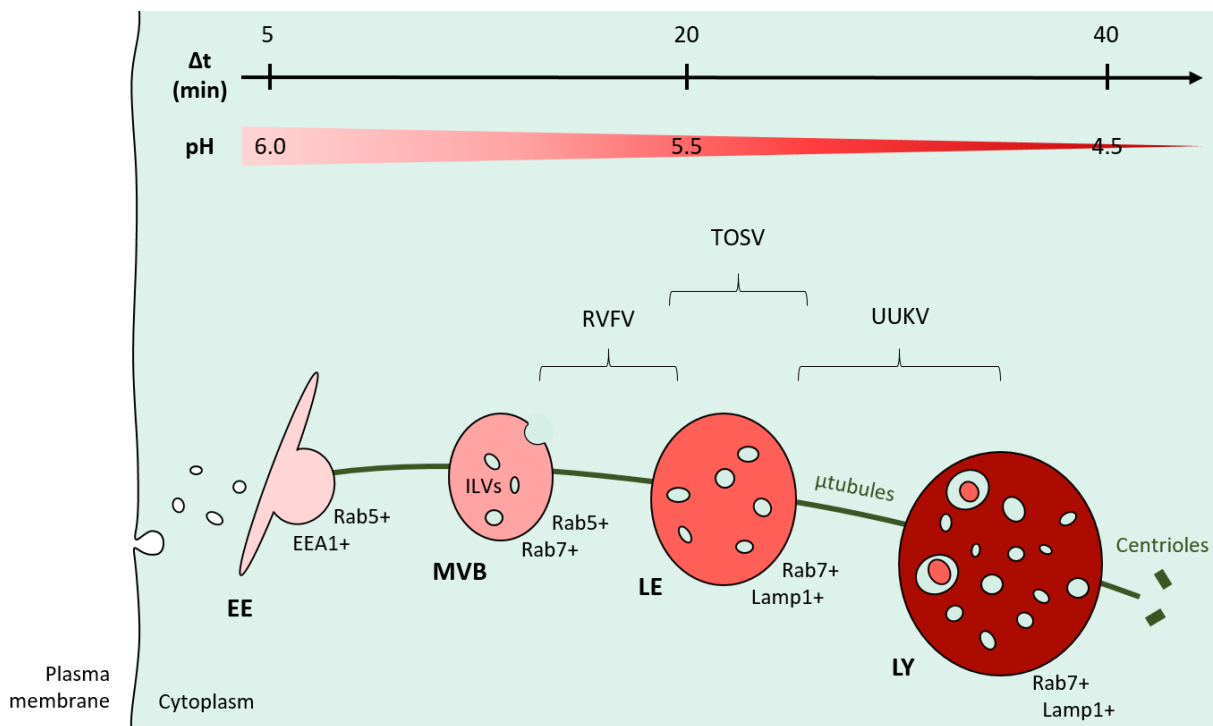


**Figure 4: Phlebovirus intracellular trafficking**

This graph shows vesicles of the endocytic pathway and locations for viral penetration are indicated by brackets. The arrows above indicate the time ( $\Delta t$ ), cargo requires to traffic from the plasma membrane and the pH level of the different endosomes. EE = early endosome, MVB = multivesicular body, LE = late endosome, LY = lysosome, ILVs = intraluminal vesicles,  $\mu$ tubules = microtubules. Adapted from<sup>43</sup>.

### 7.2.5.4 Fusion

The final step of the entry process is the release of the viral genome into the host cytosol by fusion between the viral envelope and the host endosomal membrane. Fusion is driven by the two envelope glycoproteins  $G_N$  and  $G_C$ . For RVFV and UUKV acidification is sufficient to trigger fusion<sup>71,81</sup>. In other cases additional cues, such as receptor interactions or proteolytic cleavage of viral glycoproteins or target membrane lipids, are a prerequisite for fusion<sup>82</sup>.

## Introduction

SFTSV for example is proposed to rely on serine protease-mediated proteolytic cleavage of envelope glycoproteins for fusion<sup>55</sup>. Liposome-based approaches demonstrate that RVFV and UUKV fusion at an acidic pH require the presence of bis(monoacylglycerol)phosphate (BMP) in the target membrane<sup>81,83</sup>. BMP is an anionic lipid exclusively located in the inner membrane of LEs and LYSs<sup>84</sup>. SFTSV late entry steps (during intracellular trafficking or fusion) and HRTV infection rely on the enzymatic activity of glucosylceramide synthase (UGCG)<sup>76</sup>. UGUC initiates *de novo* biosynthesis of glycosphingolipids in the Golgi apparatus by synthesizing glucosylceramide<sup>85</sup>. Interestingly, an accumulation of glucosylceramide enhances SFTSV infection<sup>76</sup>, suggesting that a specific glycolipid composition in the targeted membrane is important for SFTSV infection.

Fusion itself is a process in which a fusion protein inserts a hydrophobic domain into the target membrane to bring the viral envelope and the host membrane lipid bilayers into close proximity. Juxtaposed membranes are fused to allow the viral core to escape into the host cellular cytosol and finally infect the cell. Fusion proteins are assigned, at least, to three structurally different classes (class I, II and III), undergoing analogous functional transitions<sup>82,86,87</sup>. RVFV G<sub>C</sub> (prefusion structure) and SFTSV G<sub>C</sub> (postfusion structure) show a close structural resemblance and exhibit 25 % sequence identity. Both glycoproteins are classified class II fusion proteins, catalyzing virus particle-host membrane fusion<sup>88,89</sup>. G<sub>C</sub> glycoproteins are organized in three domains with a hydrophobic transmembrane domain and a fusion loop. Halldorsson and colleagues resolved the structure of RVFV G<sub>N</sub> and the RVFV G<sub>N</sub>-G<sub>C</sub> heterodimer and proposed the following fusion mechanism<sup>83</sup>. At a neutral pH G<sub>N</sub> & G<sub>C</sub> form heterodimers. In this prefusion state, G<sub>N</sub> shields the fusion loop of G<sub>C</sub>, which is buried within the structure (**Figure 5i**). Low pH is suggested to be perceived by G<sub>C</sub> histidine residues<sup>71,88</sup>. A drop in pH and exposure to the target membrane lead to a conformational change of G<sub>C</sub>, followed by G<sub>N</sub> moving to the side. As a consequence, the hydrophobic fusion loop is exposed, followed by its insertion into the host membrane (**Figure 5ii**). The G<sub>N</sub>-G<sub>C</sub> heterodimers dissociate, allowing redistribution of extended G<sub>C</sub> monomers on the viral membrane (**Figure 5iii**). The juxtaposed membranes fuse and G<sub>C</sub> forms stable postfusion trimers, burying the fusion loop in the just fused lipid bilayer (**Figure 5iv**). This process can be counteracted by host cell proteins. For example, by inserting in endolysosomal membranes, IFITM2 and IFITM3 change the biological properties of the target cell membrane and block RVFV fusion. This is a known innate defense mechanism against viral invasion (**Figure 2B**)<sup>90</sup>.

## Introduction

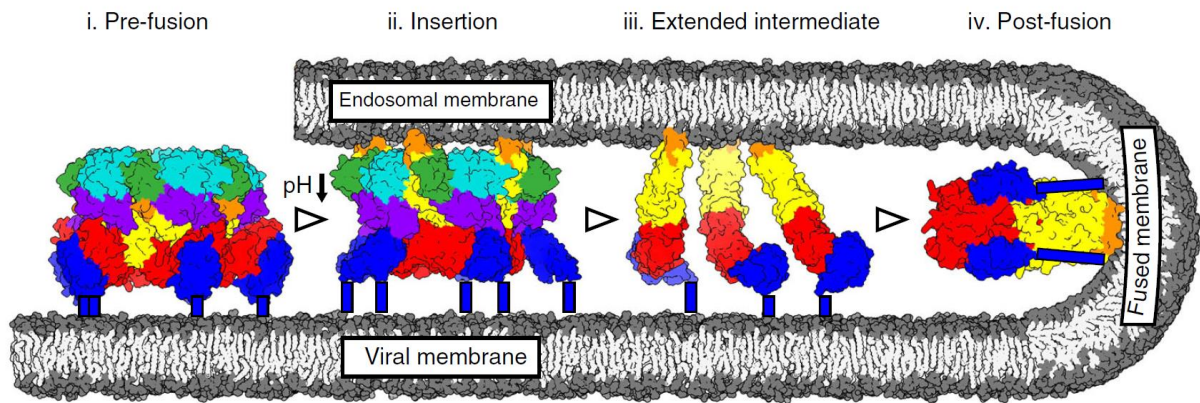


**Figure 5: RSV fusion mechanisms**

Consecutive steps of viral fusion are schematically represented from left to right. i) Pre-fusion complex made up of G<sub>N</sub>-G<sub>C</sub> heterodimers. ii) At a fusion-permissive pH level G<sub>C</sub> changes its conformation and G<sub>N</sub> moves to the side, resulting in the exposure of the fusion loop and its insertion into the host membrane. iii) G<sub>N</sub> dissociates and the extended G<sub>C</sub> redistributes in the viral envelope. iv) The endosomal and viral membrane merge, whereupon G<sub>C</sub> forms postfusion trimers, which embed the fusion loops in the fused membrane. G<sub>C</sub> domain I is colored in red, domain II in yellow, domain III in blue with the transmembrane domain as a blue rectangle and the fusion loops in orange. G<sub>N</sub> domain A is colored in teal, domain B in green and the β-ribbon in purple. The lipid bilayer is represented in grey, with the head group in dark grey and the acyl chains in light grey. Adapted from <sup>83</sup>.

Structural similarities between RSV and SFTSV G<sub>N</sub> and G<sub>C</sub> proteins suggest that the described fusion mechanism might be similar among different viruses in the *Phlebovirus* genus <sup>83,88,89,91</sup>. RSV fusion mechanisms are analogous to those reported for alpha- (*Togaviridae* family) and flaviviruses (*Flaviviridae* family) <sup>92,93</sup>, suggesting a conservation of the fusion mechanisms between these arboviruses. Once the viral core accesses the host cellular cytosol, virus replication begins.

### 7.2.6 From replication to the release of infectious viral particles

Upon fusion, viral RNPs (vRNPs) are released into the cytoplasm for transcription and replication. Due to a lack of capping ability, other *Bunyavirales*, for example the orthobunyavirus La Crosse, were reported to start transcription with a cap-snatching mechanism. In this process 5' caps from host mRNAs are cleaved off by the endonuclease domain of the viral RdRp <sup>94</sup>. The snatched cap is then used as a primer for transcription of viral RNA at the rough endoplasmic reticulum (rER). Transcription, also of RSV and UUKV, is initiated with a prime-and-realign strategy to elongate short snatched primers <sup>95,96</sup>. After priming, incorporation of a few nucleotides, the extended cap mRNA moves backwards and

## Introduction

realigns to the template. This is possible due to terminal repeat sequences. For transcription termination, a hairpin structure, formed by inverted complementary RNA sequences, is supposed to cause dissociation of the viral polymerase in the phlebovirus Punta Toro virus (PTV) <sup>97</sup>. In a transcription-coupled translation mechanism phleboviral proteins are synthesized.

Replication takes place in the cytosol and is driven by vRNPs. The terminally associated RdRp first synthesizes a complementary RNA strand (cRNA), to which newly synthesized N and L proteins attach to form a complementary RNP (cRNP). Accordingly, cRNPs then direct synthesis of progeny vRNPs. The vRNP reproduction process is amplified by using the progeny vRNPs as templates for cRNPs to produce more vRNPs. Viral transmembrane glycoproteins traffic from the rER to the Golgi apparatus whereto vRNPs also move. Together vRNPs and viral glycoproteins assemble to progeny virus particles by budding into the ER-Golgi intermediate compartment (ERGIC) or the Golgi apparatus <sup>98</sup>. As a final step newly produced viral particles are believed to be released through exocytosis of secretory vesicles <sup>13</sup>.

### 7.3 siRNA based screen for UUKV host factors

To identify novel factors involved in UUKV infection and thereby shed light onto the early virus-host cell interactions, a genome-wide siRNA screen was performed in our lab <sup>80</sup>. The human cell line HeLa expressing the UUKV receptor, DC-SIGN, was used in this approach <sup>99</sup>. Those cells were therefore highly susceptible to UUKV infection <sup>59</sup>.

An automated fluorescence microscopy-based approach was chosen to quantify cells with newly synthesized nucleoprotein N to monitor viral replication. Thereby, host cellular factors involved in UUKV entry and replication up to N protein translation could be identified. After screening two independent human genome-wide siRNA libraries (one from Dharmacon and the second from Qiagen), the fusion protein VAMP3 appeared as potential host cellular factor in both siRNA screens. In-depth characterization revealed VAMP3 as an important factor for late penetration of UUKV. VAMP3 mediates sorting endosome fusion with REs and regulates constitutive exocytosis of integrins, transferrin and the transferrin receptor to the plasma membrane <sup>100,101</sup>. VAMP3 also mediates fusion of EEs with the TGN to transport cholera toxin and ricin <sup>102</sup>, or fusion of LEs with the TGN for retrograde transport of the mannose 6-phosphate receptors <sup>103</sup>. VAMP3 also plays a role in the initiation of autophagy <sup>104</sup> and fusion between MVBs and autophagosomes <sup>105</sup>, thereby bridging the endosomal and autophagosomal pathway

## Introduction

<sup>106</sup>. Interestingly, two key autophagy proteins WIPI1 and FIP200 (also termed RB1CC1) were identified as potential host cellular factors <sup>80</sup>. In addition, the small GTPases Rab1b and Rab11a were identified as potential host cellular factors <sup>80</sup>. Besides the role of Rab1b in ER-Golgi trafficking <sup>107</sup> and the role of Rab11a in recycling endosome trafficking <sup>108</sup> both proteins have reported functions in the autophagic pathway <sup>109,110</sup>. Together those data led us to make the hypothesis that the autophagic pathway may play a role in UUKV infection.

### 7.4 Autophagy

#### 7.4.1 Historic cornerstones of autophagy research in short

Christian de Duve, Nobel Prize laureate for lysosome discovery, defined and coined the term autophagy (Ancient Greek, “self-eating”) in 1963. He described autophagy as a process by which a cell self-engulfs portions for lysosomal degradation. During starvation cells can reuse parts of their own substances for “fuel” and “renewal of their own constituents”. A limiting membrane keeps autophagy localized to prevent self-damage <sup>111</sup>. This principle still holds true today. Beyond, numerous additional functions of the autophagy pathway and concise underlying molecular mechanisms have been defined over the intervening years. Two cornerstones to define the autophagy process on a molecular level were the identification of the today termed autophagy-related genes (Atgs), required for autophagy in yeast by the Nobel Prize laureate Yoshinori Ohsumi’s lab <sup>112</sup> and the discovery of two essential linked protein conjugation systems for autophagosome formation by Noboru Mizushima and colleagues <sup>113</sup>.

#### 7.4.2 Functions of autophagy

Autophagy is a basic intracellular process for the degradation of cytoplasmic constituents, mediated by lysosomes. The first discovered function of this catabolic process is to provide nutrients and energy-rich molecules under suboptimal (e.g. starvation) conditions. Beyond, the overall purpose of autophagy is to maintain cellular integrity and metabolic homeostasis – vital cellular processes. To these ends, a variety of selective autophagy pathways exist that remove surplus or potentially harmful intracellular components. Mammalian cells specifically target nonfunctional cellular constituents such as aggregated or misfolded proteins, storage nutrients (glycogen or lipid droplets) and dysfunctional organelles such as peroxisomes, mitochondria or parts of the ER, as well as for example bacterial or viral intruders <sup>114</sup>.

## Introduction

Disturbed autophagy or malfunctioning autophagy related proteins impact human health and are associated with a broad variety of human pathophysiological conditions such as cancer, metabolic disorders, aging, infection, inflammation and neurodegenerative diseases <sup>114</sup>.

### 7.4.3 Autophagy processes in mammalian cells

In mammals, autophagy can be categorized into chaperone-mediated autophagy (CMA), microautophagy, and macroautophagy, according to how substrates are delivered into the lysosomes.

CMA uses chaperones to move cytosolic components, mostly aggregated or unfolded proteins, into the lysosome. The chaperone Hsc70 (a heat shock cognate protein of 70 kDa) recognizes proteins via a CMA-targeting pentapeptide motif (KFERQ). Hsc70 guides its cargo to the lysosome, where it is recognized by the receptor LAMP2A (lysosome associated membrane protein type 2A) and directly translocated across the lysosomal membrane for degradation by lysosomal acid hydrolases (**Figure 6**) <sup>115</sup>. Microautophagy describes the lysosomal uptake of proteins and organelles by invaginations at the sequestering membrane (**Figure 6**) <sup>116</sup>.

During macroautophagy, cargo delivery to the lysosome is mediated by specific transport vesicles, the autophagosomes. A double-membrane is formed within the cytosol (termed phagophore or isolation membrane), engulfing cytoplasmic constituents. Once this membrane is sealed, the newly formed autophagosome fuses with lysosomes to form an autolysosome, resulting in the degradation of the cargo (**Figure 6**). Autophagosome biogenesis as well as autophagosome-lysosome fusion are regulated by Atg proteins and a variety of additional proteins, including small GTPases, SNARE (soluble NSF attachment protein receptor) and VPS (vascular protein sorting). The focus of this study is on macroautophagy, hereafter referred to as autophagy for convenience, and discussed in more detail in the following chapter.

## Introduction

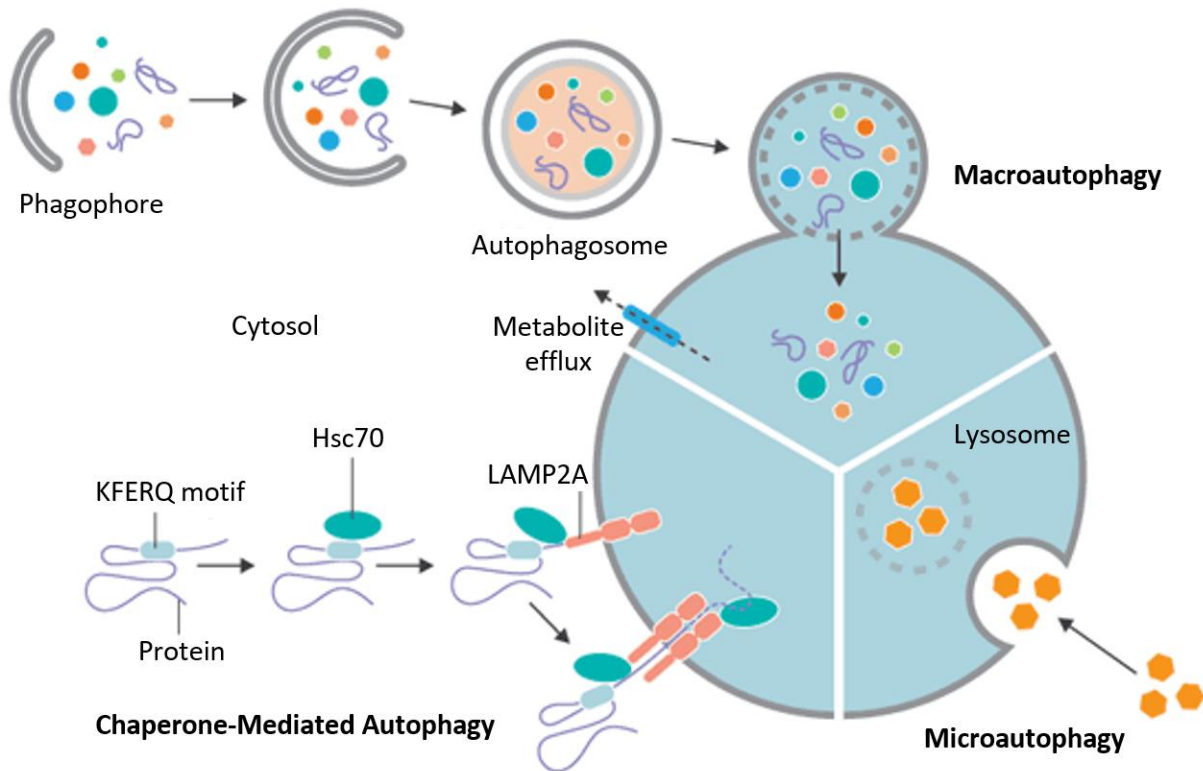


**Figure 6: Autophagy processes in mammalian cells**

Autophagy is an intracellular degradation pathway leading to lysosomal degradation. Macroautophagy involves the formation of a cytosolic double membrane, the phagophore, sequestering surplus or harmful cellular contents. The mature autophagosome is encompassed by the double membrane and fuses with the lysosome for cargo degradation. Chaperone-mediated autophagy describes a process, in which cytosolic proteins are recognized via the peptide motif KFERQ by a heat shock cognate protein of 70 kDa (Hsc70). The lysosomal associated membrane protein type 2A (LAMP2A) recognizes the Hsc70 cargo complex and together with other proteins translocates the cargo into the lysosome for degradation. Microautophagy is a process during which cytosolic content is directly internalized into vesicles from the lysosomal membrane. Adapted from Novus Biologicals (<https://www.novusbio.com/research-areas/autophagy>).

### 7.4.4 The macroautophagy process on a molecular level

#### 7.4.4.1 Regulation of the autophagic pathway

Besides a basal level of autophagy, various stimuli, e.g. starvation, stress or infection can upregulate autophagic activity. The nutrient-sensing kinase MTORC1 (mechanistic target of rapamycin complex 1) and the energy-sensing kinase AMPK (AMP-activated protein kinase) differentially phosphorylate and regulate the most upstream key autophagy regulator, the ULK1 complex<sup>117</sup>. This complex consists of ULK1, Atg13, FIP200 and Atg101. MTORC1 is active when nutrient levels are replenished<sup>118</sup> and inactivates ULK1 by phosphorylation of ULK1 serine 757<sup>117</sup>. This phosphorylation blocks AMPK interaction with ULK1 and thereby prevents

## Introduction

autophagy induction. AMPK becomes active upon ATP-depletion and inhibits MTORC1 by phosphorylation of its subunit RAPTOR<sup>119</sup>. AMPK-mediated phosphorylation of ULK1 serine 317 and serine 777 results in the activation of the ULK1 complex, and induces autophagy<sup>117</sup>.

### 7.4.4.2 Initiation of autophagy

Autophagy initiation involves the translocation of two protein complexes, namely ULK1 (Unc-51 like autophagy activating kinase 1) and PI3KC3-C1 (class III phosphatidylinositol 3-kinase complex 1), to specific sites at the ER. These translocations lead to the production of the lipid phosphatidylinositol-3-phosphate (PI3P), in turn recruiting effectors for phagophore formation.

ULK1 is mostly cytosolic and can form a heterotetrameric complex with Atg13 and FIP200, that increase the kinase activity and stabilize ULK1; and Atg101, promoting stabilization of ULK1 and Atg13<sup>118,120</sup> (**Figure 7**). Upon autophagy induction, the ULK1 complex is suggested to translocate to ER-mitochondria contact sites and Atg9-containing autophagy-specific ER exit sites, termed omegasomes<sup>121,122</sup>. The ULK1 complex remains anchored to the omegasome until the phagophore is formed and growing, and is then recycled to the cytoplasm<sup>123</sup>.

Phagophore formation is initiated by PI3KC3-C1, comprising the catalytic subunit VPS34, VPS15 (or p150), Beclin 1 and Atg14L (**Figure 7**). Under basal autophagy conditions, BECN1 was found to tether PI3KC3-C1 to microtubules by AMBRA1-mediated binding. Starvation disrupts microtubule association<sup>124</sup> and PI3KC3-C1 is recruited to phagophore initiation sites where ULK1 phosphorylates PI3KC3-C1 and activates VPS34 kinase activity<sup>125</sup>. The membrane lipid phosphatidylinositol (PI) is then phosphorylated by the activated VPS34 to generate PI3P. The charged signaling lipid PI3P recruits proteins that exhibit specific motifs, for example FYVE or F/LRRG. The four mammalian WIPI proteins are important PI3P binding proteins, that monitor phagophore formation and growth<sup>126–128</sup>. Puri and colleagues report that PI3P requires an additional protein, the small GTPase Rab11a, to specifically recruit WIPI2 to the phagophore formation site<sup>129</sup>. In contrast to the current belief, that autophagy is initiated at the ER, the importance of the RE marker Rab11a suggests that REs serve as a platform for phagophore formation<sup>129</sup> (for more details on Rab11a see chapter 7.5.2).

## Introduction

### 7.4.4.3 Phagophore elongation

Two ubiquitin-like conjugate systems, Atg12-Atg5-Atg16L1 and LC3-II are required for elongation of the phagophore and closure to form the autophagosome.

In the first step of the ubiquitin-like conjugation process, Atg7 activates Atg12 (E1 step) followed by transfer to the conjugation enzyme Atg10 (E2 step). Atg12 is then conjugated to the substrate Atg5, subsequently forming a complex with Atg16L1. WIPI1 and WIPI2 are important to recruit the Atg12-Atg5-Atg16L1 complex to the omegasome and Atg12-Atg5-Atg16L1 in turn recruits the second ubiquitin-like conjugate protein LC3 (microtubule-associated proteins 1A/1B light chain 3). The C-terminal part of the cytosolic LC3 is cleaved by the cysteine protease Atg4. This processed LC3 is called LC3-I. LC3-I is then activated by Atg7 (E1 step) and subsequently transferred to Atg3 (E2 step). Finally, the Atg12-Atg5-Atg16L1 complex mediates LC3-I lipidation by conjugation to the membranous phosphatidylethanolamine (PE) via the exposed glycine (E3 step)<sup>130</sup>. LC3-PE, most commonly called LC3-II is anchored to the inner and outer autophagosome membrane and thereby represents a robust marker for autophagosomes and autophagy. The characteristic conversion of LC3-I to LC3-II can be used to monitor autophagic flux by immunoblotting. Recruitment of fluorescently labeled LC3 from the cytosol to the autophagosome upon lipidation and the concomitant redistribution from a diffuse cytosolic distribution to the formation of punctate structures corresponding to autophagosomes, is frequently used to visualize autophagosome formation under a fluorescence microscope<sup>131</sup>.

Functionally, LC3-II is an important receptor for substrate recruitment to the extending phagophore. Recruitment to the inner phagophore membrane results in cargo uptake into the autophagosome. Anchor proteins, such as p62 or NBR1, bind ubiquitinated proteins and move these to the phagophore by binding LC3-II with their LC3-interacting region (LIR)<sup>132,133</sup>. LIR-dependent recruitment of NDP52 to the outer membrane is suggested to regulate transport of autophagosomes along actin filaments by NDP52-myosin VI interactions<sup>134</sup>. LC3-II also regulates autophagosome-lysosome fusion, by recruiting PLEKHM1<sup>135</sup> (see chapter 7.4.4.4). Upon fusion with the lysosome LC3-II is cleaved off the outer membrane by Atg4 and degraded by lysosomal enzymes on the inner leaflet<sup>131</sup>.

The source of membrane for phagophore elongation is still under debate. Various cellular organelles, including ER, ERGIC, Golgi apparatus, mitochondria as well as the plasma membrane are suggested to contribute membrane to the phagophore<sup>136-140</sup>. Atg9, a transmembrane protein, is believed to deliver membrane parts or phospholipids from different

## Introduction

donor sources to the phagophore. The small GTPase Rab1b is present on these Atg9 positive vesicles and regulates autophagosome formation <sup>141</sup> (for more details on Rab1b see chapter 7.5.1). At a basal autophagy level, Atg9 is located in the Golgi apparatus. Upon autophagy induction, Atg9 disperses into different compartments. During transient interaction with the phagophore, Atg9 is suggested to deliver membrane components to the forming phagophore <sup>142</sup>. Atg2 is required to complete phagophore closure, to eventually form the autophagosome <sup>143</sup>.

### **7.4.4.4 Autophagosome-lysosome fusion**

Fusion between the autophagosome and lysosome (yielding autolysosomes), is mediated by PI3KC3 complex 2 (PI3KC3-C2). Similar to PI3KC3-C1, PI3KC3-C2 comprises the catalytic subunit VPS34, VPS15 and Beclin 1. In a mutually exclusive manner either Atg14L or UVRAG (UV-radiation resistance-associated gene protein) can bind, defining complex 1 and 2 respectively <sup>144</sup>.

The adaptor protein termed pleckstrin homology domain-containing protein family member 1 (PLEKHM1) is a Rab7 effector. PLEKHM1 simultaneously binds Rab7 and LC3-II and thereby bridges autophagic and lysosomal membranes <sup>135</sup>. PLEKHM1 additionally recruits the tethering complex HOPS (homotypic fusion and protein sorting) <sup>135</sup>. HOPS interacts with the SNARE fusion protein syntaxin 17 that mediates autophagosome-lysosome fusion <sup>145</sup>. Syntaxin 17 only binds to the outer membrane of completed autophagosomes but not to the phagophore, therefore lysosomes only fuse with completed autophagosomes <sup>146</sup>. Finally, the cargo is degraded by lysosomal acid hydrolases.

## Introduction

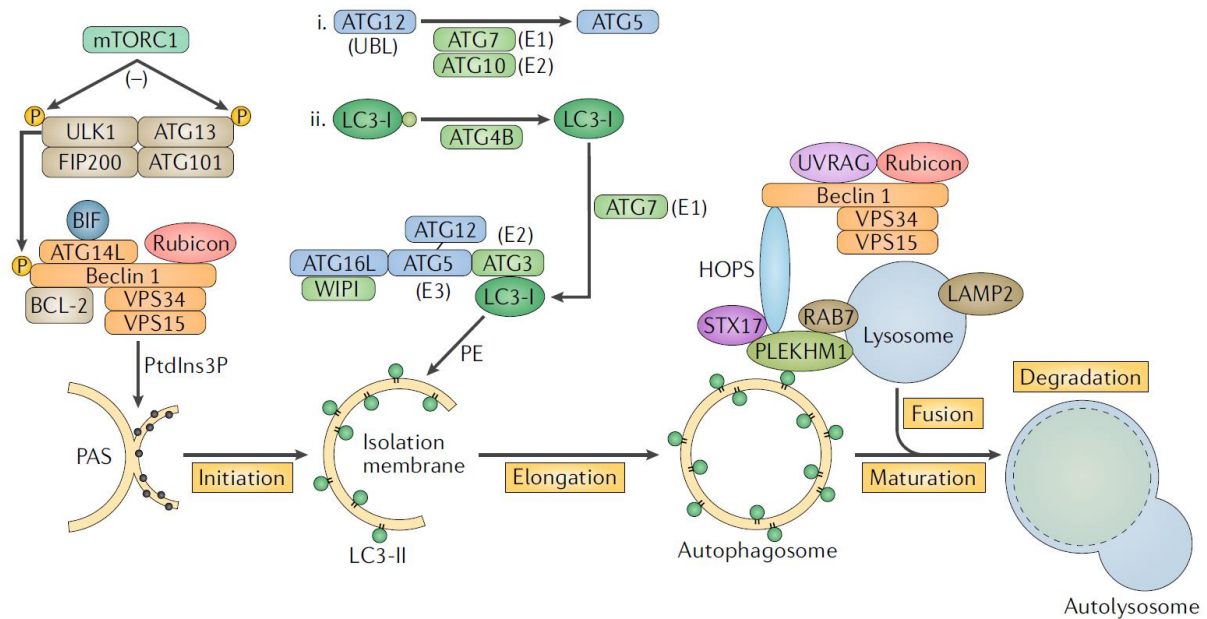


**Figure 7: Molecular basis for mammalian macroautophagy**

In the first step the ULK1 complex (comprising ULK1, Atg13, FIP200, Atg101) is translocated to the phagophore initiation site, where it activates the class III phosphatidylinositol 3-kinase complex 1 (PI3KC3-C1) (comprising VPS34, Beclin 1, VPS15, Atg14) by phosphorylation. The activated protein kinase VPS34 produces phosphatidylinositol-3-monophosphate (PI3P). WIPI1 and WIPI2 have a PI3P as well as an Atg16L binding domain and mediates binding of the Atg12-Atg5-Atg16L conjugate to the phagophore initiation site. The Atg12-Atg5-Atg16L complex enables LC3 conjugation to phosphatidylethanolamine (PE) in the phagophore membrane. LC3-PE is a receptor for autophagy substrates. PLEKHM1 binds Atg7 as well as LC3 and bridges the lysosome and the autophagosome. The subsequent autophagosome-lysosome fusion is mediated by the tethering complex HOPS, bound to PI3KC3-C2 (comprising VPS34, Beclin 1, VPS15, UVRAG), that recruits SNARE fusion proteins. PAS = preautophagosomal structure. Adapted from <sup>147</sup>.

### 7.4.5 Autophagy in viral infection

Autophagy can participate in defending host cells from pathogen invasions. Xenophagy, a selective form of autophagy, specifically recognizes and targets intracellular microorganisms for degradation to autophagosomes <sup>148</sup>. An innate immune response is initiated by autophagy after infection through activation of pattern recognition receptors (PRRs), inducing interferon production and secretion <sup>149</sup>. Pathogen degradation within the autophagosome initiates an adaptive immune response in which viral antigens are delivered onto major histocompatibility complex I or II (MHC I/II) for presentation to T lymphocytes <sup>149</sup>. Through ongoing evolutionary competition, however, viruses have evolved to circumvent the autophagy-mediated immune response and elimination, for instance by blocking key components of the autophagic pathway <sup>147</sup>. Several viruses even hijack and utilize autophagy for their own benefit, such as genome

## Introduction

replication or exocytosis of viral particles <sup>147</sup>. A wide variety of distinct virus-autophagy interactions have been described, and were recently reviewed by <sup>147,150–154</sup>. The following subchapters briefly describe the various virus-autophagy interactions, including those identified for the phleboviruses RVFV and SFTSV.

### 7.4.5.1 Autophagy as an antiviral defense mechanism

Autophagy plays an important role in mounting an innate immune response. An innate immune response is mediated by PRRs, including Toll-like receptors (TLRs), specifically recognizing pathogen-associated molecular patterns (PAMPs), resulting in induction of an antiviral interferon response. TLR7- as well as TLR9-induced interferon production in response to infection by Vesicular stomatitis Indiana virus (VSV) and herpes simplex virus type 1 (HSV-1) respectively, relies on the key autophagy protein Atg5 <sup>155,156</sup>. Moreover, TLR adapter proteins MYD88 and TRIF bind to Beclin1 to disrupt its inhibition by B cell lymphoma-2 (BCL-2) and ultimately induce autophagy (**Figure 7**). In turn autophagy can selectively degrade TRIF to inhibit TLR signaling <sup>157</sup>. The phlebovirus RVFV is suggested to induce a TLR-mediated antiviral autophagy response <sup>158</sup>. Autophagy is also suggested to have an antiviral function against SFTSV infection <sup>159</sup>.

Xenophagy, targets intracellular pathogens, such as bacteria and viruses, to the autophagosome for degradation. Some PRRs are xenophagy signaling receptors, e.g. p62, NBR1, NDP52 and optineurin and expose a cargo recognition domain (CRD) for specific recognition of pathogens, and an LC3-interacting region (LIR) for recruitment to the autophagosome. NDB52 for example possesses a CRD that specifically binds  $\beta$ -galactoside glycans, cytoplasmically exposed on pathogen-damaged endosomes, and thereby targets these endosomes to lysosomes for content degradation <sup>160</sup>. Picornaviruses for example are recognized upon  $\beta$ -galactoside exposure but as a countermeasure recruit a host protein to block this detection and prevent autophagic degradation <sup>161</sup>.

LC3-associated phagocytosis (LAP) is a recently discovered selective autophagy pathway that acts independently on autophagosomes. In LAP, LC3 is conjugated to newly formed, pathogen containing phagosomes. Phagosome-lysosome fusion results in the formation of a phagolysosome inside which pathogens are degraded <sup>162</sup>.

Autophagy is also involved in generating an adaptive immune response. Adaptive immunity involves antigen presentation on MHC complexes to T lymphocytes. Autophagy mediates

## Introduction

processing of viral antigens as well as antigen delivery to MHC-I and MHC-II complexes<sup>147</sup>. In addition, fusion between autophagosomes and MHC-II-containing vesicles results in the presentation of engulfed cytoplasmic proteins by MHC-II to CD4<sup>+</sup> T cells<sup>163</sup>.

### 7.4.5.2 Evasion of the autophagy-mediated antiviral response

To evade autophagy-mediated immune response and degradation, different viruses have the ability to block key autophagy proteins. HSV-1 and human cytomegalovirus (hCMV) express Beclin 1-blocking proteins to inhibit autophagy<sup>164,165</sup>. Kaposi's sarcoma-associated herpesvirus (KSHV) prevents LC3 processing by inhibiting binding to Atg3<sup>166</sup>.

### 7.4.5.3 Viruses exploit autophagy for their own benefit

Multiple studies demonstrate that viruses utilize the autophagic machinery, parts of it, or single autophagy-related proteins for their benefit. Viral-autophagy modifications are diverse and happen during different steps of virus life cycles, from internalization to particle release.

Ebola virus (EBOV, *Filoviridae*) particles are known to be internalized by macropinocytosis<sup>167</sup>. A recent study demonstrates that EBOV internalization depends on the autophagic proteins Beclin 1, Atg7 and LC3 due to LC3-II requirement for macropinosome biogenesis<sup>168</sup>.

Cellular entry of the two enveloped viruses Varicella zoster virus (VZV, *Herpesviridae*) and Influenza A virus (IAV, *Orthomyxoviridae*) highly depends on UVRAG. Besides its crucial role in autophagosome elongation, UVRAG is important for late endocytic transport. Infection prevents UVRAG-mediated late endosome fusion with the lysosome. VZV and IAV thereby evade lysosomal degradation<sup>169</sup>.

Various viruses utilize autophagosomes for replication purposes, e.g. members of the *Picornaviridae*, *Coronaviridae* and *Flaviviridae* families. Cytosolic double membrane vesicles provide a scaffold for the viral replication machinery and prevent detection of viral RNAs by innate immune sensors as well as degradation<sup>147</sup>. The mosquito-borne dengue virus (DENV, *Flaviviridae*), for example, induces autophagy during infection<sup>170</sup>. Silencing the key autophagy protein Atg5 impairs viral replication, indicating a proviral effect of autophagy on DENV infection<sup>170</sup>. DENV nonstructural proteins and double-stranded RNA localize to LC3-labeled vesicles, thus autophagic membranes are suggested to serve as a platform for DENV replication<sup>171</sup>. Localization of the ribosomal protein L28 to dsRNA additionally points towards a

## Introduction

translational capacity<sup>171</sup>. Lipophagy, a selective autophagic process for degradation of lipid droplets is also utilized to promote viral replication. DENV-promoted catabolism of lipid droplets provides free fatty acids and generates ATP (by  $\beta$ -oxidation) for viral replication<sup>172,173</sup>.

In addition to using autophagic membranes for replication, members of the *Herpesviridae*, *Picornaviridae* and *Flaviviridae* families can subvert the autophagic machinery for particle exocytosis<sup>147</sup>. VZV (*Herpesviridae*), an enveloped dsDNA virus for example, is released from cells in single membraned LC3-II and Rab11a-positive vesicles. Fusion with the plasma membrane releases VZV particles from the cell<sup>174</sup>.

### 7.5 Rab GTPases: Regulators of cellular trafficking

Membrane trafficking between multiple organelles of the eukaryotic cell is crucial for its existence. Rab GTPases, a family of small GTPases, ensure cargo delivery to the proper destination by defining membrane identity and controlling vesicle transport, including coat recruitment and uncoating, motility, fission, target selection and fusion. Humans express more than 60 different Rab proteins<sup>175</sup>.

Intrinsically soluble Rab proteins can only be anchored to a specific membrane upon prenylation by a Rab geranylgeranyl transferase (RabGGTase) (**Figure 8.1**). Within the target membrane, Rab proteins are then activated by guanine-nucleotide exchange factors (GEFs). The concomitant exchange of guanosine diphosphate (GDP) for guanosine triphosphate (GTP) enables binding of the active Rab proteins to effector proteins mediating downstream functions (**Figure 8.2 & Figure 8.3**). Finally, GTPase-activating proteins (GAPs) enhance the Rab protein's intrinsic GTPase activity to hydrolyze GTP to GDP and terminate its function. Guanine-nucleotide-dissociation inhibitors (GDIs) recognize and extract GDP-associated Rab proteins from the membrane by shielding the hydrophobic geranylgeranyl group (**Figure 8.4**). Solubilized Rab proteins constitute a cytoplasmic pool for redelivery to another target membrane<sup>176</sup>. Rab proteins are reversibly attached to vesicles of the endocytic and exocytic pathway. Activated Rab GTPases regulate membrane trafficking by interaction with multiple effectors, including sorting adaptors, motor linkers, tethering complexes, fusion linkers, protein kinases and phosphatases, Rab regulators and more<sup>175</sup>. Here, the specific functions of Rab1b and Rab11a are described in more detail, because these two small GTPases are host factors identified in siRNA screens as candidates with a role in UUKV infection<sup>80</sup>.

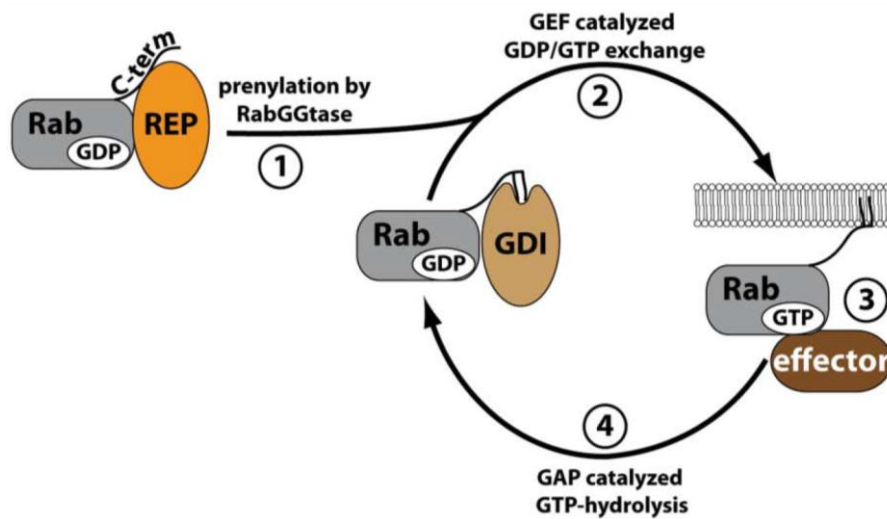


**Figure 8: Rab GTPases as molecular switches**

Rab proteins switch between an active GTP-bound and an inactive GDP-bearing state. **1)** Intrinsically soluble Rab proteins attach to a Rab escort protein (REP) to be prenylated by the Rab geranylgeranyl transferase (RabGGTase). **2)** The prenylated protein is anchored to the membrane, where guanine-nucleotide exchange factors (GEFs) activate Rab by replacing guanosine diphosphate (GDP) for guanosine triphosphate (GTP). **3)** Activated GTP-bearing Rab interacts with effectors to regulate membrane trafficking. **4)** The intrinsic Rab GTPase activity is enhanced by GTPase-activating proteins (GAPs), resulting in GTP hydrolysis to GDP, to discontinue its function. GDP associated Rab proteins are recognized and dissociated from the membrane by guanine-nucleotide-dissociation inhibitors (GDIs). Adapted from <sup>176</sup>.

### 7.5.1 Rab1b

Rab1b is predominantly present in ER and Golgi apparatus membranes and regulates vesicle trafficking between those two organelles. ER to Golgi transport is an important step for the export of secretory and plasma membrane proteins for example and is mediated inside coat protein complex (COP)-coated vesicles. Upon activation, Rab1b regulates anterograde transport of COPII-coated vesicles from ER exit sites (ERES) to the ERGIC <sup>107</sup>. The exchange of COPII for COPI is suggested to be as well regulated by Rab1b <sup>177</sup>. Rab1b indirectly activates the COPI-recruiting GTPase Arf1 by activating the Arf1-GEF Golgi-specific brefeldin A resistance factor 1 (GBF1) <sup>178–180</sup>. COPI vesicles allow anterograde transport to the Golgi as well as retrograde transport back to the ER <sup>181</sup>.

A more recently identified function of Rab1b is related to autophagosome formation. Reduced Rab1b expression compromises autophagosome formation, indicating that Rab1b is important for initial steps of autophagy. In line with these results Kakuta and colleagues report that Rab1b

## Introduction

GTPases are associated to Atg9 positive vesicles, a transmembrane protein controlling early steps of autophagosome biogenesis<sup>141</sup>. While inhibition of Sar1, a small GTPase crucial for COPII vesicle formation, blocks autophagosome formation, inhibition of Arf1, a small GTPase crucial for COPI vesicle formation, has no effect. These results indicate that early but not late steps of the secretory pathway are required for autophagy<sup>109</sup>.

### 7.5.2 Rab11

The small GTPase Rab11 subfamily comprises three isoforms: Rab11a, Rab11b and Rab25 (also referred to as Rab11c) among which Rab11a is by far the best studied. Rab11a is ubiquitously expressed in a variety of different tissues ranging from brain, lung, heart, liver, kidney and spleen to the gastrointestinal tract<sup>182</sup>. In contrast to Rab11a, Rab11b expression is restricted to the brain, heart and testes<sup>183</sup> and Rab25 is abundant in the gastric tract, kidney and lung<sup>184</sup>.

All three isoforms reside in the recycling endosome (RE), and Rab11a also in the trans-Golgi network (TGN) (**Figure 9**)<sup>185–187</sup>. Two different cellular exocytic routes are associated with these two organelles. The secretory pathway transports newly synthesized proteins from the ER via the Golgi apparatus to the plasma membrane. The recycling pathway moves internalized cargo via recycling endosomes back to the cell surface<sup>188</sup>. Indeed, the three isoforms of Rab11 control trafficking through recycling endosomes<sup>185–187</sup>. Similar functions for Rab11a and Rab11b were reported in the recycling of the transferrin receptor from the RE to the plasma membrane<sup>185,186,189</sup>. Both proteins interact with the exocyst complex to fuse REs with the plasma membrane (**Figure 9**)<sup>190</sup>. But also selective regulation of specific recycling pathways for all three Rab11 isoforms<sup>187,191</sup> and localization to distinct vesicular compartments were reported<sup>192</sup>.

Cellular uptake or a fast recycling from early EEs does not depend on Rab11a. Early (fast) recycling is regulated by Rab4<sup>193</sup>, while Rab11a regulates recycling from LEs (slow) via the RE to the cell membrane<sup>194</sup>. Besides its function in the RE, Rab11a also controls constitutive and regulated secretory pathways from the TGN to the plasma membrane (**Figure 9**)<sup>195,196</sup>. Rab11a moves vesicles primarily along microtubules by interactions with kinesin motor proteins, but also along actin filaments by interaction with myosin V<sup>197,198</sup>. In addition, Rab11a decorates MVBs in human K562 erythroleukemia cells and mediates homotypic MVB-MVB

## Introduction

fusion<sup>199</sup> and autophagosome-MVB fusion, resulting in the formation of amphisomes (**Figure 9**)<sup>200</sup>.

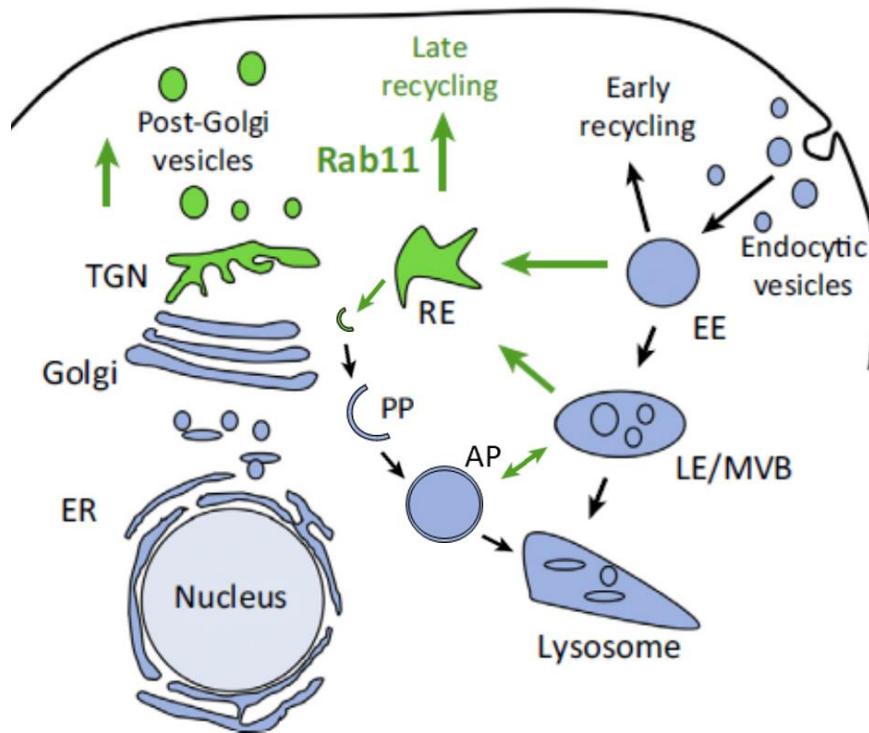


**Figure 9: Rab11-regulated processes**

The small GTPase Rab11 is present on recycling endosomes (REs), the trans-Golgi network (TGN) and multivesicular bodies (MVBs) to regulate endosomal recycling, secretion, phagophore (PP) formation and amphisome formation. AP = autophagosome, EE = early endosome, ER = endoplasmic reticulum, LE = late endosome. Adapted from<sup>108</sup>.

Other research groups showed that Rab11a- & Rab11b-dependent vesicle transport from REs contributes to autophagosome formation and delivers key autophagy proteins, including ULK1 and Atg16L1<sup>110,201</sup>. In line with these results and in addition to the current belief that autophagosomes are derived from the ER, Puri and colleagues propose an emergence from Rab11a-positive REs<sup>129</sup> (**Figure 9**). Rab11a-positive membranes serve as a platform for phagophore formation. Simultaneous recognition of PI3P and Rab11a allows WIPI2 recruitment. In turn, WIPI2 binds Atg16L1, thereby giving rise to the site of autophagosome formation (**Figure 10**).

## Introduction

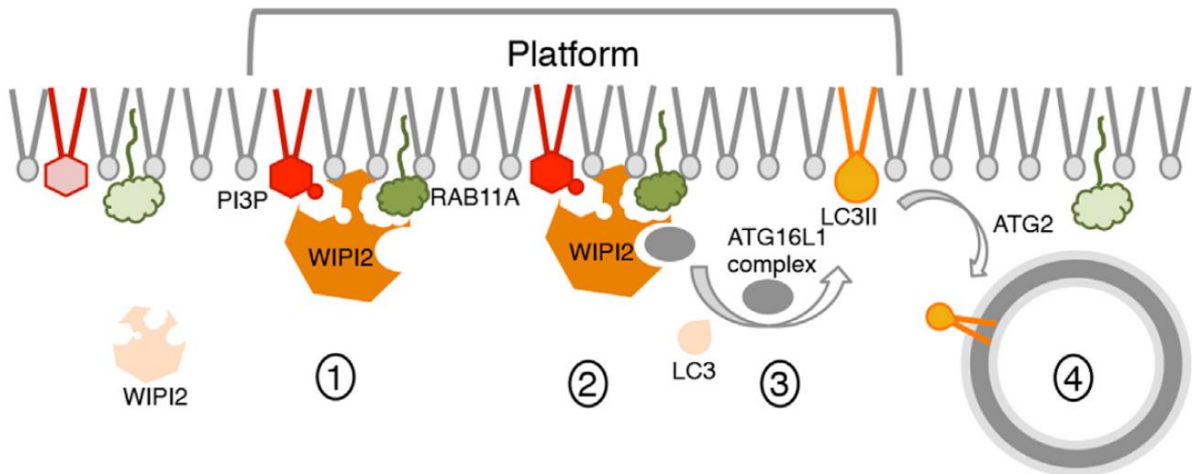


**Figure 10: Rab11a positive membrane as a compartment for phagophore formation**

1) PI3P and Rab11a-positive membranes may constitute a platform for autophagosome formation by recruiting WIPI2. 2) WIPI2 in turn would recruit Atg16L1. 3) Atg16L1 would then form a complex with two other autophagy-related proteins. The Atg16L1 complex is an E3-like enzyme, catalyzing LC3 lipidation (LC3-II formation). 4) The autophagosome marker LC3-II recruits cargo and elongates the phagophore. Atg2, present in the vicinity of the phagophore formation platform, completes autophagosome closure. Adapted from <sup>129</sup>.

## 7.6 Relationship between autophagy and endocytosis

In short, autophagy describes a process for lysosomal degradation of intracellular components. Cytoplasmic constituents are engulfed in a double membrane, termed autophagosome and fusing with the lysosome to form the autolysosome. During endocytosis, extracellular components are internalized at the plasma membrane and trafficked through early endosomes to late endosomes and finally fuse with the lysosome (**Figure 9**).

Both pathways intersect already at their very initial stage, i.e. the cellular plasma membrane serves as membrane donor for endosomes and autophagosomes (note: further membrane sources are involved in autophagosome formation. See chapter 7.4.4.3). Clathrin- and dynamin-dependent formation of Atg16L1 positive vesicles at the plasma membrane is involved in phagophore formation <sup>137</sup>. Clathrin-mediated endocytosis presents also a possible means to deliver membrane and content to EEs <sup>75</sup>.

Autophagy and endocytosis directly intersect by fusion of autophagosomes with endosomes, termed amphisome formation. Autophagosome-MVB fusion is proposed to be regulated by Rab11a (**Figure 9**) <sup>200</sup> and VAMP3 <sup>105</sup>. For maturation, autophagosomes acquire LAMPs and

## Introduction

vATPases. These proteins are also found on MVBs, LEs and LYs, indicating that both maturation processes are accompanied by acidification. Both pathways involve Rab7, a protein for LE maturation and autophagosome-lysosome fusion<sup>75,147</sup>. Accumulating evidences support the idea that autolysosome formation relies on a functional endocytic pathway because disruption of early endosome trafficking or MVB formation leads to an accumulation of autophagosomes and amphisomes<sup>202,203</sup>.

### 8 Objectives of the study

The aim of my PhD project is to investigate early phlebovirus-host cell interactions. Genome-wide siRNA screens previously performed in our lab <sup>80</sup> identified VAMP3 as a host cellular factor critical for UUKV late penetration into HeLa cells. VAMP3 is a SNARE protein present in recycling endosomes and involved in exocytic processes and autophagy <sup>100,101,104,105</sup>. In addition to VAMP3 a number of other autophagy-related proteins appeared as potential host factors in the siRNA screens, namely WIPI1, FIP200, Rab1b, and Rab11a. This led to **our hypothesis that autophagy plays a role in the early steps of UUKV infection.**

The knowledge on the interplay between phleboviruses and autophagy is very limited. Individual studies on RVFV and SFTSV propose an antiviral role of autophagy in infection <sup>158,159</sup>. To date no study is published, describing the role of autophagy in UUKV infection. To test our working hypothesis and whether UUKV relies on the autophagic pathway for infection, I examined the role of several autophagy-related proteins as well as that of autophagosome maturation in UUKV infection.

## 9 Materials and Methods

### 9.1 Materials

#### 9.1.1 Devices and Instruments

Device / Instrument	Provider
Bacteria centrifuge Avanti J-20 XP	Beckman Coulter, Brea, USA
Bacteria incubator	Memmert, Schwabach, Germany
Bacteria shaker Multitron Pro	Infors, Bottmingen, Switzerland
Blotting system (iBlot gel transfer device)	Invitrogen, Thermo Fisher Scientific, Carlsbad, USA
Cell culture centrifuge Megafuge 40R	Thermo Fisher Scientific, Waltham, USA
Cell culture incubator C200	Labotect, Göttingen, Germany
Cell culture wide field microscope	Hund, Wetzlar, Germany
Flow cytometer BD FACSCalibur	BD Bioscience, Franklin Lakes, USA
Flow cytometer BD FACSCelesta	BD Bioscience, Franklin Lakes, USA
Flow cytometer BD FACSVers	BD Bioscience, Franklin Lakes, USA
Fluorescence plate reader, Typhoon Trio, variable mode imager	GE Healthcare, Chicago, USA
Freezer -80°C	Thermo Fisher Scientific, Waltham, USA
Fridge 4°C	Liebherr, Kirschdorf, Germany
Laboratory centrifuge 5430R	Eppendorf, Hamburg, Germany
Leica SP5 laser confocal scanning microscope	Leica Microsystems, Wetzlar, Germany
Leica SP8 laser confocal scanning microscope	Leica Microsystems, Wetzlar, Germany
Licor Odyssey CLx	Licor, Lincoln, USA
Malassez counting chamber	Brand, Wertheim, Germany
Nanophotometer NP80 Touch	Implen, Munich, Germany
pH-meter FiveEasy	Mettler-Toledo, Columbus, USA
Precision scale EW220-3NM	Kern, Balingen, Germany
Rocker Polymax 1040	Heidolph, Schwabach, Germany
Rotor SW 32 Ti	Beckman Coulter, Brea, USA
Rotor SW 60 Ti	Beckman Coulter, Brea, USA
Scale 650-2NM	Kern, Balingen, Germany

## Materials and Methods

SDS-PAGE chamber (Novex Mini-Cell)	Invitrogen, Thermo Fisher Scientific, Carlsbad, USA
Ultracentrifuge L8-60M	Beckman Coulter, Brea, USA
Water bath	GFL, Burgwede, Germany

### 9.1.2 Consumables

Consumable	Provider
12 mm round cover glasses	Marienfeld, Lauda-Königshofen, Germany
24 well plate, flat bottom, Cellstar	Greiner bio-one, Frickenhausen, Germany
6 well plate, flat bottom, Cellstar	Greiner bio-one, Frickenhausen, Germany
96 well plate, U-bottom, Cellstar	Greiner bio-one, Frickenhausen, Germany
Cell culture flask T125 (Cell Star, Ref. 660160)	Greiner bio-one, Frickenhausen, Germany
Cell culture flask T25 (Cellstar, Ref. 690160)	Greiner bio-one, Frickenhausen, Germany
Cell culture flask T75 (Cellstar, Ref. 658170)	Greiner bio-one, Frickenhausen, Germany
Centrifuge tubes, open top, polyclear SW32	Seton, Petaluma, USA
Centrifuge tubes, open top, polyclear SW60	Seton, Petaluma, USA
Cryotube, 2 mL	Greiner bio-one, Frickenhausen, Germany
Microscopy slides	Marienfeld, Lauda-Königshofen, Germany
Needle, 0.4 x 19 mm	BD Bioscience, Franklin Lakes, USA
Precast Protein gels, 10 % Bis-Tris, NuPAGE	Thermo Fisher Scientific, Waltham, USA
Sterile filter 0.22 $\mu$ M, bottle top filter	Merck, Darmstadt, Germany
Sterile filter 0.22 $\mu$ M, Luer Lock for syringe	Whatman, Maidstone, United Kingdom
Sterile filter 0.45 $\mu$ M, Luer Lock for syringe	Whatman, Maidstone, United Kingdom
Syringe, Luer Lock, 3 mL	BD Bioscience, Franklin Lakes, USA
Transfer stack, PVDF (iBlot)	Invitrogen, Thermo Fisher Scientific, Carlsbad, USA

## Materials and Methods

### 9.1.3 Commercial kits

Kit	Provider
CalPhos Mammalian Transfection Kit (Ref. 631312)	Clontech Laboratories, Mountain View, USA
DAB Peroxidase Substrate Kit	Vector Laboratories, Burlingame, USA
DNA Plasmid Plus Midi Kit	Qiagen, Hilden, Germany

### 9.1.4 Chemicals and Reagents

Chemical / Reagent	Provider
Acetic acid	Merck, Darmstadt, Germany
Agarose (for LB agar plates)	Carl Roth, Karlsruhe, Germany
Albumin Fraction V, powder (BSA)	Carl Roth, Karlsruhe, Germany
Alexa Fluor 488 NHS Ester (succinimidyl ester)	Thermo Fisher Scientific, Waltham, USA
Alexa Fluor 568 NHS Ester (succinimidyl ester)	Thermo Fisher Scientific, Waltham, USA
Alexa Fluor 647 NHS Ester (succinimidyl ester)	Thermo Fisher Scientific, Waltham, USA
Ammonium chloride (NH <sub>4</sub> Cl)	Sigma-Aldrich, St. Louis, USA
Ampicillin	Carl Roth, Karlsruhe, Germany
Bafilomycin A <sub>1</sub>	Sigma-Aldrich, St. Louis, USA
Blasticidin	Invivogen, San Diego, USA
Bovine Albumin Fraction V (7.5 % solution) (BSA)	Thermo Fisher Scientific, Waltham, USA
Calcium chloride (CaCl <sub>2</sub> )	Sigma-Aldrich, St. Louis, USA
Carboxymethyl cellulose (CMC)	Sigma-Aldrich, St. Louis, USA
Citric acid monohydrate	Sigma-Aldrich, St. Louis, USA
Coomassie brilliant blue G-250	Thermo Fisher Scientific, Waltham, USA
Crystal violet	Sigma-Aldrich, St. Louis, USA
D(+)-Saccharose	Carl Roth, Karlsruhe, Germany
Dimethyl sulfoxide (DMSO)	Merck Millipore, Burlington, USA
Enhanced chemoluminescent substrate (ECL), SuperSignal West Pico	Thermo Scientific, Schwerte, Germany

## Materials and Methods

Ethanol	Merck, Darmstadt, Germany
Ethylenediaminetetraacetic acid (EDTA) 0.5 M pH8	Invitrogen, Thermo Fisher Scientific, Carlsbad, USA
Fetal bovine serum (FBS)	Thermo Fisher Scientific, Waltham, USA
Fetal calf serum (FCS)	Merck, Darmstadt, Germany
Formaldehyde solution 37 % (used for flow cytometry)	Merck, Darmstadt, Germany
Glycerol	Labochem international, Einhausen, Germany
Kanamycin	Carl Roth, Karlsruhe, Germany
LB Medium Powder	Carl Roth, Karlsruhe, Germany
Lipofectamine 2000 transfection reagent	Invitrogen, Thermo Fisher Scientific, Carlsbad, USA
Lipofectamine RNAiMAX transfection reagent	Invitrogen, Thermo Fisher Scientific, Carlsbad, USA
Magnesium chloride (MgCl <sub>2</sub> ) hexahydrate	Merck, Darmstadt, Germany
Methanol	VWR International, Radnor, United States
Milk powder, blotting grade	Carl Roth, Karlsruhe, Germany
Mowiol 4-88	Sigma-Aldrich, St. Louis, USA
N-tosyl-L-phenylalanine chloromethyl ketone (TPCK)-treated trypsin	Sigma-Aldrich, St. Louis, USA
Paraformaldehyde solution, 16 % w/v, methanol free (used for imaging)	Alfa Aesar, Haverhill, USA
Penicillin-Streptomycin 100X solution	Pan Biotech, Aidenbach, Germany
Phosphate buffered saline (PBS)	Merck, Darmstadt, Germany
Protease inhibitor cocktail tablets	Roche, Basel, Switzerland
Protein Standard, SeeBlue Plus2 Prestained (Ref. LC5925)	Thermo Fisher Scientific, Waltham, USA
Puromycin	Invivogen, San Diego, USA
Rapamycin (dissolved in Methanol)	Sigma-Aldrich, St. Louis, USA
Saponin	Serva, Heidelberg, Germany
Sodium azide (NaN <sub>3</sub> )	Merck, Darmstadt, Germany
Sodium bicarbonate solution 7.5 %	Thermo Fisher Scientific, Waltham, USA

## Materials and Methods

Sodium chloride (NaCl)	Bernd Kraft, Oberhausen, Germany
Sodium citrate monobasic	Sigma-Aldrich, St. Louis, USA
Tris base	Carl Roth, Karlsruhe, Germany
Triton X-100	Merck, Darmstadt, Germany
Trypan blue solution 0.4 %	Sigma-Aldrich, St. Louis, USA
Trypsin/EDTA 10X	Pan Biotech, Aidenbach, Germany
Tryptone	Sigma-Aldrich, St. Louis, USA
Tryptose phosphate broth (TPB)	Sigma-Aldrich, St. Louis, USA
Tween 20	Carl Roth, Karlsruhe, Germany
Ultrapure agarose	Thermo Fisher Scientific, Waltham, USA
Vybrant Dye Cycle Green	Thermo Fisher Scientific, Waltham, USA
Wortmannin (dissolved in Methanol)	Merck, Darmstadt, Germany
Yeast extract	Sigma-Aldrich, St. Louis, USA

### 9.1.5 Buffers and Solutions

Buffer / Solution	Supplements
Coomassie staining solution	Methanol 50 % Acetic acid 10 % Coomassie brilliant blue 0.25 % (w/v) in dH <sub>2</sub> O
Crystal violet staining solution	Crystal violet 0.25 % (w/v) Ethanol 10 % Formaldehyde 7.4 % in dH <sub>2</sub> O
FACS buffer (FB)	FCS 2 % in PBS 1X
FACS permeabilization buffer (FPB)	FCS 2 % EDTA 5 mM NaN <sub>3</sub> 0.02 % (w/v) Saponin 0.1 % (w/v) in PBS 1X

## Materials and Methods

Fixative solution	Methanol 40 % Acetic acid 10 % in dH <sub>2</sub> O
LB agar	Agarose 13% in LB medium
LB medium	Tryptone 1 % yeast extract 0.5 % NaCl 171 mM in H <sub>2</sub> O
LDS sample buffer 4X, NuPAGE	Thermo Fisher Scientific, Waltham, USA
Lysis buffer	Triton X-100 0.01 % Protease inhibitors in TNE 1X
Mowiol mounting medium	Glycerol 33 g Mowiol 4-88 13 g Tris base 66 mL (use 100 mM Tris base stock solution, adjusted to pH 8.5) ad 100 mL dH <sub>2</sub> O
MOPS SDS running buffer 20X, NuPAGE	Thermo Fisher Scientific, Waltham, USA
TBS-Tween (TBST)	Tween 20 0.1% in TBS 1X
Tryptose phosphate broth (TPB)	29.5 % (w/v)
Carboxymethyl cellulose (CMC)	Carboxymethyl cellulose 3.2 % (w/v) NaCl 0.85 % (w/v) autoclaved
HEPES - NaCl - EDTA (HNE), pH 7.4 10X stock solution	HEPES 100 mM NaCl 1 M EDTA 20 mM 0.22 μM sterile filtered after pH adjustment
Tris-buffered saline (TBS), pH 7.6 10X stock solution	Tris base 200 mM NaCl 1.5 M 0.22 μM sterile filtered after pH adjustment

## Materials and Methods

### 9.1.6 Media used for cell culture and infection assays

Medium (Provider)	Supplements
<b>Complete DMEM</b> DMEM, high glucose, with GlutaMAX (Gibco, Karlsruhe, Germany) Ref: 61965-026	FCS 10 % Penicillin 100 units/mL Streptomycin 100 µg/mL
<b>Complete GMEM</b> GMEM, high glucose, with L-glutamine (Gibco, Karlsruhe, Germany) Ref: 11710-035	TPB 10 % FBS 5 % Penicillin 100 units/ml Streptomycin 100 µg/mL
<b>Freezing medium</b>	FCS (or FBS for BHK-21 cells) 90 % DMSO 10 %
<b>Infection medium</b> (pH 7.0 – 7.4): DMEM, high glucose, with GlutaMAX (Gibco, Karlsruhe, Germany) Ref: 61965-026	HEPES 20 mM BSA 0.2 % MgCl <sub>2</sub> 2 mM CaCl <sub>2</sub> 1 mM
<b>Opti-MEM</b> , with L-glutamine (Gibco, Karlsruhe, Germany) Ref: 11058-021	None
<b>Overlay solution</b> 1:1 dilution of solution A and B	Solution A: Agarose 1.8 % in dH <sub>2</sub> O Solution B: Sodium bicarbonate 0.45 % in complete GMEM
<b>pH 5 buffer</b> RPMI with GlutaMAX (Gibco, Karlsruhe, Germany) Ref: 61870	BSA 0.2 % Citric acid 2.1 mg/ml Sodium citrate 5.6 mg/ml 0.22 µM sterile filtered after pH adjustment
<b>pH 7 buffer</b> (pH 7): RPMI with GlutaMax (Gibco, Karlsruhe, Germany) Ref: 61870	BSA 0.2 % HEPES 30 mM 0.22 µM sterile filtered after pH adjustment

## Materials and Methods

### 9.1.7 Plasmids

Plasmid	Description	Provider
pCDNA3-VSV-G	Vesicular Stomatitis Indiana virus G-protein (VSV-G) expression vector for lentivirus pseudotyping	Zennou et al., 2010 <sup>204</sup>
P8.71	Packaging vector for lentiviral particle production	Zennou et al., 2010 <sup>204</sup>
pIKO.1puro Atg3 F1 pIKO.1puro Atg3 F2 pIKO.1puro Bec1	Transgene vector, encoding shRNA against Atg3 or Beclin 1, a puromycin resistance and the packaging signal for lentivirus particle production	Dr. Nathan Brady (John Hopkins, Baltimore, USA)
pEGFP-Rab5 WT	Expression plasmid for eGFP-Rab5a WT	Lozach et al., 2010 <sup>37</sup>
pEGFP-Rab5 S34N	Expression plasmid for eGFP-Rab5a dominant negative mutant	Lozach et al., 2010 <sup>37</sup>
pEGFP-Rab11a WT	Expression plasmid for eGFP-Rab11a WT	Prof. Urs Greber (University of Zürich, Zürich, Switzerland)
pEGFP-Rab11a S25N	Expression plasmid for eGFP-Rab11a dominant negative mutant	
pEGFP-Rab11a Q70L	Expression plasmid for eGFP-Rab11a constitutively active mutant	
pEGFP-LAMP1	Expression plasmid for eGFP-LAMP1 WT	Dr. Thomas Heger (ETH, Zürich, Switzerland)

### 9.1.8 siRNAs

siRNA 5'-3'	Sequence	Provider
ATG5_1	GGAUGCAAUUGAAGCUCAU	Thermo Fisher Scientific, Waltham, USA
ATG5_2	GAACCAUACUAUUUGCUUU	
ATG5_3	GCUAUAUCAGGAUGAGUA	
ATG7_1	GGAACACUGUAUAACACCA	
ATG7_2	CGCUUAACAUUGGAGUUCA	
ATG7_3	GAAGCUCCCAAGGACAUA	
ATP6V1A	CAUGGUCCAUAUUCGUGA	
BECN1_1	CAGUUACAGAUGGAGCUAA	

## Materials and Methods

BECN1_2	GCAGUCAAAGAAGAGGUU	
BECN1_3	CAGAUACUCUUUAGACCA	
FIP200_1 (RB1CC1)	CGAUAGACAGUAGACGAAU	
FIP200_2 (RB1CC1)	GCCUAGAACAACUAACGAA	
FIP200_3 (RB1CC1)	GUCGUCUCCUAAUCCUAUA	
RAB11A_1	CAACAAUGUGGUUCCUAUU	
RAB11A_2	GAGAUUUACCGCAUUGUUU	
RAB11A_3	GGAGUAGAGUUUGCAACAA	
RAB11B_1	CUAACGUAGAGGAAGCAUU	
RAB11B_2	GCAACGAGUUCAACCUUGGA	
RAB1B_1	GCUGAAAUCAAAAAGCGGA	
RAB1B_2	AGAGCGACCUCACCACCAA	
RAB1B_3	GCACCAGCCUUAACCCUCA	
SiSel NC1 (scrambled)	No sequence information available	
WIPI1_1	GCACUAUUGCUGCCCAUGA	
WIPI1_2	GAAACUCCCUGAAAACAGU	
WIPI1_3	CCCUCUCAACGAUCCAGAA	
VAMP3.4	CCCAAUAUGAAGAUAAACUA	Qiagen, Hilden, Germany

### 9.1.9 Viruses

- **Uukuniemi virus strain 23** (UUKV) was isolated from *Ixodes ricinus* ticks<sup>205</sup>. The strain results from five consecutive plaque purifications in chicken embryo fibroblasts followed by passages in BHK-21 cells<sup>35</sup>.
- **Influenza A virus (A/Puerto Rico/8/1934(H1N1))** (IAV), was produced with the reverse genetics system on MDCK cells and kindly provided by Dr. Susann Kummer, group of Prof. Kräusslich, Virology, Heidelberg.
- **Semliki Forest virus** (SFV)<sup>37</sup>
- **Rift Valley fever virus delta NSs eGFP** (RVFV  $\Delta$ NSs-eGFP) was produced and tittered on Vero E6 cells by Nicole Cordes, former group member of Dr. Lozach, Virology, Heidelberg

## Materials and Methods

### 9.1.10 Bacteria

- *E. coli* **DH5a**, chemically competent from Gibco, genotype: F– 80dlacZM15 (lacZYA-argF) U169 recA1 endA1 hsdR17(rk-, mk+) phoA supE44 – thi-1 gyrA96 relA1, was used for plasmid production.

### 9.1.11 Mammalian cells

Cell line	Origin
BHK-21	Received from Roberta Mancini (ETH, Zürich, Switzerland)
HEK 293T	Received from ETH, Zürich, Switzerland
HeLa DC-SIGN (referred to as HeLa)	Lozach et al., 2005 <sup>99</sup>
HeLa DC-SIGN BFP-LC3 (referred to as HeLa BFP-LC3)	Transduced with the lentivirus system by Dr. Verena Lang (formerly group of Prof. Nathan Brady, John Hopkins, Baltimore, USA). Sorted with the cell sorter by Dr. Monika Langlotz (Flow Cytometry & FACS Core Facility (FFCF), Heidelberg, Germany).
HeLa DC-SIGN shATG3 (referred to as HeLa shATG3)	Prepared in this thesis (chapter 9.3.5)
HeLa DC-SIGN shBECN1 (referred to as HeLa shBECN1)	Prepared in this thesis (chapter 9.3.5)
HeLa (referred to as parental HeLa)	Received from ETH, Zürich, Switzerland
Huh7 <i>ATG14L</i> KO	
Huh7 <i>ATG16L1</i> KO	
Huh7 <i>ATG3</i> KO	Prepared with the CRISPR/Cas9 genome-editing system, kindly provided by Dr. Keisuke Tabata, group of Prof. Bartenschlager, Molecular Virology, Heidelberg
Huh7 <i>ATG5</i> KO	
Huh7 <i>ATG7</i> KO	
Huh7 <i>ATG9L1</i> KO	
Huh7 control	
Huh7 <i>FIP200</i> KO	

## Materials and Methods

### 9.1.12 Primary antibodies

Target protein (antibody name)	Species	Dilution	Method	Provider
Actin	Mouse monoclonal	1:1000	WB	Santa Cruz (Ref. sc-58679)
Atg3	Rabbit polyclonal	1:1000	WB	Cell Signaling (Ref. 3415)
Atg7	Rabbit monoclonal	1:200	WB	Cell Signaling (Ref. 8558)
Beclin 1	Rabbit polyclonal	1:1000	WB	Cell Signaling (Ref. 3738)
DC-SIGN / CD209 (conjugated FITC)	Mouse monoclonal	1:50	Flow cytometry	R&D Systems (Ref. FAB161F)
IAV-N	Mouse monoclonal	1:250	Flow cytometry	Merck Millipore (Ref. MAB8257)
Rab11a	Rabbit polyclonal	1:1000 1:50	WB microscopy	Cell Signaling (Ref. 2413)
Rab1b	Mouse monoclonal	1:100	WB	Sigma Aldrich (Ref. SAB1400720)
SFV-E2	Mouse monoclonal	1:400	Flow cytometry	Prof. Margaret Kielian
UUKV (U2)	Rabbit polyclonal	1:1000	Focus-forming assay	Dr. Pierre-Yves Lozach
UUKV-N (8B11A3)	Mouse monoclonal	1:400	Flow cytometry	Dr. Anna Överby
$\alpha$ -tubulin	Mouse monoclonal	1:1000	WB	Sigma Aldrich (Ref. T5168)
$\beta$ -actin	Mouse monoclonal	1:1000	WB	Sigma-Aldrich (Ref. A2228)

## Materials and Methods

### 9.1.13 Secondary antibodies

Antibody name	Species	Dilution	Method	Provider
Anti-mouse AF488	Goat	1 : 500	Flow cytometry	Thermo Fisher Scientific
Anti-mouse AF647	Goat	1 : 500	Flow cytometry	Thermo Fisher Scientific
Anti-mouse HRP	Goat	1 : 10 000	WB	Santa Cruz
Anti-rabbit AF405	Goat	1 : 500	Microscopy	Thermo Fisher Scientific
Anti-rabbit HRP	Goat	1 : 10 000	WB	Santa Cruz

### 9.1.14 Image Analysis Programs

Program	Application
FlowJo V10	Flow cytometer data analysis
Icy	Bioimage analysis
ImageJ	Bioimage analysis
Odyssey Image Studio Software	Protein analysis

### 9.1.15 Services

Company / Facility	Service
Flow Cytometry & FACS Core Facility (FFCF), Heidelberg, Germany	Cell sorting
Advanced Biological Screening Facility, Heidelberg, Germany	siRNA ordering

## Materials and Methods

### 9.2 Cellular biology methods

#### 9.2.1 Mammalian cell culture

All cell lines were cultured at 37°C in a humidified atmosphere (90 % relative humidity) with 5 % CO<sub>2</sub>. BHK-21 cells were kept in cell culture flasks in complete GMEM, all other mammalian cell lines were kept in cell culture flasks in complete DMEM. Cells were monitored with a wide field microscope and split twice a week by a 1:10 to 1:20 dilution according to their confluency. For passaging, trypsin/EDTA was added onto PBS-washed cells for 2-5 minutes to detach adherent cells. Complete medium was added to inactivate trypsin and to resuspend the cells. For long term storage, cells were cryopreserved and kept at -80°C or in liquid nitrogen. For cryopreservation the cells were pelleted at 300 x g for 5 minutes and taken up in FBS or FCS. 10 % DMSO was added dropwise while swirling the cells in FBS. 1 mL freezing medium contained 1-3x10<sup>6</sup> cells and was frozen in one cryotube. Slow temperature decrease was allowed overnight in isopropanol tanks inside a -80°C freezer and cells were then taken out the isopropanol tank and kept at -80°C or in liquid nitrogen.

#### 9.2.2 Cell lysis

Adherent cells were lysed by adding 200 µL lysis buffer per well of a 24 well plate. After 15 minutes incubation on ice, the cells were scraped off with a pipet tip and transferred into a 1.5 mL reaction tube and incubated again 15 minutes on ice. Next, the cell lysate was centrifuged for 20 minutes at 12 000 x g at 4°C. Cell lysates were stored at -20°C and further used for SDS-PAGE and western blot (chapter 9.4.2).

#### 9.2.3 Heat shock transformation and plasmid preparation

Chemically competent *E. coli* DH5α cells were thawed on ice. 20 ng plasmid (chapter 0) was added to 50 µL *E. coli* DH5α cells and gently mixed. After 30 minutes incubation on ice, the bacteria were heat-shocked for 30 seconds at 42°C in a water bath and returned onto ice. 250 µL LB medium were added. Bacteria were incubated for 1 h at 37°C and shaken at 145 rpm. 100 µL bacterial suspension was then plated onto selective LB-agarose plates. The plates were incubated at 37°C overnight. Bacterial colonies were visible after 16 hours incubation.

To amplify the transformed plasmid, a single colony was picked with a sterile pipet tip, inoculated into 50 mL selective LB medium and incubated for 14-16 h at 37°C while shaken at 145 rpm. The bacterial suspension was pelleted in 50 mL conical tubes by centrifugation at 5000 x g at 4°C for 10 minutes. The supernatant was discarded, and the plasmids were prepared

## Materials and Methods

from the pellet with the DNA Plasmid Plus Midi Kit according to the manufacturer's instructions. The DNA concentration was measured with the nanophotometer.

### 9.2.4 Cell transfection with siRNAs and DNA plasmids using Lipofectamine

siRNAs (listed in chapter 9.1.8) were introduced into the cells by reverse transfection using Lipofectamine RNAiMAX transfection reagent according to the manufacturer's instructions. In the case of Huh7 cells DMEM was used for transfection instead of Opti-MEM. The utilized siRNA concentrations and incubation times are indicated in the respective figure legends. For the endocytic bypass assay (chapter 9.2.5.4) and the drug-addition time course (chapter 9.2.5.5), reverse transfection was performed in 24 well plates with 25 000 or 30 000 HeLa cells. For all other flow cytometry-based infection assays (chapters 9.2.5.1 - 9.2.5.3), reverse transfection was performed in 6 well plates with 200 000 HEK 293T cells, 125 000 HeLa cells, 125 000 parental HeLa cells or 300 000 Huh7 cells. For imaging-based infection assays, reverse transfection was performed in 24 well plates with 12 mm round cover glasses and 20 000 HeLa cells.

Applied transfection conditions for Figure 11:

siRNA	Experiment number	Concentration [nM]	Time [h]
Applied transfection conditions for infection assay			
ATG5	1 + 2	20	72
	3 + 4	10	48
ATG7	1 + 2	10	72
	3 + 4	10	48
	5	50	72
BECN1	1	10	48
	2	50	72
FIP200 (RB1CC1)	1 – 4	20	72
RAB1B	1 + 2	20	72
	3	20	48
RAB11A	1	20	48
	2 + 3	10	72
WIPI1	1 – 5	20	72
Applied transfection conditions for SDS-PAGE and WB			
ATG7	1	20	72
RAB1B	1	20	72
RAB11A	1	10	48

Lipofectamine 2000 transfection reagent was used according to the manufacturer's instructions to introduce 0.5 µg DNA plasmids (listed in chapter 0) for 20-24 h. For flow cytometry-based infection assays (chapter 9.2.5.1), plasmid transfection was performed in 24 well plates, and 50

## Materials and Methods

000 HeLa cells were seeded 18-22 h before transfection. For imaging-based infection assays, 70 000 HeLa cells were seeded 18-22 h before transfection onto 12 mm round cover glasses (chapter 9.2.7.2).

### 9.2.5 Flow cytometry-based infection assays

Infections assays addressing different steps of the viral life cycle are described in the following subchapters.

#### 9.2.5.1 Infection assays

Cells were detached with PBS/EDTA 0.5 mM for 5-7 min, transferred into a 15 mL conical reaction tube and washed in 10 mL complete DMEM to remove the EDTA. Cells were pelleted at 300 x g for 5 minutes and resuspended in warm infection medium. For infection with IAV, the infection medium was supplemented with 1 µg/mL TPCK-treated trypsin to cleave the surface exposed hemagglutinin and thereby allow IAV infection. 200 000 cells per sample were seeded into a 96 well plate with U-bottoms. Cells were again pelleted and infected in suspension with 100 µL warm infection medium containing the viral particles. The utilized viral particles and MOIs are indicated in the figure legends. 1 hpi the inoculum was removed and replaced by 200 µL warm complete DMEM. After additional 5 h or 7 h incubation (specified in the figure legends) at standard conditions, the cells were fixed and immunostained to determine infectivity by flow cytometry (specified in section 9.2.6).

Plasmid-transfected HeLa cells (chapter 9.2.4) were directly infected in the 24 well plate. The number of cells per well was determined by detaching cells from one well (distinct for counting) with trypsin/EDTA. A final volume of 300 µL viral particles diluted in warm infection medium was added onto the adherent cells for infection. 1 hpi the inoculum was removed and replaced by 500 µL warm complete DMEM. After additional 7 h incubation, the cells were fixed and immunostained to determine infectivity by flow cytometry (specified in section 9.2.6).

#### 9.2.5.2 Binding assay with Alexa Flour-labeled viral particles

Cells were detached with PBS/EDTA 0.5 mM for 5-7 min, transferred into a 15 mL conical reaction tube and washed in 10 mL complete DMEM to remove the EDTA. Cells were pelleted at 300 x g for 5 minutes and resuspended in cold infection medium. 200 000 cells per well seeded into a 96 well plate with U-bottoms. To assure, that endocytic processes are stopped, the cells were kept on ice for 10 min. Cells were then pelleted in a precooled centrifuge at 300 x g for 5 minutes and resuspended in 100 µL cold infection medium with UUKV-AF488 or UUKV-AF647 particles . The MOIs are indicated in the figure legends. After binding on ice

## Materials and Methods

for 90 min, the cells were washed twice with cold PBS and directly measured for surface fluorescence with the flow cytometer (specified in section 9.2.6).

### **9.2.5.3 Internalization assay using trypan blue**

UUKV-AF488 was bound to cells on ice in two separate 96 well plates as described in chapter 9.2.5.2. Cells in the first plate were washed with precooled infection medium to remove unbound viral particles and kept on ice until the second 96 well plate was ready. Cells in the second 96 well plate were washed with warm infection medium and incubated for 10 minutes in a 37°C warm water bath, followed by additional 30 minutes in the incubator. Both plates were then washed once with precooled PBS and directly measured with the FACSCelesta. To differentiate between plasma membrane-bound and internalized UUKV-AF488 particles, 0.01 % trypan blue was added to each sample and measured a second time. Data were analyzed with the software FlowJo V10.

### **9.2.5.4 Plasma membrane-virus fusion assay (endocytic bypass assay)**

130 000 Huh7 *ATG7* KO cells or Huh7 control cells were seeded into a 24 well plate 18-22 h before infection. HeLa cells transfected with siRNAs (chapter 9.2.4) were used for the endocytic bypass assay. The number of cells per well was determined by detaching cells from the counting well with trypsin/EDTA and counting them in the Malassez counting chamber. The adherent cells were washed once with infection medium. To assure, that endocytic processes have stopped, the cells were kept on ice for 10 min. A final volume of 300 µL cold infection medium with viral particles was added to the adherent cells. The respective MOIs are indicated in the figure legends. After virus particle binding on ice for 1 h, the inoculum was removed and 300 µL warm pH5 buffer or 300 µL warm pH7 buffer were added to the cells. The 24 well plates with HeLa cells or Huh7 cells were quickly transferred to a 37°C water bath for 90 seconds or 60 seconds, respectively. After the incubation period, the pH5 buffer or pH7 buffer were quickly removed and 1 mL complete DMEM + 20 mM HEPES ± 100 mM ammonium chloride (NH<sub>4</sub>Cl) were added to the cells. Cells were incubated for 6 h (HeLa cells) or 8 h (Huh7 cells) in the incubator. The cells were then fixed and immunostained. The infectivity was determined by flow cytometry (specified in section 9.2.6).

### **9.2.5.5 Drug-addition time course**

HeLa cells transfected with siRNAs (chapter 9.2.4) were used for the drug-addition time course. The number of cells per well was determined by detaching cells from the counting well with trypsin/EDTA and counting them in the Malassez counting chamber. The adherent cells were washed once with infection medium. To assure, that endocytic processes have stopped, the cells

## Materials and Methods

were kept on ice for 10 min. Viral particles in 300  $\mu$ L cold infection medium were added to the adherent cells. The respective MOIs are indicated in the figure legends. After virus particle binding on ice for 1 h, the inoculum was removed and 500  $\mu$ L warm complete DMEM was added to each well. A rapid temperature shift was guaranteed by letting the 24 well plate float in a 37°C warm water bath for 10 minutes, followed by incubation in the incubator. The complete DMEM was replaced by complete DMEM with 50 mM NH<sub>4</sub>Cl at different time points (0 / 5 / 10 / 20 / 40 / 80 minutes after the temperature shift to 37°C). Control samples were incubated without addition of NH<sub>4</sub>Cl. HeLa cells were in total incubated 6 h and subsequently fixed and immunostained. Infectivity was measured by flow cytometry (specified in section 9.2.6).

### 9.2.6 Cell fixation and immunostaining for flow cytometry

To assess infectivity, cells were washed twice with PBS, detached with 100  $\mu$ L trypsin/EDTA and transferred into a 96 well plate with U-bottoms. Trypsin was inactivated by adding 100  $\mu$ L complete medium. Cells were again washed with PBS and fixed in 100  $\mu$ L PBS/formaldehyde 3.7 % for 20 minutes at RT. After another PBS washing step, cells were permeabilized in 200  $\mu$ L FACS permeabilization buffer (FPB) for 5 min. The cells were pelleted by centrifugation at 300 x g and resuspended in 100  $\mu$ L diluted primary antibodies. The anti-UUKV-N antibody 8B11A3 or the anti-SFV-E2 antibody (both diluted 1:400 in FPB) were added to the cells and incubated 1 h at RT. Or the anti-IAV-N antibody (diluted 1:250 in FPB) was added to the cells and incubated on ice for 1 h. After a washing step with 200  $\mu$ L FPB, the cells were resuspended in 200  $\mu$ L diluted secondary antibodies anti-mouse AF647 or anti-mouse AF488 (1:500 in FPB) and incubated for 1 h at RT or on ice (for IAV infected samples). Cells were then washed twice with PBS and kept on ice until measurement with the flow cytometer. Data were analyzed with the software FlowJo V10.

To assess DC-SIGN expression on the cell surface, cells were washed twice with PBS, detached with 100  $\mu$ L trypsin/EDTA and transferred into a 96 well plate with U-bottoms. Trypsin was inactivated by adding 100  $\mu$ L complete medium. Cells were washed with cold FACS buffer, and stained in 100  $\mu$ L anti-DC-SIGN antibody (diluted 1:50 in FACS buffer) for 1 h at 4°C in the dark. Cells were then washed twice with PBS and kept on ice until measurement with the flow cytometer. Data were analyzed with the software FlowJo V10.

### 9.2.7 Imaging-based assays

Imaging-based assays to assess autophagosome formation and UUKV localization to LC3- or Rab11a-decorated vesicles, are described in the following subchapters.

## Materials and Methods

### **9.2.7.1 Autophagy activation in HeLa BFP-LC3 C2 cells**

50 000 HeLa or HeLa BFP-LC3 C2 cells were seeded on 12 mm round cover glasses in a 24 well plate 14-18 h before drug addition. The cells were washed once with complete DMEM and then exposed to 1 mL complete DMEM supplemented with 100 nM bafilomycin A<sub>1</sub>, 1 μM rapamycin or 100 nM wortmannin for 4 h. The cells were washed with PBS and fixed with 150 μL PBS/methanol free paraformaldehyde 4 % for 20 minutes at RT. After a washing step with PBS, the cells were incubated with 100 nM Vybrant Dye Cycle Green (nuclear stain) for 30 minutes in the incubator. After two additional washing steps with PBS, the 12 mm round cover glasses were mounted in 8 μL mowiol mounting medium on a microscopy slide and dried over night at 4°C. Images were acquired with the Leica SP5 Laser Confocal Scanning Microscope (chapter 9.2.8).

### **9.2.7.2 Colocalization assay for UUKV-AF568 with eGFP-Rab11a**

Plasmid-transfected HeLa cells grown on 12 mm round cover glasses in a 24 well plate (chapter 9.2.4) were used for this colocalization assay. The number of cells per well was determined by detaching cells from the distinct well for cell counting with trypsin/EDTA and counting them in the Malassez counting chamber. The adherent cells were washed once with infection medium. To assure, that endocytic processes have stopped, the cells were kept on ice for 10 minutes. A final volume of 300 μL cold infection medium with UUKV-AF568 particles (MOI 0.5) was added to the adherent cells. After binding on ice for 1 h, the inoculum was replaced by 500 μL warm complete DMEM. The temperature was rapidly shifted by letting the 24 well plates float in the 37°C water bath for the first 10 minutes, followed by incubation in the incubator. After the indicated incubation period (0 / 5 / 10 / 15 / 20 / 30 minutes after the temperature shift to 37°C), cells were quickly washed with cold PBS and fixed with 150 μL PBS/methanol free paraformaldehyde 4 % for 20 minutes in the incubator. After two additional washing steps with PBS, the 12 mm round cover glasses were mounted in 8 μL mowiol mounting medium on a microscopy slide and dried over night at 4°C. Images were acquired with the Leica SP8 Laser Confocal Scanning Microscope (chapter 9.2.8).

### **9.2.7.3 Colocalization assay for UUKV-AF568 with BFP-LC3**

50 000 HeLa BFP-LC3 C2 cells were seeded on 12 mm round cover glasses in a 24 well plate 14-18 h before infection. UUKV-AF568 was bound to HeLa BFP-LC3 C2 cells at an MOI of 2 and internalization was allowed as described in chapter 9.2.7.2. Fixation, nuclei staining and acquisition was performed as described in chapter 9.2.7.1.

## Materials and Methods

### 9.2.8 Confocal fluorescence microscopy

Multichannel 2D images or 3D stacks were acquired with a confocal laser scanning microscope (Leica SP5 or Leica SP8) using a 63X oil immersion objective. Images were recorded with an excitation wavelength of 405, 488, 561 and/or 640 nm and stacks had a z-spacing of 300 nm.

### 9.3 Virology methods

#### 9.3.1 Production of UUKV particles & SFV particles

UUKV particles and SFV particles were produced in BHK-21 cells. 14-18 h before infection,  $12 \times 10^6$  BHK-21 cells were seeded in 35 mL complete GMEM into T175 cell culture flasks and incubated overnight. Cells were washed once with warm complete GMEM without FBS (GMEM with 10 % TPB, Penicillin 100 units/ml, Streptomycin 100  $\mu\text{g}/\text{mL}$ ). 5  $\mu\text{L}$  UUKV particle preparation (unpurified cell culture supernatant of infected cells) was added in 15 mL warm complete GMEM without FBS and added to the BHK-21 cells in the T175 cell culture flask. The desired MOI was around 0.1. Analogously, 1  $\mu\text{L}$  SFV was added to the cells for SFV production. For 1 h incubation in the incubator, the cell culture flasks were carefully swirled every 15-20 min. The inoculum was discarded and replaced by 35 mL warm complete GMEM without FBS. Virus particles in the supernatant were harvested when a cytopathogenic effect was visible in the widefield microscope, usually 48-72 hpi. The supernatant was cleared by centrifugation at  $1500 \times g$  and  $4^\circ\text{C}$  in 50 mL conical reaction tubes and subsequently semipurified through a sucrose cushion (chapter 9.3.2).

#### 9.3.2 UUKV & SFV semipurification

The supernatant was transferred into SW32 ultracentrifugation tubes. The supernatant from the UUKV particle production was underlayered with 2.5 mL HNE/sucrose 25 % (w/v, 0.22  $\mu\text{M}$  sterile filtered). The supernatant from the SFV particle production was underlayered with 2.5 mL HNE/sucrose 20 % (w/v, 0.22  $\mu\text{M}$  sterile filtered). The samples were centrifuged at  $100\,000 \times g$  at  $8^\circ\text{C}$  for 2 h. The supernatant was decanted. 300  $\mu\text{L}$  HNE 1X was added as a resuspension buffer to the virus particle pellets and incubated on ice. After 1-2 h the pellets were resuspended by up- and down pipetting and pooled. The viral particle preparation was cleared by centrifugation at  $3000 \times g$  and  $4^\circ\text{C}$  for 15 min. The supernatant containing the viral particles was then aliquoted and stored at  $-80^\circ\text{C}$ .

## Materials and Methods

### 9.3.3 UUKV titration by focus-forming assay

To determine the titer of semipurified (chapter 9.3.2) or labeled (chapter 9.3.5) UUKV particle preparation, a focus-forming assay was performed in BHK-21 cells. 100 000 BHK-21 cells per well were seeded in complete GMEM in a 24 well plate. 14-18 hours after seeding, a ten-fold serial dilution of viral particles was freshly prepared in complete GMEM without FBS. The BHK-21 cells were washed with complete GMEM without FBS. Next, 200  $\mu$ L complete GMEM without FBS and 200  $\mu$ L virus preparation dilution was added to the cells. After 1 h incubation, 400  $\mu$ L CMC with complete GMEM (1:1 dilution) was added to the cells. After 72 h incubation the virus preparation titers were recorded as follows. The cells were carefully washed with complete GMEM without FBS and once with PBS. Next, the cells were fixed with PBS/formaldehyde 3.7 % for 20 minutes at RT. The BHK-21 cells were then washed with FPB and 300  $\mu$ L U2 primary antibody (diluted 1:1000 in FPB) was added. After 1 h incubation at RT, the cells were again washed with FPB and incubated with 300  $\mu$ L anti-rabbit HRP secondary antibody (diluted 1:200 in FPB) for 1 h at RT. After another washing step with FPB, the cells were stained with DAB peroxidase substrate kit according to the manufacturer's instructions and the foci were counted.

### 9.3.4 SFV titration by plaque assay

To determine the titer of semipurified SFV particle solution (chapter 9.3.2), a plaque assay was performed in BHK-21 cells. 100 000 BHK-21 cells per well were seeded in complete GMEM in a 24 well plate. 14-18 h after seeding, ten-fold serial dilution of viral particles was freshly prepared in complete GMEM without FBS. The BHK-21 cells were washed with complete GMEM without FBS. Next, 200  $\mu$ L complete GMEM without FBS and 200  $\mu$ L virus preparation dilution was added to the cells. After 1 h incubation, the inoculum was replaced by warm overlay medium (1.8 % agarose and complete GMEM with 0.45 % sodium bicarbonate, 1:1 diluted). After 1 h incubation, the agarose was solid and the plates were inverted. After another 47 h of incubation, the agarose pads were removed carefully. Next, 300  $\mu$ L crystal violet staining solution were added and the plate was incubated for 20 minutes at RT. After careful washing of the cells under slow-flowing water, plaques were counted.

### 9.3.5 UUKV labeling and purification

To purify viral particles immediately after the labeling, a linear sucrose gradient, ranging from 15 to 60 % sucrose (w/v), was prepared in advance. Sucrose solutions containing 15 %, 30 %, 45 % or 60 % sucrose (w/v) were prepared in HNE 1X. The different sucrose solutions were layered on top of each other, starting with of the highest sucrose concentration and ending with

## Materials and Methods

the lowest sucrose concentration. 900  $\mu$ L sucrose solution were pipetted into a SW60 ultracentrifugation tube and frozen, before 900  $\mu$ L the next sucrose solution were added. The sucrose gradients were kept frozen and thawed overnight at 4°C before use.

Proteins on the surface of semipurified UUKV particles (chapter 9.3.2) were nonspecifically labeled with an Alexa Fluor NHS Ester, which reacts with primary amines. A semipurified UUKV particle preparation containing minimum 150  $\mu$ g UUKV glycoproteins  $G_N$  &  $G_C$  per mL particle preparation (the glycoprotein concentration was quantified by SDS-PAGE and coomassie staining, see chapter 9.4.1), was required for efficient labeling and subsequent particle purification. The molar ratio of  $G_N$  &  $G_C$  to dye was 1 to 2.5. The required amount of Alexa Fluor NHS Ester was freshly dissolved in 50  $\mu$ L HNE 1X and then added to the particle preparation. After 2 h incubation on a rocker in the dark at RT, the virus particle solution was layered on top of a linear sucrose gradient. Next, ultracentrifugation was performed for 90 minutes at 100 000 x g at 4°C. A milky band at a density corresponding to 45 % sucrose was extracted with a syringe attached to a needle and further analyzed to assess infectivity by foci-forming assay (chapter 9.3.3).

### **9.3.6 Generation of HeLa cells stably expressing shRNA against Atg3 or Beclin 1 by lentivirus transduction**

Lentiviruses were produced on HEK 293T cells. For this, HEK 293T cells were transfected with three plasmids: P8.71 (packaging vector), pCDNA3-VSV-G (pseudotype vector) and plKO.1puro Atg3 F1 or plKO.1puro Atg3 F2 or plKO.1puro Bec1 (transgene vector). Transfection was performed with the CalPhos Mammalian Transfection kit according to the manufacturer's instructions. 24 h and 48 h after the transfection, the medium was replaced by fresh complete GMEM. 72 h after the transfection, the supernatant was cleared by centrifugation for 5 minutes at 500 x g and 0.45  $\mu$ M sterile filtered. Lentivirus particle preparations were then stored at -80°C.

These lentivirus particles were used to generate cell lines stably expressing shRNA against Atg3 or Beclin 1. For this, 125 000 HeLa cells per well were seeded in a 6 well plate and incubated overnight. After 14-18 h, the cell culture supernatant was replaced by 1.15 mL lentivirus particle containing cell supernatant. 6 hpi and 24 hpi the supernatant was again replaced by 1.15 mL lentivirus particle containing cell supernatant. 32 hpi lentiviral particles were replaced by complete DMEM. When the cells were confluent, they were transferred from the 6 well plate to a T25 cell culture flask and selected on complete DMEM supplemented with 5  $\mu$ g/mL puromycin.

## Materials and Methods

### 9.4 Biochemistry methods

#### 9.4.1 Viral protein analysis by SDS-PAGE & coomassie staining

To quantify UUKV glycoprotein  $G_N$  &  $G_C$  concentrations, different volumes of viral particle preparations (5 / 10 / 15  $\mu$ L) were incubated with LDS sample buffer. The particle samples, and 2  $\mu$ L protein ladder were loaded on a precast 10 % Bis-Tris protein gel. For normalization, known concentrations of BSA (62.5 / 125 / 250 / 500 / 1000 ng) in LDS sample buffer were also loaded onto the gel. Electrophoresis was performed under nonreducing conditions in MOPS SDS running buffer at 125 V for 1 h 30 min. The gel was incubated in fixative solution for 1 h rocking and then stained in coomassie staining solution for 2 h rocking. Destaining of the gel was achieved by multiple washing steps in washing solution while rocking. The gel was then imaged with the Licor Odyssey scanner. The Odyssey Image Studio Software or ImageJ were used for quantitative analysis of band signal intensities. An example for the calculation of UUKV glycoprotein concentrations can be found in our review <sup>206</sup>.

To assess which proteins are fluorescently labeled with the Alexa Fluor NHS Ester, protein gels with the fluorescently labeled viral particles were scanned on the fluorescence plate reader before fixation.

#### 9.4.2 Cellular protein analysis by SDS-PAGE & Western blot

To assess cellular protein expression, cell lysates (chapter 9.2.2) in LDS sample buffer were denatured for 5 minutes at 95°C and loaded on a precast 10 % Bis-Tris protein gel. Electrophoresis was performed under nonreducing conditions in MOPS SDS running buffer at 125 V for 1 h 30 min. Subsequently, the proteins were transferred to a Polyvinylidene difluoride (PVDF) membrane with a dry blotting system (iBlot). Membranes were blocked in TBS-Tween (TBST)/milk 5 % for 1 h at RT on the rocker. Primary antibodies were diluted as indicated in chapter 9.1.12 in TBST/milk 5% or TBST/BSA 5% according to the provider's recommendations and incubated over night at 4°C. After three 10 minutes washing steps in TBST on the rocker at RT, the membranes were incubated with HRP-conjugated secondary antibodies (chapter 9.1.13), diluted in TBST/milk 5 %. Again, three washing steps were performed for 10 minutes with TBST on the rocker. Bound secondary antibodies were detected by exposure to an enhanced chemiluminescent (ECL) HRP substrate and developed on a foto film and digitalized using a scanner. The band and intensities were determined with ImageJ.

### **9.5 Image analysis**

#### **9.5.1 LC3-puncta quantification with ImageJ**

To determine the number of BFP-LC3 puncta per cell, 3D stacks were inverted and minimal projected. The noise was reduced with the Gaussian Blur filter. Puncta were selected by applying a threshold and the Watershed algorithm was used to separate overlapping objects. Next, cells were selected one after another to count puncta with the “Analyze particles” plugin.

#### **9.5.2 Colocalization analysis with Icy**

Colocalization was determined with the bioimage analysis software Icy <sup>207</sup>. The spot detector was used to detect viral particles and define their location as a region of interest (ROI). The ROI statistics function was then used to obtain the average pixel intensity of other markers (eGFP-LAMP1 or BFP-LC3) within these ROIs. A threshold was then applied to define viral particle ROIs that colocalize with eGFP-LAMP1 or BFP-LC3.

### **9.6 Statistical analysis**

Data analysis was performed using GraphPad Prism software. The standard deviation (SD) was plotted and statistical significance was assessed with a two-tailed unpaired Student's t test.

# 10 Results

## 10.1 Autophagy-related proteins in UUKV infection

The first part of my PhD thesis I focused on the role of autophagy-related proteins in UUKV infection. Therefore, we specifically reduced the expression of autophagy-related proteins or overexpressed mutants and assessed the effect on UUKV-N protein expression. We selected the four autophagy-related proteins appearing as potential host factors in our siRNA screens, namely WIPI1, FIP200, Rab1b and Rab11a<sup>80</sup> as well as further key autophagy proteins involved in different steps of the macroautophagic pathway. This included FIP200 (part of the initiation complex), Beclin 1 and Atg14L (nucleation complex), Atg9L1 and WIPI1 (phagophore formation), Atg3, Atg5, Atg7 and Atg16L1 (autophagosome elongation)<sup>208</sup> (**Figure 7**). We also tested the small GTPases Rab1b and Rab11a because the first is involved in the autophagosome formation<sup>109</sup> and the second forms a platform for autophagosome assembly<sup>129</sup>.

### 10.1.1 UUKV infection upon silencing autophagy-related proteins

To assess the effect of autophagy-related proteins on UUKV infection, siRNA- or shRNA-mediated silencing was performed in the human cell line HeLa. The cells used in this approach expressed the UUKV receptor DC-SIGN, the same line utilized for the siRNA screens from which we obtained our autophagy-related host cellular candidates<sup>80</sup>. After 6 h infection, newly synthesized UUKV nucleoprotein (UUKV-N) was immunostained, detected by flow cytometry and positive cells were quantified. An infection rate of 20-40 % was targeted to enable the detection of infection decrease but also a potential increase due to silencing of the respective proteins. Data were normalized to a scrambled siRNA control. Positive control siRNAs against VAMP3, as known host factors involved in UUKV late penetration<sup>80</sup>, or against the vacuolar proton pump (siATP6V1A), were used. The late penetrating UUKV requires this proton pump to maintain a low pH in endosomal compartments for fusion.

Silencing of Atg7 and Rab11a, each with three nonoverlapping siRNAs, significantly reduced UUKV infection by around 50 % (**Figure 11a**). To assess silencing efficiency, cell lysates were analyzed by SDS-PAGE and WB for Atg7, Rab1b, and Rab11a. After immunostaining a decreased Atg7 and Rab11a expression was detected as a result of specific siRNA transfection (**Figure 11c**). Reduced protein expression in combination with a decreased infection level supported a possible role of Atg7 and Rab11a in UUKV infection. Silencing of Rab1b with three nonoverlapping siRNAs reduced UUKV-N protein expression to 69 %, 61 % and 29 %

## Results

(**Figure 11a**) while Rab1b expression was clearly decreased (**Figure 11c**), indicating also a potential role of Rab1b in UUKV infection.

A significant but weaker reduction in UUKV-N protein replication, amounting 42 %, 13 % and 30 %, was measured for siRNAs targeting *ATG5* (**Figure 11b**). For *FIP200* none of the tested siRNAs modified the infection level. For *BECN1* and *WIPI1* only 1 out of 3 siRNA reduced infection by 50 % while the other two nonoverlapping siRNAs had no effect (**Figure 11a**). As in all four experiments positive control siRNAs targeting vATPase (si*ATP6VIA*) or *VAMP3* significantly reduced UUKV infection, siRNAs were successfully delivered into HeLa cells. But assessment of si*WIPI1*, si*ATG5*, si*BECN1* and si*FIP200* silencing efficiency would be a prerequisite to conclude on the protein's role in UUKV infection.

## Results

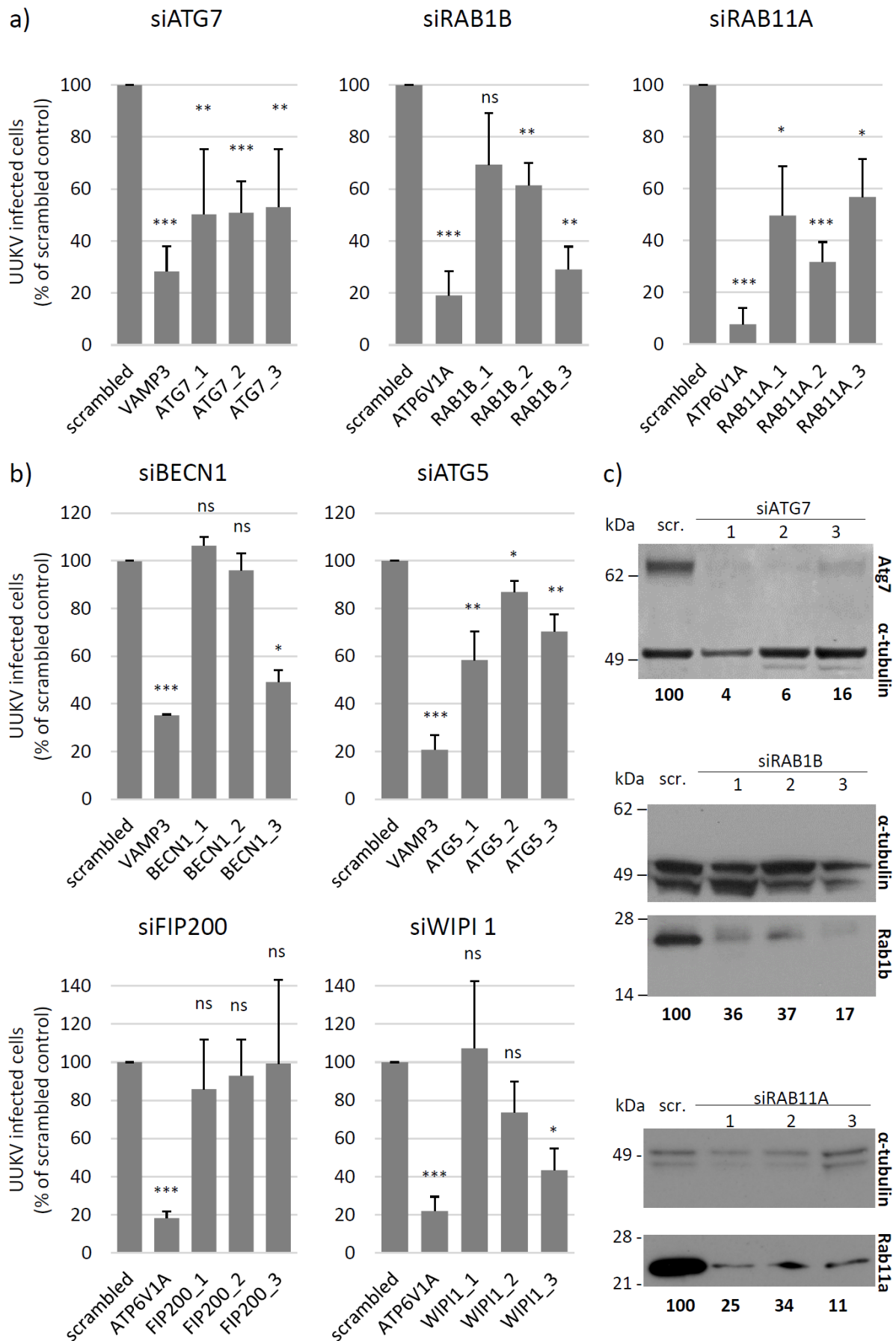
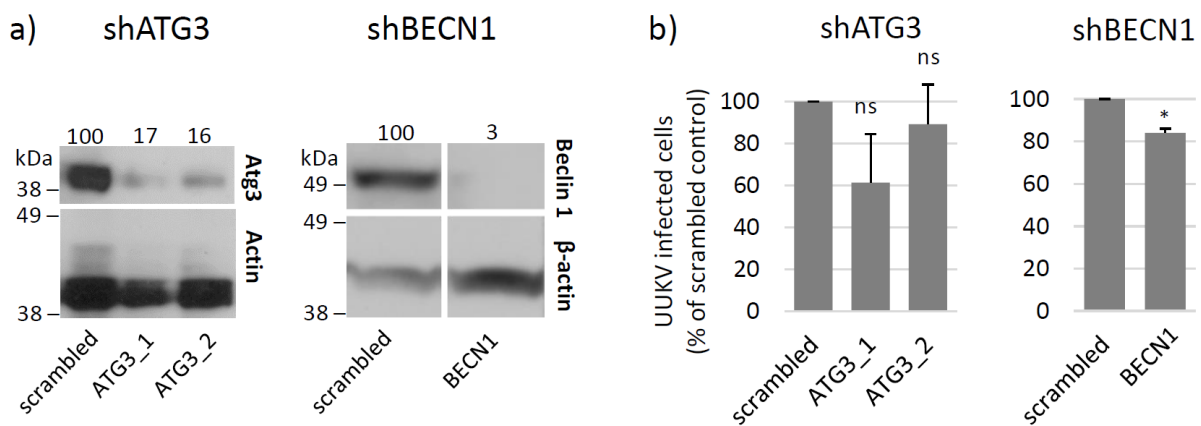


Figure 11: Atg7, Rab1b and Rab11a were involved in UUKV infection in HeLa cells

## Results

(a-b) HeLa cells were transfected with siRNAs (transfection conditions are specified in chapter 9.2.4) and exposed to UUKV at a MOI of 0.125 for 6 h. After fixation and permeabilization, infected cells were immunostained for UUKV-N and analyzed by flow cytometry. Data were normalized to scrambled control and represent means  $\pm$  standard deviation (SD),  $n = 2-5$ , two-tailed unpaired t-test,  $***p \leq 0.001$ ,  $**p \leq 0.01$ ,  $*p \leq 0.05$ , ns stands for nonsignificant. (c) HeLa cells were transfected siRNAs (transfection conditions are specified in chapter 9.2.4), lysed and analyzed by SDS-PAGE and Western Blot (WB). Band intensity is indicated below the blots.

To further assess the effect of autophagy-related proteins on UUKV infection, a shRNA-based approach was performed. Lentivirus transduction was used to express shRNAs against the two key autophagy proteins Atg3 and Beclin 1 in HeLa cells and silencing was assessed with immunostaining by WB (**Figure 12a**). shRNA targeting *ATG3* did not significantly modify UUKV-N protein expression (**Figure 12b**) while Atg3 expression was clearly reduced (**Figure 12a**). Despite efficient silencing mediated by the shRNA targeting *BECN1* (**Figure 12a**), a weak but significant reduction in infected cells was detected upon UUKV infection (**Figure 12b**). Together these results suggest no or only a minor role for Atg3 and Beclin 1 respectively in UUKV infection.



**Figure 12: Atg3 and Beclin 1 play a minor role in UUKV infection**

(a) HeLa cells were transduced with lentiviruses to stably express shRNA, lysed and analyzed by SDS-PAGE and WB. Band intensity is indicated above the blots. (b) HeLa cells expressing shRNAs were exposed to UUKV at a MOI of 0.125 for 6 h. After fixation and permeabilization, infected cells were immunostained for UUKV-N and analyzed by flow cytometry. Data were normalized to the scrambled shRNA control and represent means  $\pm$  SD,  $n = 3$  for shATG3,  $n = 2$  for shBECN1, two-tailed unpaired t-test,  $***p \leq 0.001$ ,  $**p \leq 0.01$ ,  $*p \leq 0.05$ , ns stands for nonsignificant.

## Results

### 10.1.2 Rab11a is involved in UUKV infection

To complement siRNA-based infection assays, suggesting an involvement of Rab11a in UUKV infection, infection was additionally assessed in the presence of dominant negative or constitutively active mutants of Rab11a. To this end the GTP binding-defective Rab11a S25N mutant (dominant negative mutant), the GTPase-deficient Rab11a Q70L mutant (constitutively active mutant) and Rab11a WT (control), all tagged with the eGFP, were used. Additionally, the known UUKV entry factor Rab5 WT (control) and the GTP binding-defective Rab5 S34N mutant (dominant negative mutant), also tagged with eGFP, were expressed. Transfection of HeLa cells with eGFP-Rab11a WT/S25N/Q70L or eGFP-Rab5 WT/S34N expression plasmids allowed selection of efficiently transfected cells based on high eGFP expression. In accordance with previous findings in A549 and BSC40 cells<sup>37</sup>, which do not express DC-SIGN, UUKV-N protein expression in HeLa cells was also significantly reduced in the presence of Rab5 S34N in comparison to Rab5 WT expression (**Figure 13**). While expression of eGFP-Rab11a Q70L had no effect on infection, eGFP-Rab11a S25N significantly reduced the percentage of infected cells (**Figure 13**). Together these results indicate that Rab11a contributes to UUKV infection.

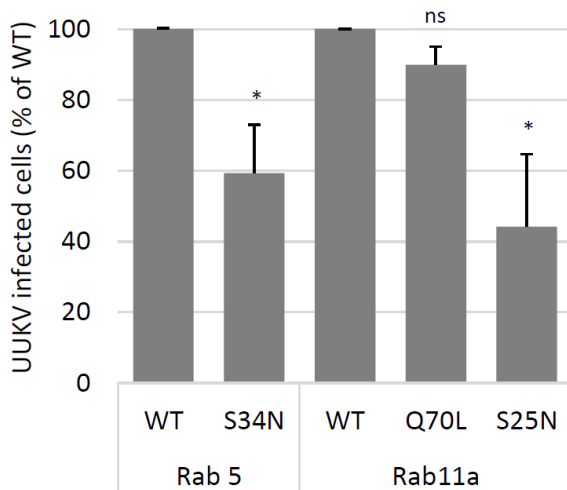


**Figure 13: Rab11a was involved in UUKV infection in HeLa cells**

HeLa cells were transfected with different expression plasmids coding for eGFP-Rab5 WT/S34N or eGFP-Rab11a WT/Q70L/S25N for 24 h and exposed to UUKV at a MOI of 1 for 8 h. After fixation and permeabilization, infected cells were immunostained for UUKV-N and analyzed by flow cytometry. Infection was assessed in cells expressing a high level of eGFP. Data were normalized to Rab5 WT or Rab11a WT and represent means  $\pm$  SD, n = 3, two-tailed unpaired t-test, \*\*\*p  $\leq$  0.001, \*\*p  $\leq$  0.01, \*p  $\leq$  0.05, ns stands for nonsignificant.

## Results

### 10.1.3 UUKV infection in Huh7 cells knocked out for key autophagy proteins

A human hepatocellular carcinoma cell line, Huh7, was chosen to determine, whether the role of autophagy-associated proteins in UUKV infection was cell specific. In addition, investigations were extended to additional autophagy factors. Huh7 cells are known to be sensitive to UUKV infection<sup>37</sup>. Knockout mutants were generated with the CRISPR/Cas9 genome-editing system. Efficient knockout was proven with immunostaining by WB (data not shown from our collaborator). In a flow cytometry-based infection assay UUKV-N was quantified 8 hours post infection (hpi), as described above (chapter 10.1.1). In accordance with our results from siRNA- and shRNA-mediated silencing approaches (**Figure 11b**, **Figure 12b**), *FIP200* or *ATG3* knock out had no effect on infection (**Figure 14a**). Likewise, knockout of *ATG5*, *ATG9L1*, *ATG14L* and *ATG16L1* did not impact UUKV infection (**Figure 14a**). Solely the knockout of *ATG7* significantly reduced UUKV-N expression (**Figure 14a**) and efficient knockout of *ATG7* was confirmed with immunostaining by WB (**Figure 14b**). In line with infection assays in HeLa cells (**Figure 11a**), these data from Huh7 cells supported a role of Atg7 in UUKV infection.

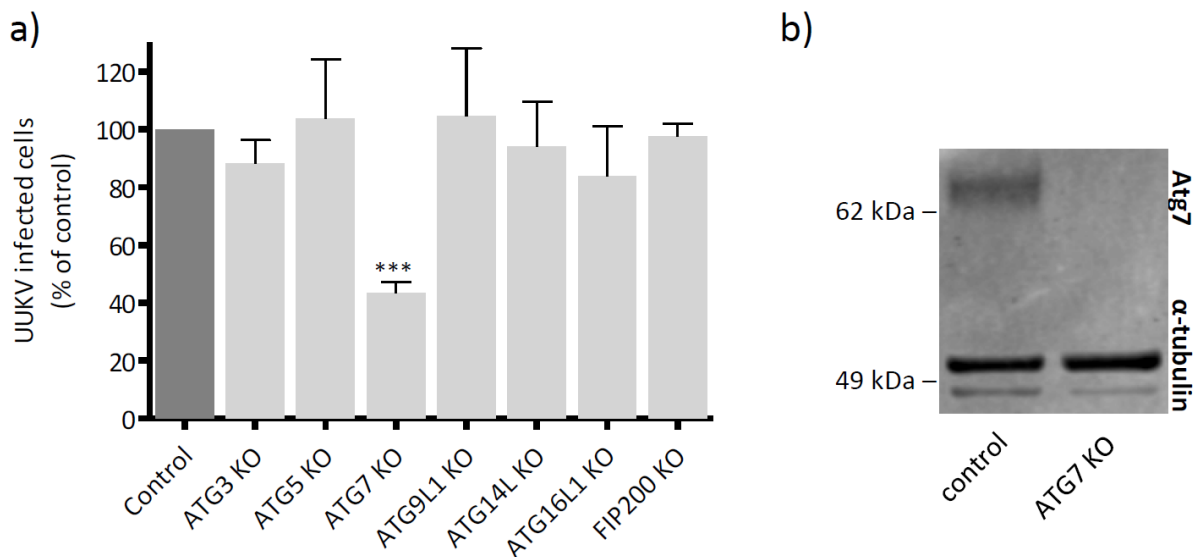


**Figure 14: Atg7 was involved in UUKV infection in Huh7 cells**

(a) Huh7 knockout (KO) cells were exposed to UUKV at a MOI of 0.5 for 8 h. After fixation and permeabilization, infected cells were immunostained for UUKV-N and analyzed by flow cytometry. Data were normalized to control and represent means  $\pm$  SD,  $n = 3$ , two-tailed unpaired t-test, \*\*\* $p \leq 0.001$ , \*\* $p \leq 0.01$ , \* $p \leq 0.05$ , ns stands for nonsignificant (b) Huh7 *ATG7* KO cells were lysed and analyzed by SDS-PAGE and WB.

## Results

Altogether these results show that only a subset of assessed autophagy-related proteins were involved in UUKV infection. The strongest effects on UUKV-N protein expression arose from Atg7 and Rab11a. In the second part of the thesis I therefore focused on the characterization of Atg7 and Rab11a functions in UUKV infection and examined during which step of infection these two proteins played a role.

### **10.2 Production of fluorescently labeled UUKV particles to study early virus-host cell interactions**

Fluorescently labeled viral particles are a useful tool to study UUKV binding to the host cell membrane and internalization by flow cytometry or to visualize viral particles by fluorescence microscopy to study intracellular trafficking. Envelope proteins of viral particles can be labeled nonspecifically with amine-reactive dyes coupled to various fluorophores. Here we used Alexa Fluor succinimidyl ester dyes that covalently bind free amine groups in the UUKV envelope glycoproteins G<sub>N</sub> and G<sub>C</sub> (**Figure 16a**).

In the labeling procedure, Alexa Fluor fluorescent dyes were added to the viral particle preparation in a defined molar ratio of dye to viral envelope glycoproteins. Hence, UUKV envelope glycoproteins G<sub>N</sub> and G<sub>C</sub> were semiquantified on a SDS-PAGE gel stained with coomassie blue to assess the molarity in the virus stock. The details of this procedure are explained in **Figure 15**.

## Results

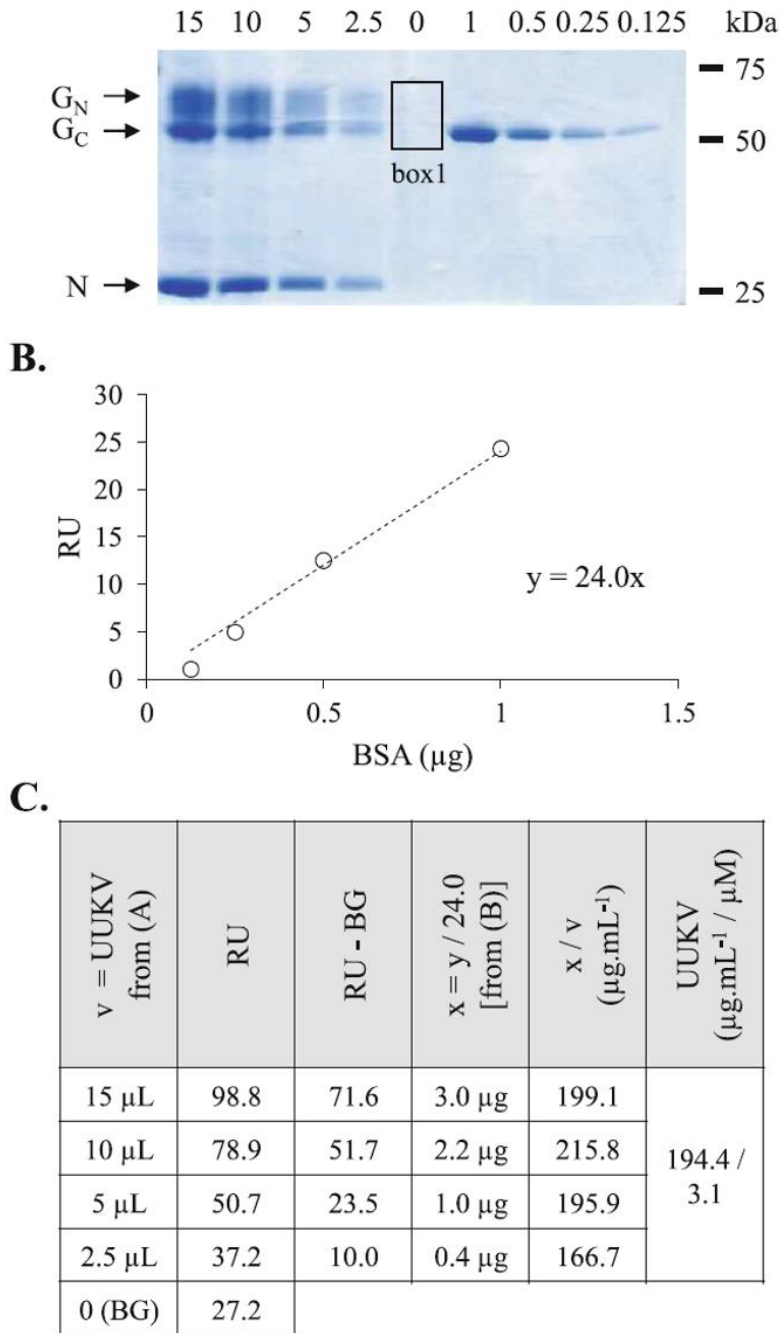


**Figure 15: Semiquantification of UUKV  $G_N$  and  $G_C$**

(a) UUKV particles, semipurified through a 25 % sucrose cushion, and BSA standards were analyzed under nonreducing conditions on SDS-PAGE and then by coomassie staining. The mean pixel intensity of each band was measured within the same defined square by using the software ImageJ. An empty well was used to define the background value (BG) and subtracted from all other values. (b) BSA standards were blotted to correlate the relative units (RU) with a protein quantity. An equation defining the linear trend line ( $y=24x$ ) was obtained. (c) UUKV glycoproteins were normalized against BSA. To this end the BG was subtracted from the values obtained in (a) (RU-BG). Next, the linear trend line obtained in (b) enabled quantification of  $G_N$  and  $G_C$ . To calculate the molarity, we considered  $G_N$  and  $G_C$  as one protein with a molecular weight of 63 400 Da i.e.  $(0.194 \text{ g/L}) / (63 \text{ 400 g/mol}) = 3.1 \times 10^{-6} \text{ mol/L}$ . The concentration (w/v) and molarity of  $G_N$  and  $G_C$  are indicated in the right column. Adapted from <sup>206</sup>

## Results

A protocol with optimized labeling conditions was established and is represented schematically in **Figure 16a**. Binding of Alexa Fluor fluorescent dyes to viral envelope proteins was allowed during 2 h incubation period on a rocker in dark at room temperature. The molar ratio of UUKV glycoproteins  $G_N$  &  $G_C$  to dye was 1 to 2.5. To purify viral particles, the virus solution was layered on top of a linear sucrose gradient, ranging from 15 % to 60 % sucrose (w/v). After ultracentrifugation for 90 minutes at 100 000 x g and 4°C, a milky band was visible at a density corresponding to 45 % sucrose. The band was extracted with a syringe and it was further analyzed to assess whether it contains infectious labeled viral particles. A transparent colored band, most likely comprising the unbound dye molecules, remained on top of the gradient, as expected.

Infectivity of labeled virus stocks was determined on BHK-21 cells by a focus forming unit assay. Titers between  $5 \times 10^7$  ffu/mL (focus forming units per milliliter) and  $4 \times 10^8$  ffu/mL were obtained. In-gel fluorescence of an SDS-PAGE gel was acquired and exhibited two fluorescent bands corresponding to  $G_N$  and  $G_C$  (**Figure 16b**), verifying that Alexa Fluor fluorescent dyes successfully bound to UUKV envelope glycoproteins. Subsequent Coomassie staining confirmed the presence of the three major structural proteins N,  $G_N$  and  $G_C$  (**Figure 16b**). The absence of a fluorescent band corresponding to UUKV-N proved that Alexa Fluor fluorescent dyes could not access and label this protein located inside viral particles, suggesting that viral particles were intact. **Figure 16c** shows confocal imaging of UUKV-AF568 on HeLa cells. After binding on ice (0 mpi) viral particles formed a ring with a certain distance to the nucleus, indicating that UUKV-AF568 was bound to the plasma membrane. At 30 mpi a fraction of virus particles was present in the nuclear periphery, suggesting that UUKV-AF568 successfully entered HeLa cells (**Figure 16c**). Summarizing, integrity and efficient fluorescent labeling of UUKV particles was demonstrated.

## Results

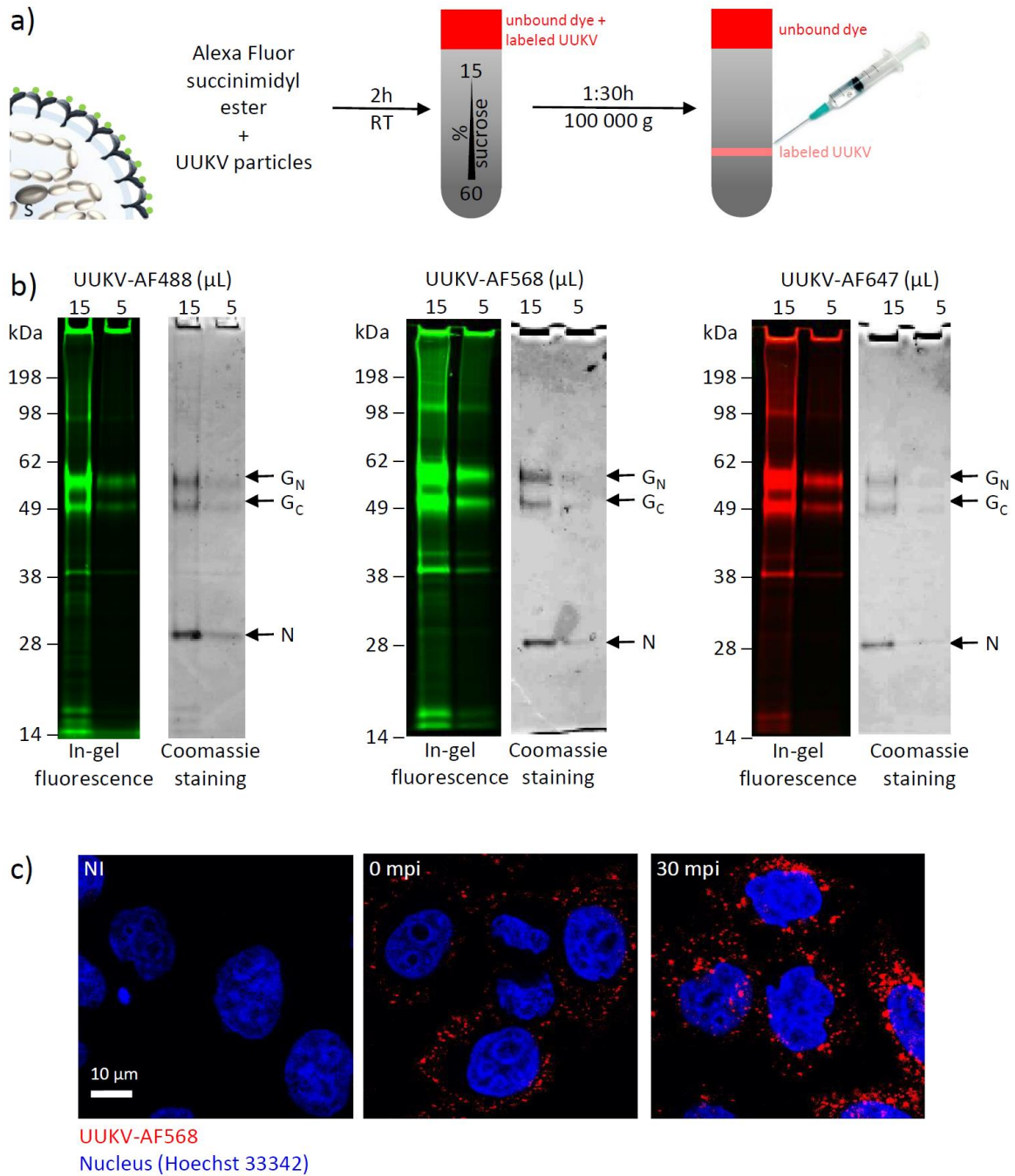


**Figure 16: UUKV labeling with Alexa Fluor succinimidyl ester dyes**

(a) UUKV particle labeled with Alexa Fluor dye (green) and schematic representation of the protocol for UUKV labeling with Alexa Fluor succinimidyl esters: Viral particles were semipurified through a 25% sucrose cushion and incubated with the Alexa Fluor dye for 2 h at room temperature (RT). The molar ratio of UUKV glycoproteins  $G_N$  &  $G_C$  to dye was 1 to 2.5. Viral suspension was loaded on a linear 15-60 % sucrose gradient and centrifuged for 90 minutes at 100 000 x g. The milky appearing band containing viral particles was extracted with a syringe. Left illustration adapted from <sup>206</sup> (b) Labeling of viral particles and particle integrity were analyzed under nonreducing conditions on SDS-PAGE for In-gel-fluorescence (acquired with Fluorescence image reader, **left panels**), and then by coomassie staining (**right panels**). (c) UUKV-AF568 was bound to HeLa cells on ice at a MOI of 2 for 1 h. After 0 minutes or 30 minutes at 37°C cells were fixed, exposed to the nuclear staining Hoechst and acquired with the confocal microscope.

## Results

### 10.3 The role of Rab11a in UUKV infection

Rab11a is a small GTPase involved in recycling endosomes trafficking and believed to form a platform for autophagosome assembly<sup>129</sup>. We showed that Rab11a was involved in infection of HeLa cells by UUKV (**Figure 11a, Figure 13**). To follow up on the specific function of Rab11a in UUKV infection we investigated its implication in the different steps of the viral life cycle from attachment to replication.

#### 10.3.1 Rab11a is involved in UUKV entry

In a first step, we determined whether Rab11a regulated UUKV infection during the viral entry process (from endocytosis up to fusion) or replication. To this end, I used an assay consisting in bypassing virus endocytosis. This means that release of the viral genome into the cytosol did not rely on the virus entry pathway through the endocytic machinery (**Figure 17a**). Viral particles were bound to the cells on ice and acid-activated fusion of the viral envelope with the plasma membrane was induced by acidification at pH5 and 37°C for 90 seconds. To prevent viral particles from entering cells via the natural infection route during the remaining 6 h infection period, ammonium chloride (NH<sub>4</sub>Cl) was then added to the incubation medium. The weak base NH<sub>4</sub>Cl instantaneously neutralized the pH in host intracellular vesicular compartments and thereby inhibited fusion of viral particles from endosomes.

The efficiency of the NH<sub>4</sub>Cl-containing incubation buffer was assessed by using a pH7 buffer for the 90 seconds treatment instead of the pH5 buffer. As illustrated in **Figure 17b-c** (left diagram), addition of 50 mM NH<sub>4</sub>Cl after pH7 treatment completely blocked infection at MOI 4 and MOI 10, proving that 50 mM NH<sub>4</sub>Cl was sufficient to prevent UUKV infection via the natural infection route. Hence, 50 mM NH<sub>4</sub>Cl could be applied during the 6 h incubation period after pH5 treatment, to assure that only those viral particles replicated, that have entered by plasma membrane fusion. At MOI 4 and 10, the infection level in cells silenced for Rab11a could be restored to the infection level in scrambled control cells when we bypassed the entry pathway (**Figure 17b-c**). Thus, Rab11a was not required for infection after fusion.

## Results

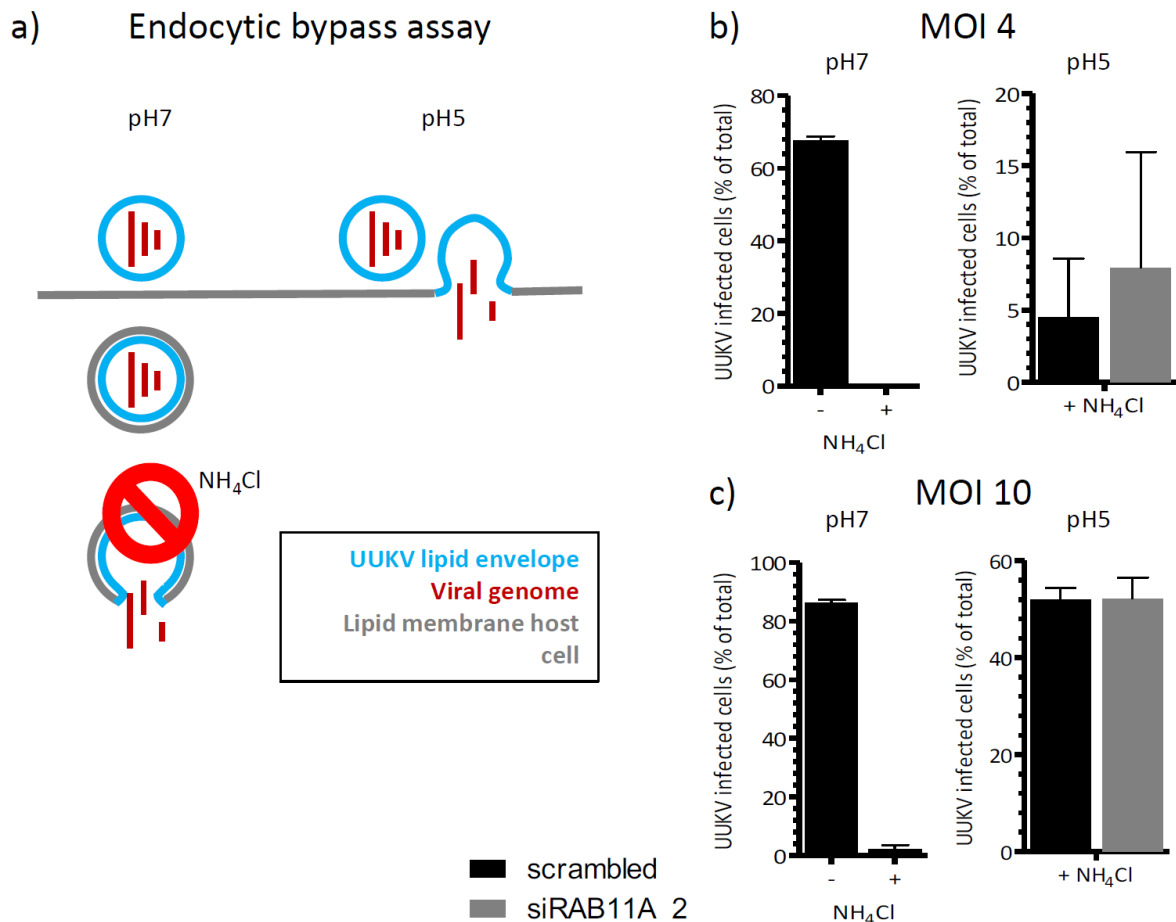


**Figure 17: Rab11a plays a role during UUKV entry in HeLa cells**

(a) Schematic representation of the endocytic bypass assay: Infection at pH7 occurred by receptor-mediated endocytosis and subsequent trafficking to acidic late endosomal compartments. Virus fusion from acidic compartments could be inhibited with the weak base ammonium chloride (NH<sub>4</sub>Cl). At pH5 UUKV envelope fused with the plasma membrane and the viral genome was released into the cytosol without the necessity of host entry factors. (b-c) HeLa cells were transfected with 20 nM siRNA targeting *RAB11A* for 72 h. UUKV was bound to HeLa cells on ice at a MOI of 4 (b) or 10 (c) for 1 h. Cells were exposed to pH5 or pH7 buffer for 90 seconds at 37°C and incubated for 5 h in the presence or absence of 50 mM NH<sub>4</sub>Cl. After fixation and permeabilization, infected cells were immunostained for UUKV-N and analyzed by flow cytometry.

The viral entry route of UUKV before fusion and virus genome release into the cytosol, can be subdivided into three steps: binding, internalization and endosomal transport to a compartment with acidic luminal pH where fusion occurs. To precisely define in which viral entry step Rab11a was involved, we addressed them individually.

## Results

### 10.3.2 Rab11a does not modify expression of the UUKV receptor DC-SIGN

Following the virus entry pathway, we started by assessing UUKV receptor expression in the absence of Rab11a. The cell surface expression of DC-SIGN was assessed after immunostaining by flow cytometry. Silencing with three nonoverlapping siRNAs targeting *RAB11A* had no effect on cell surface expression of DC-SIGN in comparison to transfection with a scrambled siRNA control (**Figure 18a-b**). As expected, almost no expression could be detected in the parental HeLa cells (**Figure 18a-b**) lacking endogenous DC-SIGN expression. Hence, silencing Rab11a did not modify DC-SIGN expression.

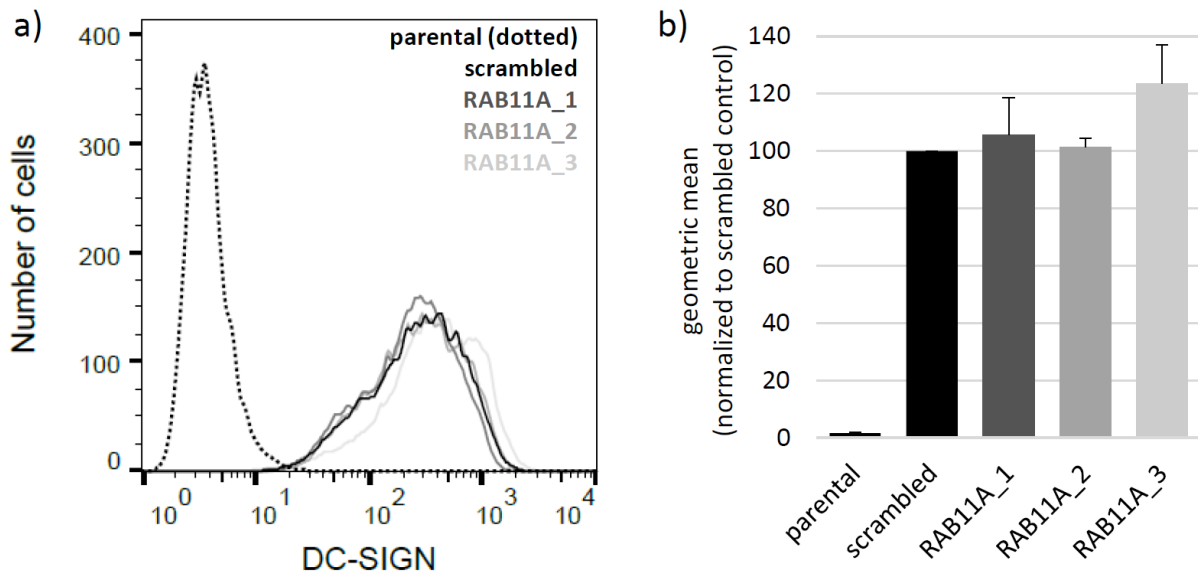


**Figure 18: DC-SIGN expression was not modified on HeLa cells following Rab11a silencing**

(a) HeLa cells were transfected with 20 nM siRNA targeting *RAB11A* for 48 h, immunostained for DC-SIGN and analyzed by flow cytometry. DC-SIGN expression of single representative samples was plotted in a histogram. (b) The average of geometric mean values  $\pm$  SD for DC-SIGN expression were normalized to scrambled siRNA,  $n = 2$ .

### 10.3.3 Rab11a is not involved in UUKV binding to HeLa cells

Binding efficiency to HeLa cells was determined with fluorescently labeled viral particles by flow cytometry. The cells were first transfected with si*RAB11A* or a scrambled siRNA and exposed to UUKV-AF647 with MOI 0.1, 1 and 10. Binding capacity to cells silenced for Rab11a and transfected with a scrambled siRNA was similar and increased with increasing

## Results

MOIs (**Figure 19a-b**). These results suggested that a lack in Rab11a expression did not impact UUKV binding to HeLa cells.

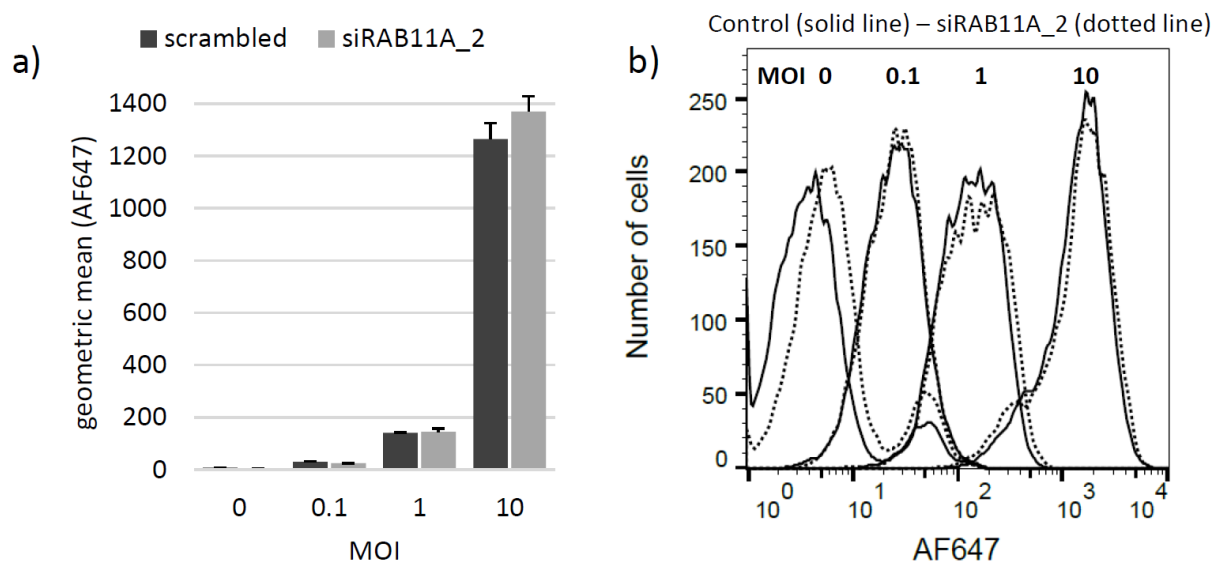


**Figure 19: Silencing of Rab11a did not impair UUKV binding to HeLa cells**

(a) HeLa cells were transfected with 20 nM siRNA targeting *RAB11A* for 72 h. UUKV-AF647 was bound to the cells on ice for 1 h 30 minutes and analyzed by flow cytometry. Data represent the average of geometric mean values for AF647 expression  $\pm$  SD,  $n = 1$ , two-tailed unpaired t-test, \*\*\* $p \leq 0.001$ , \*\* $p \leq 0.01$ , \* $p \leq 0.05$ , ns stands for nonsignificant. (b) Virus binding of single representative samples was plotted in a histogram.

### 10.3.4 Rab11a is not involved in internalization of UUKV particles into HeLa cells

To study internalization of UUKV particles, we made use of the quenching effect of Trypan blue on green fluorescent dyes. HeLa cells were infected with UUKV-AF488 and each sample was acquired twice, first in absence and then in presence of Trypan blue. As Trypan blue is not membrane permeant, it does not enter living cells. Consequently, only the fluorescence signal of UUKV-AF488 on the plasma membrane can be quenched, and internalized viral particles still emit green fluorescence. The proportion of internalized viral particles could be calculated by forming the ratio of the signal after and before addition of Trypan blue.

As a positive control UUKV-AF488 was bound to HeLa cells on ice. Under these conditions, addition of 0.01 % Trypan blue reduced the fluorescence signal for AF488 by 85 % (**Figure 20a**). These results confirmed that the applied concentration of Trypan blue quenched the

## Results

fluorescence signal from UUKV-AF488 that were bound to the plasma membrane. The residual signal for the cells transfected with a scrambled siRNA or siRNA against Rab11a was considered background and subtracted from all samples (applies for **Figure 20b**).

To determine the percentage of viral particles internalized into HeLa cells, infection was allowed for 40 minutes at 37°C after binding on ice. Addition of Trypan blue caused a relative reduction in AF488 fluorescence signal to 12 % in presence of a scrambled siRNA and a reduction to 10 % after silencing Rab11a (**Figure 20b**). These results indicated that the percentage of internalized viral particles was comparable in HeLa cells transfected with a scrambled or Rab11a-targeting siRNA, and suggested that Rab11a did not interfere with UUKV uptake.

Binding assays (**Figure 19, Figure 28**) illustrated that binding of fluorescently labeled viral particles to cells could be detected at MOIs between 1 and 2.5. This range was considerably lower than the MOI 25 used for this internalization assay (**Figure 20**). Application of a high MOI could saturate the infection. Hence, nonspecific internalization mechanisms potentially disguised Rab11a-dependence as a rate-limiting step for viral internalization. It will therefore be important to repeat the internalization assay with a lower MOI.

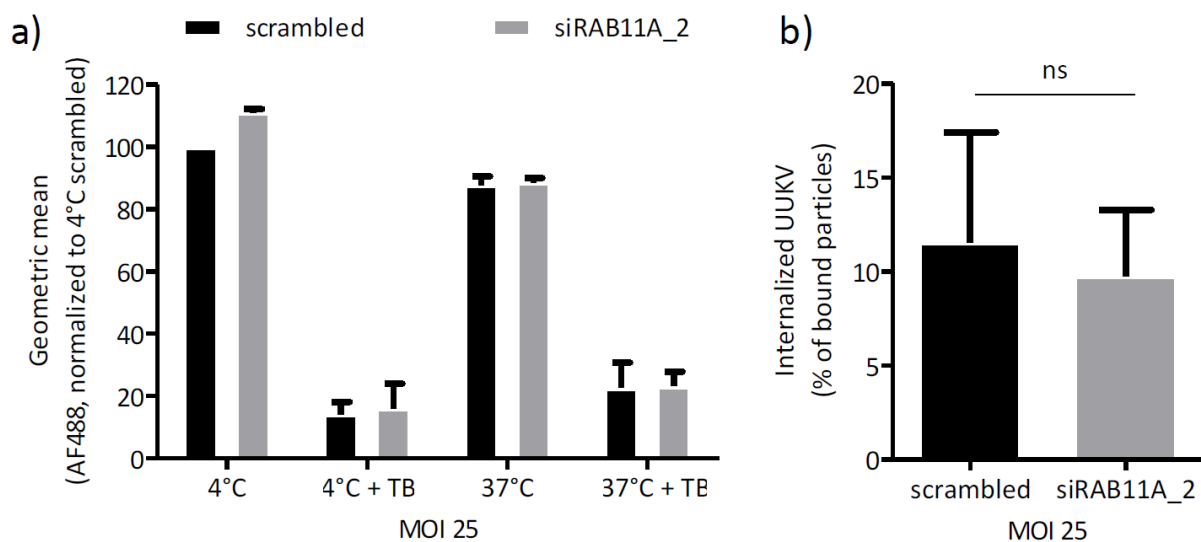


**Figure 20: UUKV-AF488 internalization efficiency was not impacted by Rab11a silencing in HeLa cells**

(a-b) HeLa cells were transfected with 20 nM siRNA targeting *RAB11A* for 72 h. UUKV-AF488 was bound to the cells on ice at a MOI of 25 for 1 h 30 minutes. After 40 minutes at 37°C each sample was acquired by flow cytometry first without, then with 0.01 % TB (Trypan blue). Data represent means  $\pm$  SD, n = 2, two-tailed unpaired t-test, \*\*\*p  $\leq$  0.001, \*\*p  $\leq$  0.01, \*p  $\leq$  0.05, ns stands for nonsignificant.

## Results

### 10.3.5 Rab11a silencing delays UUKV fusion

To assess virus intracellular trafficking, a penetration kinetic was performed in the presence and absence of Rab11a. In this drug-addition time course, viral particles were bound to HeLa cells on ice and infection was allowed by a temperature shift to 37°C. NH<sub>4</sub>Cl was added at different time points following infection to block the fusion of all viral particles that entered into the endosomal system but not yet penetrated. Infection was measured by monitoring newly synthesized protein N after immunofluorescence staining and analysis by flow cytometry.

According to previous results, UUKV infection was decreased by around 70 % in cells transfected with a siRNA targeting *RAB11A* compared to a scrambled control (**Figure 11a, Figure 21**). As expected, the relative infection level in cells transfected with scrambled siRNA was higher the later NH<sub>4</sub>Cl was added. When NH<sub>4</sub>Cl was added 80 mpi, around 40 % of the cells were infected relative to those not treated with NH<sub>4</sub>Cl. This was in stark contrast to cells silenced for Rab11a. Even when NH<sub>4</sub>Cl was added 80 mpi, a relative infection level of only 1 % could be reached. These results indicate that downregulation of Rab11a delays productive intracellular trafficking of UUKV.

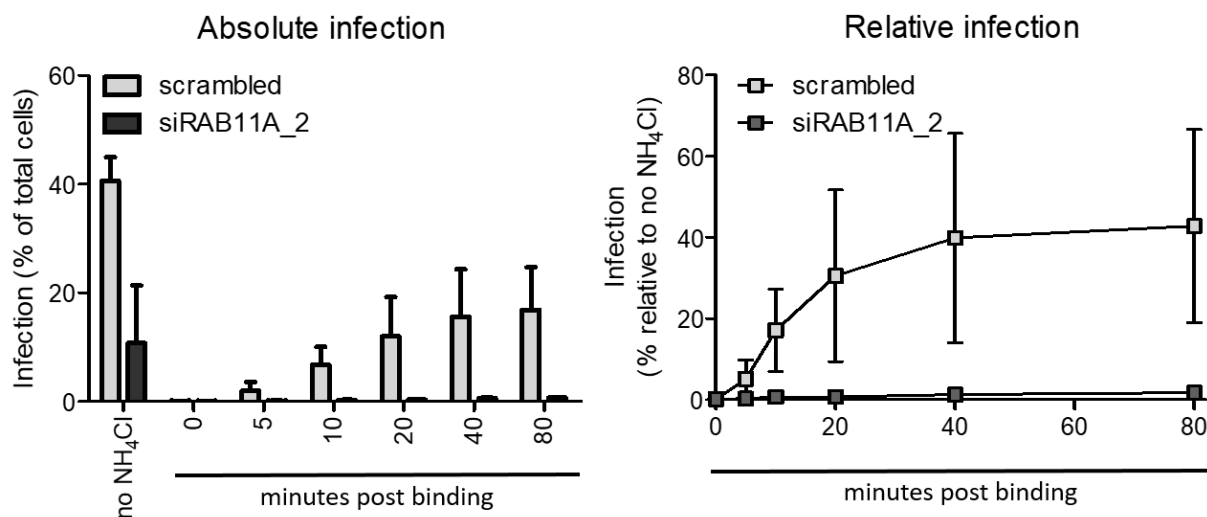


Figure 21: **siRAB11A** delays UUKV fusion

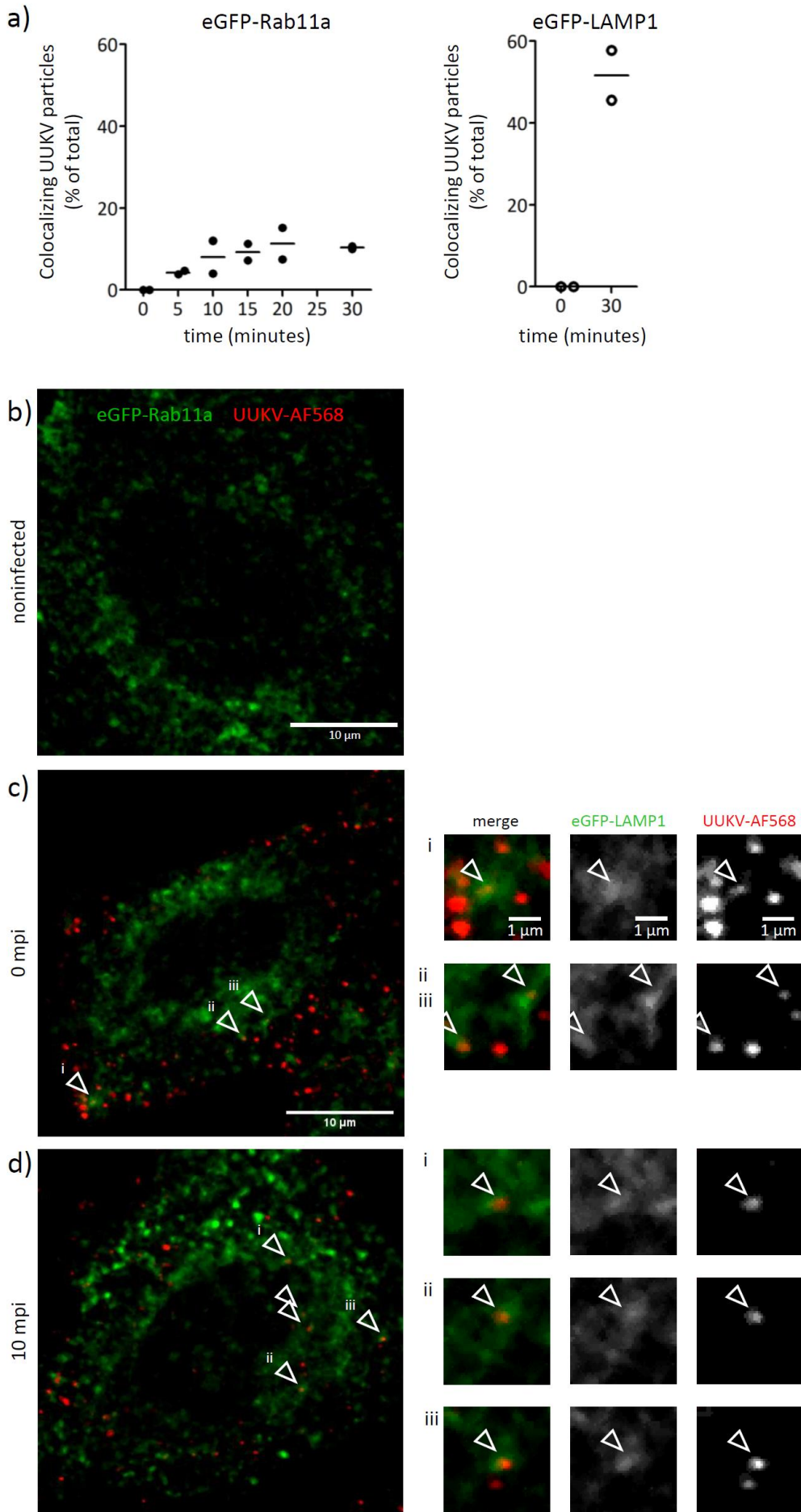
HeLa cells were transfected with 20 nM siRNA targeting *RAB11A* for 72 h. UUKV was bound to the cells on ice at a MOI of 0.5 for 1 h. During 6 h incubation at 37°C, NH<sub>4</sub>Cl was added after different time periods. After fixation and permeabilization, infected cells were immunostained for UUKV-N and analyzed by flow cytometry.

## Results

### 10.3.6 A minor fraction of UUKV-AF568 associates with eGFP-Rab11a positive vesicles

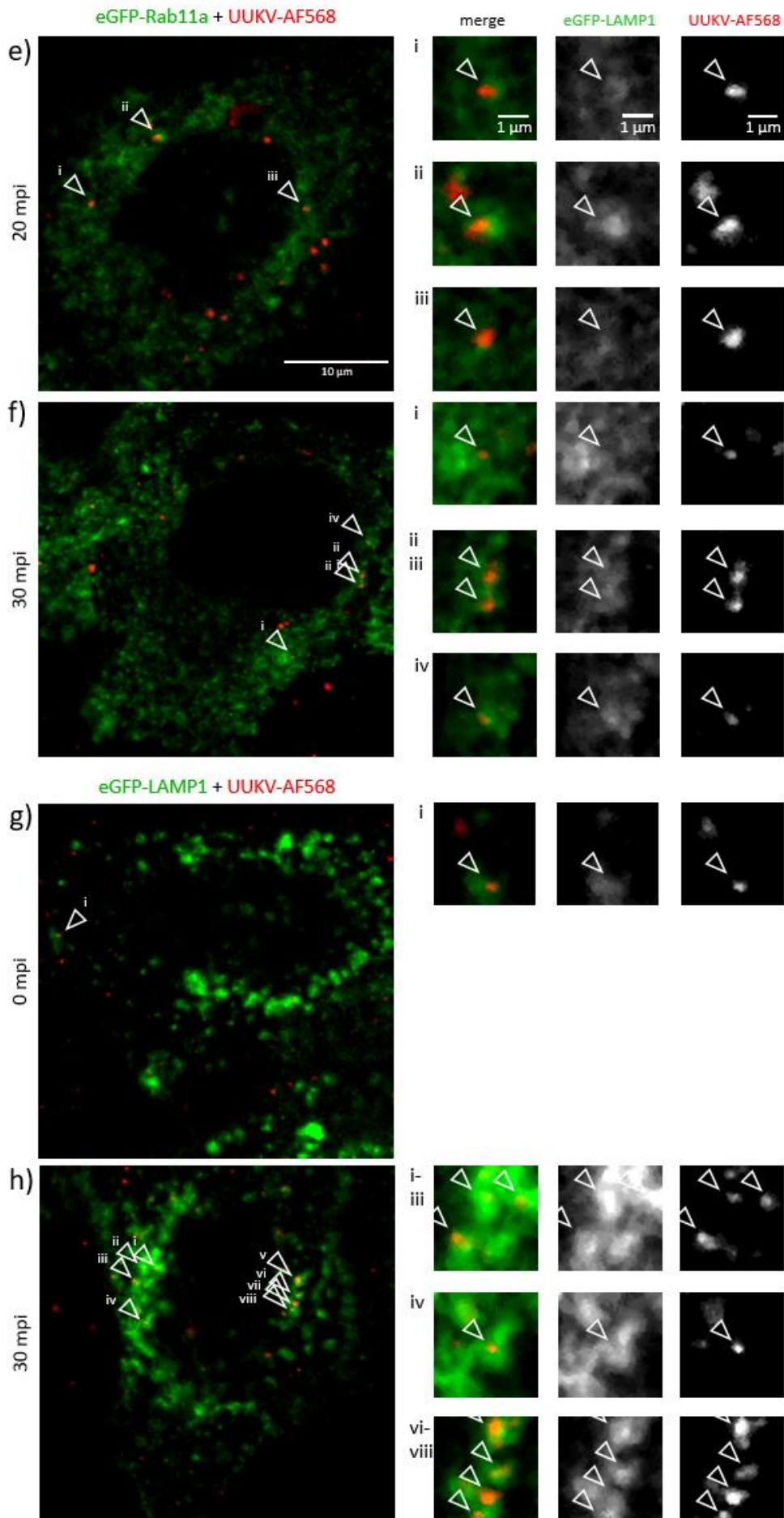
Preceding experiments suggest Rab11a to play a role in UUKV entry. Thereupon we wanted to ascertain whether viral particles enter Rab11a-decorated vesicles during viral entry. Infection of eGFP-Rab11a WT-expressing HeLa cells was synchronized by virus binding on ice. Infected cells were then shifted to 37°C to permit virus entry for different periods of time. Viral particles were identified with the spot detector of the bioimage analysis program Icy<sup>209</sup> and the percentage of viral particles colocalizing with Rab11a in each cell was quantified, based on eGFP-Rab11a signal intensity within viral spots. Upon binding on ice (0 mpi) 5 % UUKV-AF568 particles colocalized with eGFP-Rab11a (**Figure 22a+c**). This was considered as background and was therefore subtracted from all samples. After 5 minutes at 37°C, 4 % viral particles colocalized with eGFP-Rab11a. After 10 minutes at 37°C a plateau, amounting to 10 % colocalization, was reached (**Figure 22a+d-f**). Simultaneously assessed colocalization between UUKV-AF568 and eGFP-LAMP1 amounted to 5 % at 0 mpi. After background subtraction, 51 % UUKV particles colocalize with eGFP-LAMP1 at 30 minutes after the shift to 37°C (**Figure 22a+g-h**). Taken together, these results suggest that only a minority of viral particles (maximum 10 %) associate with Rab11a-positive vesicles, thus a lot less than associating with eGFP-LAMP1.

## Results



The legend for figure 22 can be found on the following pages

## Results



The legend for figure 22 can be found on the following page

## Results

**Figure 22: About 10 % UUKV-AF568 colocalize with eGFP-Rab11a**

(a) HeLa cells were transfected with an eGFP-Rab11a or eGFP-LAMP1 expression plasmid for 24 h. UUKV-AF568 at a MOI of 0.5 was bound to the cells on ice. Cells were shifted to 37°C and NH<sub>4</sub>Cl was added after different periods of time. After 6 h incubation, the cells were fixed at 37°C and imaged with the confocal microscope. Percentage of UUKV-AF568 colocalizing with eGFP-Rab11a or eGFP-LAMP1 per cell n = 13-27 for each sample. Data represent means ± SD, n = 2. (b-f) Representative images of HeLa cells transfected with eGFP-Rab11a and infected for different periods of time. (g-h) Representative images of HeLa cells transfected with eGFP-LAMP1 and infected for different periods of time. Scale bar = 10 μM or 1 μM on magnified panels.

### 10.3.7 Rab11a – extending investigations to other cell lines, viruses and protein family members

Up to this point all experiments investigating the role of Rab11a in viral infection were performed with UUKV in HeLa cells. We next investigated whether our findings were specific to these HeLa cells expressing DC-SIGN (HeLa). To this end, we assessed the impact of silencing Rab11a on infection in parental HeLa (lacking the expression of DC-SIGN), HEK 293T, and Huh7 cells. All are known to be sensitive to UUKV<sup>37</sup>. Cells were transfected with siRNA against *RAB11A* and then exposed to UUKV. Infected cells were subjected to immunofluorescence staining and analyzed by flow cytometry. Infection was decreased by roughly 50 to 75 %, depending on the cell line (Figure 23).

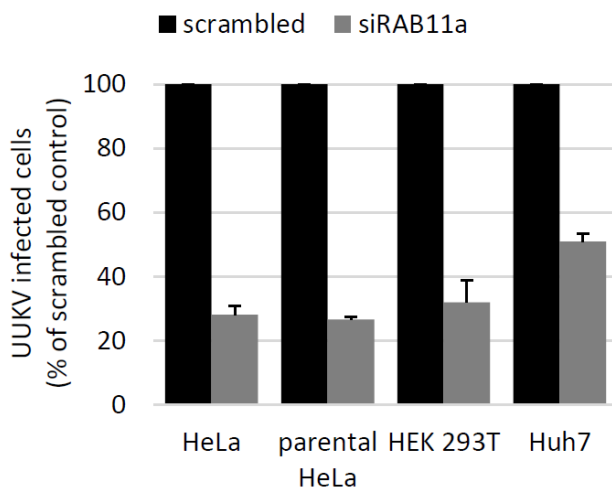


**Figure 23: UUKV relies on the host factor Rab11a for the infection of multiple cell lines**

Different cell lines were transfected with 20 nM siRNA targeting *RAB11A* for 72 h and exposed to UUKV at a MOI of 0.125 (HeLa), 4 (parental HeLa), 1 (HEK 293T), 0.5 (Huh7) for 6 h. In contrast to HeLa cells, parental HeLa cells did not express the UUKV receptor DC-SIGN. After fixation and permeabilization, infected cells were immunostained for UUKV-N and analyzed by flow cytometry. Data were normalized to scrambled siRNA and represent mean ± SD, n = 2.

## Results

To evaluate whether Rab11a could play a role in infectious entry of unrelated or related viruses, we investigated the early penetrating alphavirus Semliki Forest (SFV), the late penetrating orthomyxovirus Influenza A (strain Puerto Rico 8, IAV) and the phlebovirus Rift Valley fever (RVFV) by using RVFV  $\Delta$ NSs-eGFP (**Figure 24**). In this RVFV strain the major virulence factor NSs<sup>210</sup> was replaced by eGFP and could therefore be used under BSL-2 conditions. Infection was assessed by flow cytometry as described previously (chapter 10.1.2), using eGFP as readout for RVFV or after immunostaining against the viral nucleoprotein (IAV-N) and envelope glycoprotein E2 (SFV-E2) for IAV and SFV, respectively. Upon silencing of the vacuolar ATPase with siATP6V1A infectivity of all viruses drops dramatically, confirming their dependence on vacuolar acidification for infection, as reported previously<sup>71,211,212</sup>. Contrasting with IAV, SFV, and RVFV  $\Delta$ NSs-eGFP, only infection by UUKV was significantly reduced upon Rab11a silencing, i.e. by 58 %. These results show that Rab11a does not play an important role in infection by IAV, SFV, and even the closely related phlebovirus RVFV.

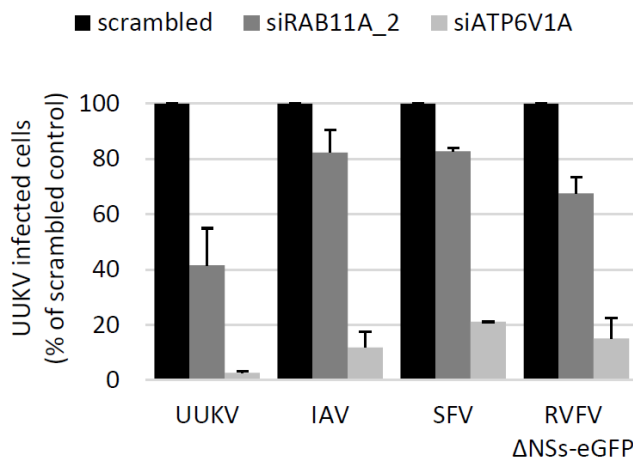


**Figure 24: Rab11a was not important for infection by IAV, SFV and RVFV**

HeLa cells were transfected with 20 nM siRNA targeting *RAB11A* for 72 h and exposed to UUKV, SFV, IAV and RVFV  $\Delta$ NSs-eGFP at a MOI of 0.1 for 6 h. After fixation and permeabilization, infected cells were immunostained for UUKV-N and analyzed by flow cytometry. Data were normalized to scrambled siRNA and represent mean  $\pm$  SD, n = 2. UUKV = Uukuniemi virus, IAV = Influenza A virus, SFV = Semliki Forest virus, RVFV = Rift Valley fever virus.

Rab11b is an isoform of Rab11a with partially overlapping functions. To evaluate its effect on UUKV infection, a flow cytometry-based infection assay was performed. Silencing of *RAB11B* with two nonoverlapping siRNAs, reduced UUKV-N protein replication by around 44 % and

## Results

58 % (**Figure 25a**). As positive control siRNAs targeting *RAB11A* and *ATP6V1A* significantly reduced UUKV infection, siRNAs were successfully delivered into HeLa cells. But assessment of si*RAB11B* silencing efficiency would be a prerequisite to conclude on the protein's role in UUKV infection. A silencing approach targeting *RAB11A* and *RAB11B* simultaneously, reduced UUKV-N protein replication by 45 % and 72 % (**Figure 25a**). This effect on infection was not significantly different from the single siRNAs. To evaluate the effect of Rab11b silencing on DC-SIGN expression, cells were immunostained for DC-SIGN after siRNA transfection. Neither si*RAB11B\_1* nor si*RAB11B\_2* modified the DC-SIGN expression level as compared to the scrambled siRNA (**Figure 25b**). These results suggest that Rab11b was not involved in DC-SIGN maturation and secretion to the plasma membrane.

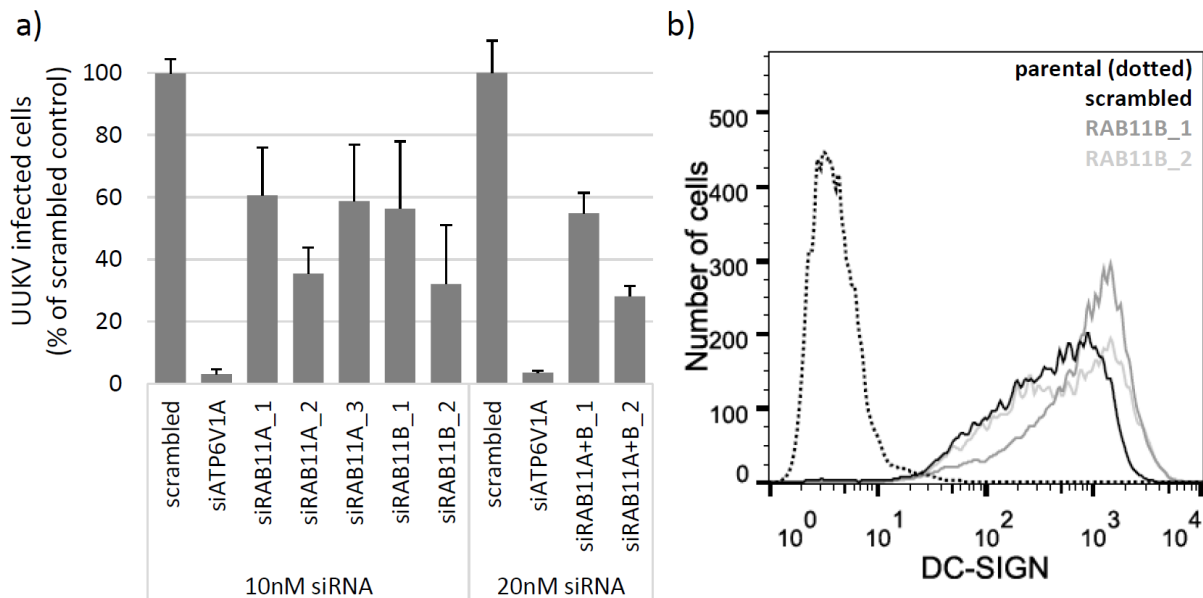


**Figure 25: Rab11b was involved in UUKV infection and has no effect on DC-SIGN expression in HeLa cells**

**(a)** HeLa cells were transfected with 10 nM siRNA targeting *RAB11A*, *RAB11B*, both, or *ATP6V1A* for 72 h and exposed to UUKV at a MOI of 0.125 for 6 h. After fixation cells were immunostained for UUKV-N and analyzed by flow cytometry. Data were normalized to scrambled control and represent means  $\pm$  standard deviation (SD),  $n = 2$  **(b)** HeLa cells were transfected with 10 nM siRNA targeting *RAB11B* for 72 h, immunostained for DC-SIGN and analyzed by flow cytometry. DC-SIGN expression of single representative samples was plotted in a histogram.  $n = 1$ .

Summarizing all experiments aiming to determine the role of Rab11a in viral infections, we demonstrated that Rab11a played an important role in UUKV infection, most likely during trafficking of viral particles through the endocytic machinery. This effect was observed in

## Results

different cell lines and appeared specific to UUKV as compared to other tested viruses, including the related phlebovirus RVFV. The Rab11 subfamily member Rab11b also played an important role in UUKV infection.

## Results

### 10.4 The role of Atg7 in UUKV infection

In addition to Rab11a, we also found a key autophagy-related protein that is involved in the phagophore elongation, Atg7<sup>213</sup>, to be important for UUKV infection in HeLa and Huh7 cells (**Figure 11, Figure 14**). With the same approaches used to characterize the role of Rab11a in infection, we also investigated the importance of Atg7 in UUKV attachment, internalization, intracellular trafficking and replication.

#### 10.4.1 Atg7 is involved in UUKV entry

As a first step we used the endocytic bypass assay to differentiate whether Atg7 was involved in UUKV entry or replication (**Figure 17a**). The classical entry pathway (at pH7) was clearly blocked upon addition of 50 mM NH<sub>4</sub>Cl. This assured that infection in presence of pH5 buffer with subsequent exchange for complete medium with NH<sub>4</sub>Cl solely resulted from viral particles that have entered by fusion from the plasma membrane. The N protein level upon acid-activated fusion (at pH5) was comparable in Huh7 control cells and Huh7 *ATG7* KO cells, meaning that Atg7 was not required for viral replication. From these results, combined with those showing that knockout of *ATG7* significantly impaired UUKV infection (**Figure 14**), we concluded that Atg7 is involved in UUKV entry and not viral replication.

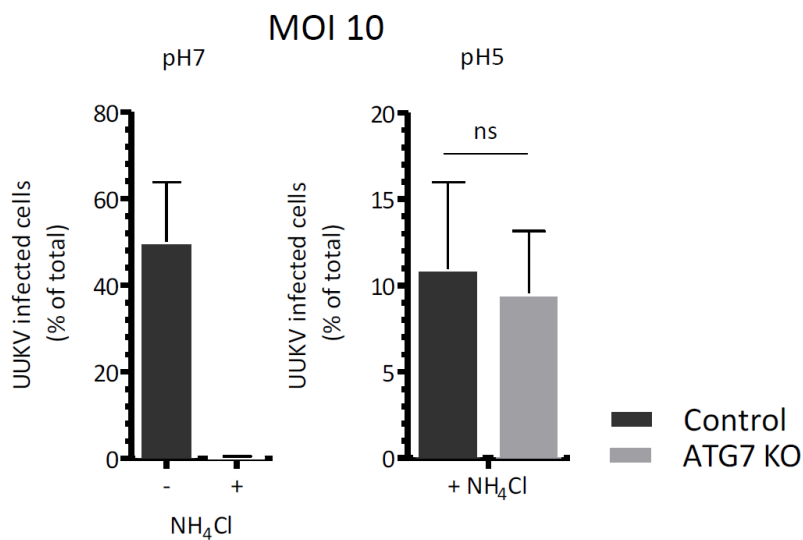


**Figure 26: Atg7 played a role in UUKV entry into Huh7 cells**

UUKV was bound to Huh7 cells on ice at a MOI of 10 for 1 h. Cells were treated for 60 seconds with pH5 or pH7 buffer at 37°C and infection was allowed for 8 h in the presence or absence of NH<sub>4</sub>Cl. After fixation and permeabilization, infected cells were immunostained for UUKV-N and analyzed by flow cytometry. Data represent mean ± SD, n = 2, two-tailed unpaired t-test, \*\*\*p ≤ 0.001, \*\*p ≤ 0.01, \*p ≤ 0.05, ns stands for nonsignificant.

## Results

To define during which step in viral entry Atg7 played a role, assays specifically addressing receptor expression, binding and internalization were performed.

### 10.4.2 Atg7 does not perturb expression of the UUKV receptor DC-SIGN

To assess whether Atg7 silencing impaired the expression of the UUKV receptor DC-SIGN at the cell surface<sup>54</sup>, siRNA-transfected cells were immunostained against the lectin and analyzed by flow cytometry. Parental HeLa cells, lacking endogenous expression of DC-SIGN, were used as negative control. HeLa cells transfected with a scrambled siRNA were used as a positive control. HeLa cells transfected with all three nonoverlapping siRNAs silencing *ATG7* (**Figure 11b**) resulted in a DC-SIGN expression level similar to HeLa cells transfected with scrambled siRNAs (**Figure 27a-b**). These results suggest no modification of the DC-SIGN expression level due to silencing Atg7. Consequently, the reason for a reduced UUKV infection rate upon Atg7 silencing was not related to a decrease in the number of receptor molecules at the cell surface.

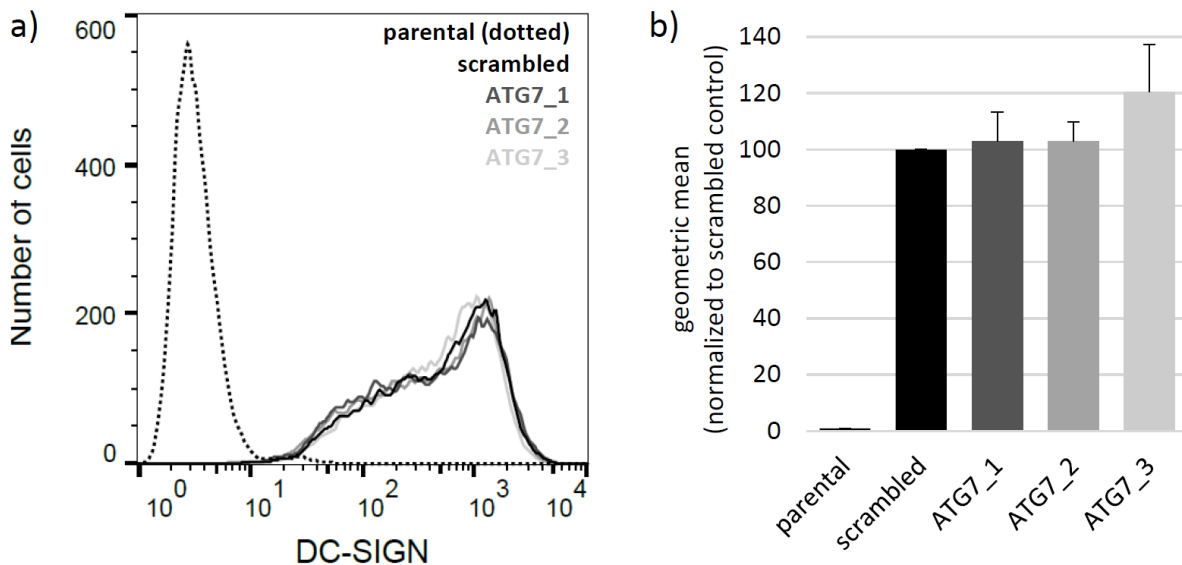


**Figure 27: DC-SIGN expression was not modified by siATG7 in HeLa cells**

(a) HeLa cells were transfected with 10 nM siRNA targeting *ATG7* for 48 h, immunostained for DC-SIGN and analyzed by flow cytometry. DC-SIGN expression of single representative samples was plotted in a histogram. (b) The average of geometric mean values  $\pm$  SD for DC-SIGN expression were normalized to scrambled siRNA, n = 3.

## Results

### 10.4.3 Atg7 does not play a major role in UUKV binding to Huh7 cells

The ability of viral particles to bind Huh7 cells was assessed with fluorescently labeled viral particles by flow cytometry. UUKV-AF488 was allowed to attach to Huh7 cells for 1 h 30 minutes on ice. At MOI 0.1, 0.5, and 2.5, binding efficiency to Huh7 control cells and Huh7 *ATG7* KO cells was similar (**Figure 28a-b**). At MOI 12.5 binding efficiency to Huh7 *ATG7* KO cells was slightly decreased by 26 % (**Figure 28a-b**), suggesting a minor implication of *Atg7* in UUKV attachment to Huh7 cells when high MOIs were used. However we assessed *Atg7* silencing on UUKV infection at MOIs below 1 (**Figure 11a, Figure 14a**), under conditions in which no difference in virus binding was observed. Consequently, the *Atg7*-mediated effect on infection was not due to limited binding in the range of MOIs used for infection.

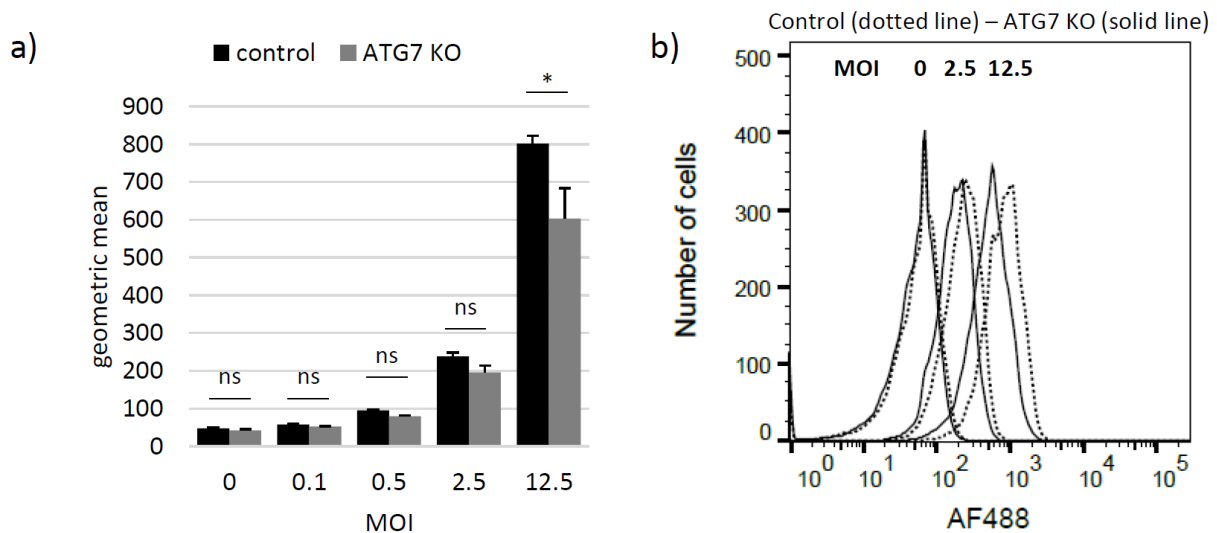


**Figure 28: Atg7 had no major impact on UUKV-AF488 binding to Huh7 cells**

(a) UUKV-AF488 was bound to Huh7 cells on ice for 1 h 30 minutes and analyzed by flow cytometry. Data represent average geometric mean values for AF488 expression  $\pm$  SD,  $n = 3$ , two-tailed unpaired t-test, \*\*\* $p \leq 0.001$ , \*\* $p \leq 0.01$ , \* $p \leq 0.05$ , ns stands for nonsignificant. (b) Virus binding of single representative samples was plotted in a histogram.

### 10.4.4 Atg7 is not involved in internalization of UUKV particles into Huh7 cells

As described previously, internalization could be assessed in a Trypan blue-based infection assay (chapter 10.3.4). UUKV-AF488 particles were bound to Huh7 cells on ice. Addition of Trypan blue resulted in a quenching of the green fluorescence (**Figure 29a**). The residual signal was considered background and subtracted from all measurements. After 40 minutes warming,

## Results

15 % and 19 % of the bound particles were internalized into Huh7 control and *ATG7* KO cells, respectively. Together these results indicated that *Atg7* did not play a role in the uptake of UUKV particles. Binding assays demonstrated that application of a lower MOI between 1 and 2.5 would have been sufficient to detect viral particles (**Figure 19**, **Figure 28**). As mentioned in chapter 10.3.4, application of a high MOI could disguise *Atg7*-dependence as a rate limiting step due to nonspecific internalization mechanisms. It is therefore advisable to perform this assay with a lower MOI.

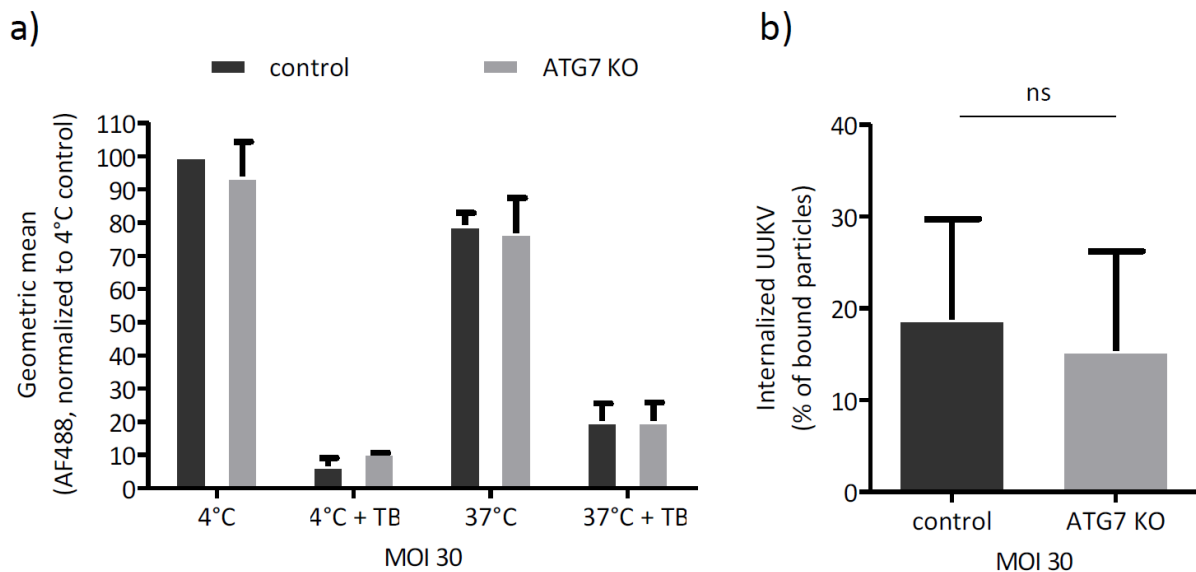


**Figure 29: *ATG7* knockout did not impact UUKV internalization into Huh7 cells**

(a-b) UUKV-AF488 was bound to Huh7 cells on ice at a MOI of 30 for 1 h 30 minutes. After 40 minutes at 37°C each sample was acquired by flow cytometry first without, then with 0.01 % Trypan blue. TB = Trypan blue. Data represent means  $\pm$  SD,  $n = 2$ , two-tailed unpaired t-test, \*\*\* $p \leq 0.001$ , \*\* $p \leq 0.01$ , \* $p \leq 0.05$ , ns stands for nonsignificant.

Summarizing all experiments on the role of *Atg7* in UUKV infection we demonstrated that *Atg7* was merely involved in intracellular trafficking of viral particles.

### 10.5 A cell line expressing blue fluorescent protein-tagged LC3 to study the role of autophagosomes in UUKV infection

To follow up our investigation into a potential role of autophagy in UUKV infection, we established a cell line stably expressing LC3, an autophagic marker, tagged with the blue fluorescent protein (BFP-LC3). LC3 appears as an accumulation of punctate structures within

## Results

autophagic membranes, which can be visualized by fluorescence microscopy when BFP-LC3 is expressed<sup>131</sup>.

### 10.5.1 Fluorescently labeled LC3 decorates autophagosomes in HeLa BFP-LC3 stable cell line

HeLa cells stably expressing DC-SIGN were transduced with lentiviruses to stably express BFP-LC3. To select cells that were transduced, we used the antibiotic blasticidin as lentiviruses encode a resistance gene. HeLa cells presented a diffuse blue fluorescent signal and/or punctate structures when they were imaged with a confocal microscope (**Figure 30**), demonstrating successful transduction and expression of BFP-LC3.

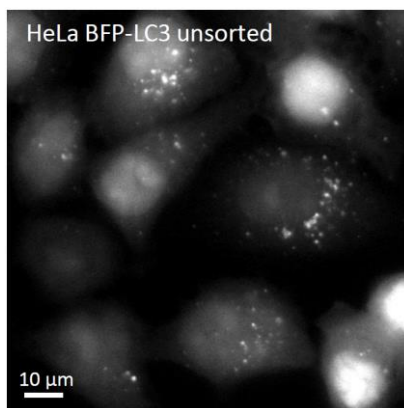


*Figure 30: HeLa BFP-LC3 stable cell line heterogeneously expressed LC3.*

Unsorted HeLa BFP-LC3 cells were grown on a coverslip, fixed and imaged with a wide-field fluorescent microscope. Scale bar = 10 μM.

However, the heterogeneous level of LC3 expression, from low to strong (**Figure 30**), made it difficult to quantify puncta, a typical marker for autophagic activity. To obtain a cell line homogeneously expressing LC3 at the single cell level, low and high expressers of BFP-LC3 were sorted by fluorescence activated cells sorting using FACS Diva (**Figure 31**).

## Results

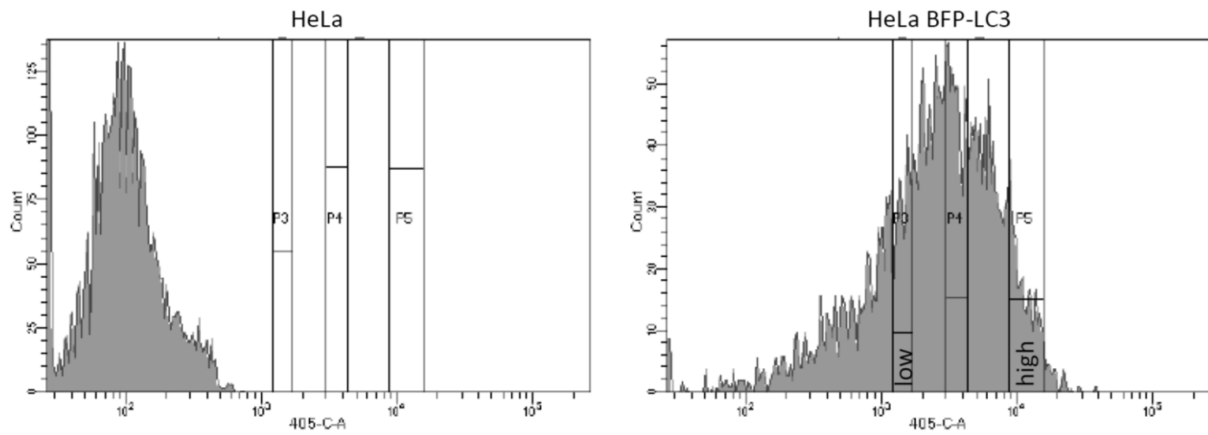


**Figure 31: Sorting subpopulations of HeLa based on BFP-LC3 expression**

From the transduced HeLa BFP-LC3 cells, clonal cell populations were sorted for low and high levels of BFP-LC3 expression with a cell sorter.

Single BFP-LC3 puncta, corresponding to autophagosomes, were better visible in cells with a low BFP-LC3 expression (clone C2, **Figure 32a-b**) than in cells with a high BFP-LC3 expression (clone D10, **Figure 32a-b**). Please, note the high basal autophagic activity in HeLa cells. The sensitivity of the clone C2 cells to UUKV was next assessed 6 hpi, after immunostaining against the protein N and analysis by flow cytometry (**Figure 32c**). The low level of BFP-LC3 expressed in clone C2 cells had no adverse effect on UUKV infection compared to HeLa cells. Because LC3 puncta were clearly visible and susceptibility to UUKV infection unaltered, the clone C2 line was chosen for further experiments.

## Results

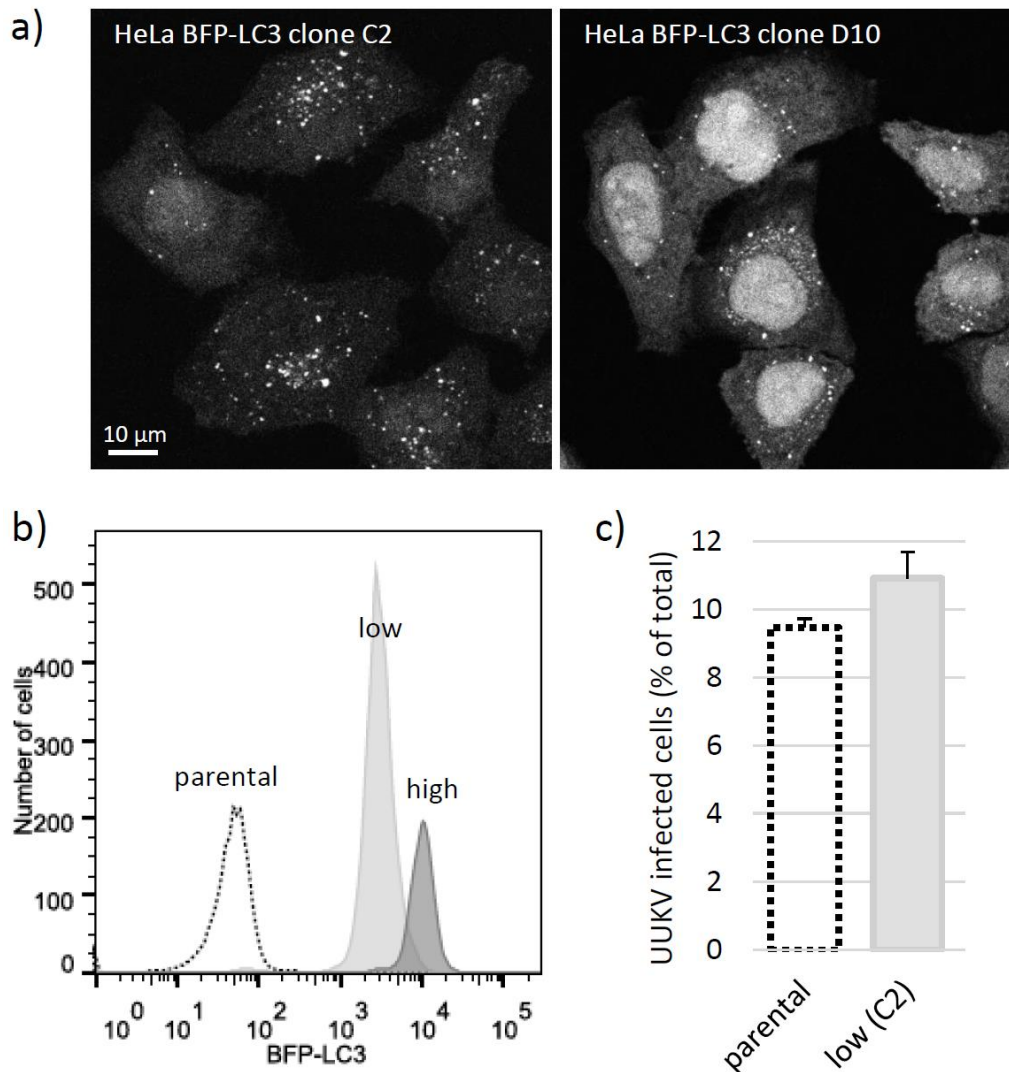


**Figure 32: BFP-LC3 expression and UUKV infection in two expresser clones of HeLa BFP-LC3 cells**

(a) HeLa BFP-LC3 cells expressing a low (C2) or high (D10) level of BFP-LC3 were grown on a coverslip, fixed and imaged with a confocal microscope. Scale bar = 10 μM. (b) HeLa, HeLa BFP-LC3 C2 or D10 cells were analyzed by flow cytometry for blue fluorescence associated to the cells. (c) Parental HeLa or HeLa BFP-LC3 C2 cells were exposed to UUKV at a MOI of 0.125 for 6 h. After fixation and permeabilization, infected cells were immunostained for UUKV-N and analyzed by flow cytometry. Data represent means ± SD, n = 1.

The following experiment aimed to assess the response of HeLa BFP-LC3 C2 to activation and inhibition of autophagy with drugs. Rapamycin inhibits a key regulator of autophagy, mTOR, and thereby activates autophagy<sup>214</sup>. Bafilomycin A<sub>1</sub> is an inhibitor of the vacuolar proton pump (vATPase), necessary to establish an acidic endosomal pH, and inhibits fusion of autophagosomes with lysosomes<sup>215,216</sup>. This block in a late step of the autophagic pathway leads to an accumulation of autophagosomes<sup>131</sup>. Wortmannin prevents autophagosome formation through inhibition of phosphatidylinositol-3-kinases<sup>217</sup>.

## Results

Cells exposed to the drugs were fixed and a stack of entire cells was acquired with a confocal microscope. Nontreated (NT) HeLa BFP-LC3 C2 cells expressed punctate structures, indicating a basal autophagic activity (**Figure 33**). Rapamycin treatment increased the number of punctate structures per cell, bafilomycin A<sub>1</sub> intensified the accumulation even more (**Figure 33**). Wortmannin decreases the formation of BFP-LC3 positive vesicles (**Figure 33**). Altogether these results indicated that autophagy-targeting drugs could induce or inhibit the formation of BFP-positive punctate structures.

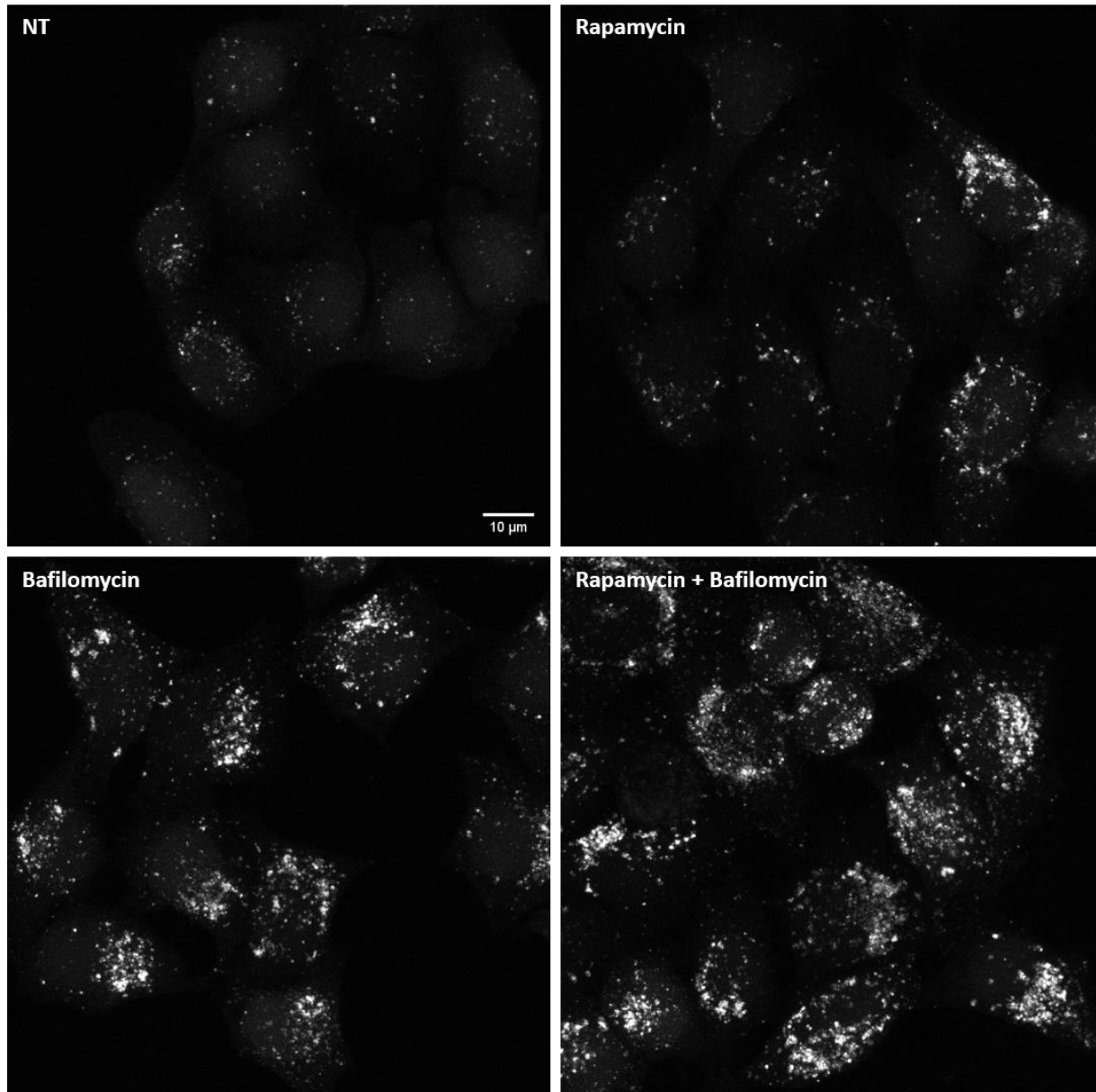


**Figure 33: BFP-LC3 puncta accumulate in HeLa BFP-LC3 C2 cells upon treatment with bafilomycin A1 or rapamycin, and are eliminated by wortmannin treatment**

HeLa BFP-LC3 C2 cells were treated for 4 h with bafilomycin A<sub>1</sub>, rapamycin or wortmannin. After fixation a z-stack of entire cells was imaged with the confocal microscope. Images are presented as a maximum z-projection. BFP-LC3 (white). Scale bar = 10 μM.

## Results

### 10.5.2 The impact of siATG7 on autophagosome formation

The following experiments were performed to investigate the level of autophagic activity upon Atg7 silencing. First, the silencing efficiency of siRNAs targeting *ATG7* in HeLa BFP-LC3 C2 cells was analyzed by SDS-PAGE and WB. After immunostaining, no more Atg7 expression was detected as a result of specific siRNA transfection with 10 nM or 50 nM of the three nonoverlapping siRNAs for 72 h (**Figure 34**).

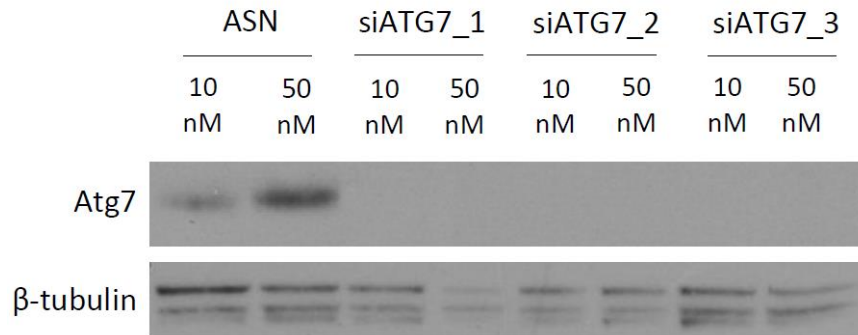
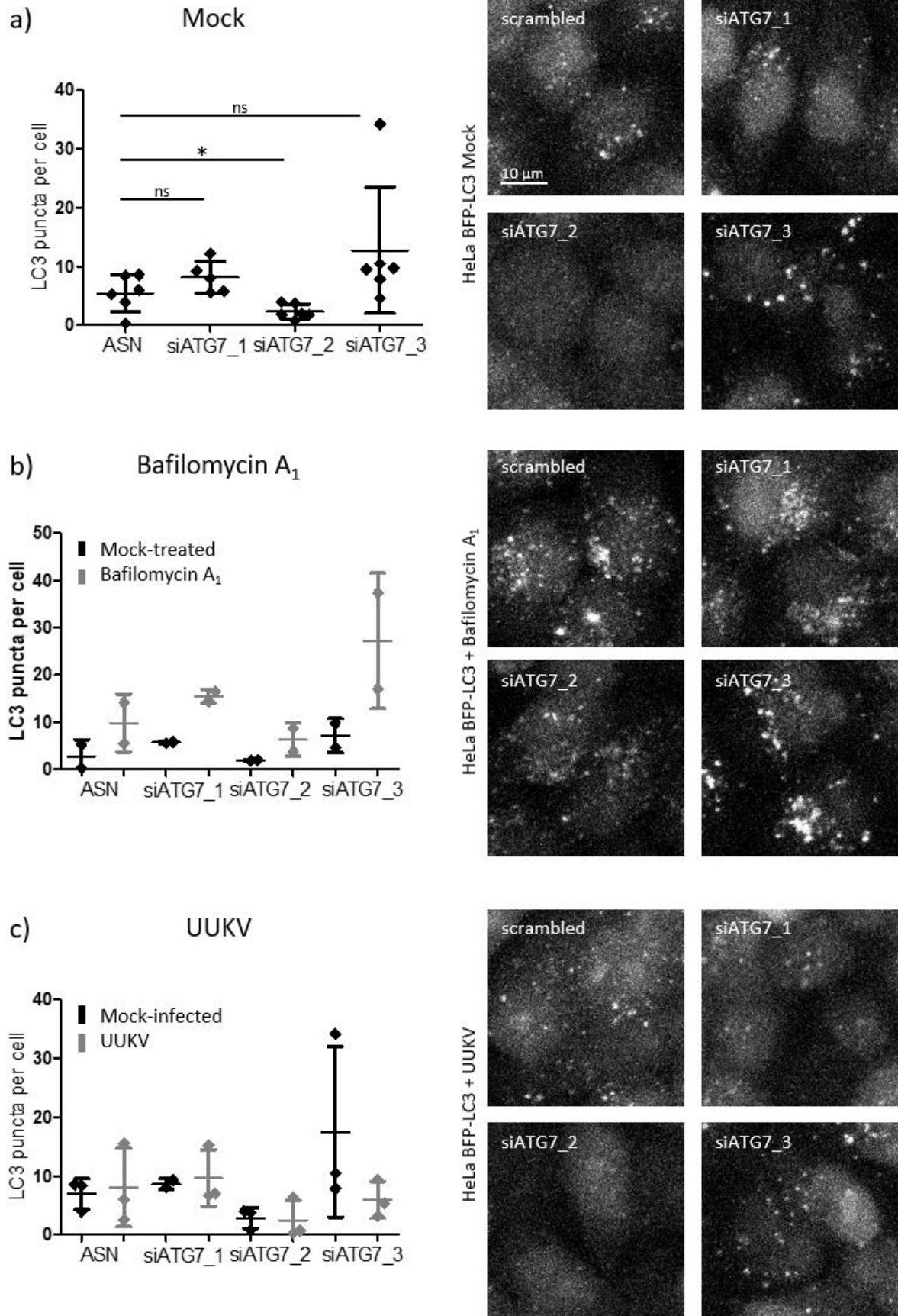


**Figure 34: Atg7 was silenced by siRNA-mediated silencing in HeLa BFP-LC3 C2 cells**

HeLa BFP-LC3 C2 cells were transfected for 72 h with 10 nM or 50 nM siRNAs targeting *ATG7*, lysed and analyzed by SDS-PAGE and Western Blot (WB).

BFP-LC3 puncta, which are associated with autophagosomes, were quantified in HeLa BFP-LC3 C2 cells transfected with the three nonoverlapping siRNAs against *ATG7*. Punctate structures above a manually defined threshold were counted with the ImageJ analyze particles plugin after noise reduction with the Gaussian Blur function and separation of overlapping objects with the Watershed function. Interestingly only siATG7\_2 reduced the number of BFP-LC3 puncta per cell, while siATG7\_1 and siATG7\_3 did not modify the number of BFP-LC3 puncta per cell compared to the scrambled siRNA control (**Figure 34a**). Addition of 100 nM bafilomycin A<sub>1</sub> for 4 h increased the number of puncta in all four samples (**Figure 34b**). Infection with UUKV had no effect on BFP-LC3 puncta accumulation in the four different samples (**Figure 34c**). In summary these results indicated that only one out of the three siRNAs against Atg7 inhibited autophagosome formation. UUKV infection did not lead to a change in the number of autophagosomes per cell 16 hpi.

## Results



The legend for figure 35 can be found on the following page.

## Results

### *Figure 35: BFP-LC3 puncta accumulation after Atg7-silencing in HeLa BFP-LC3 C2 cells*

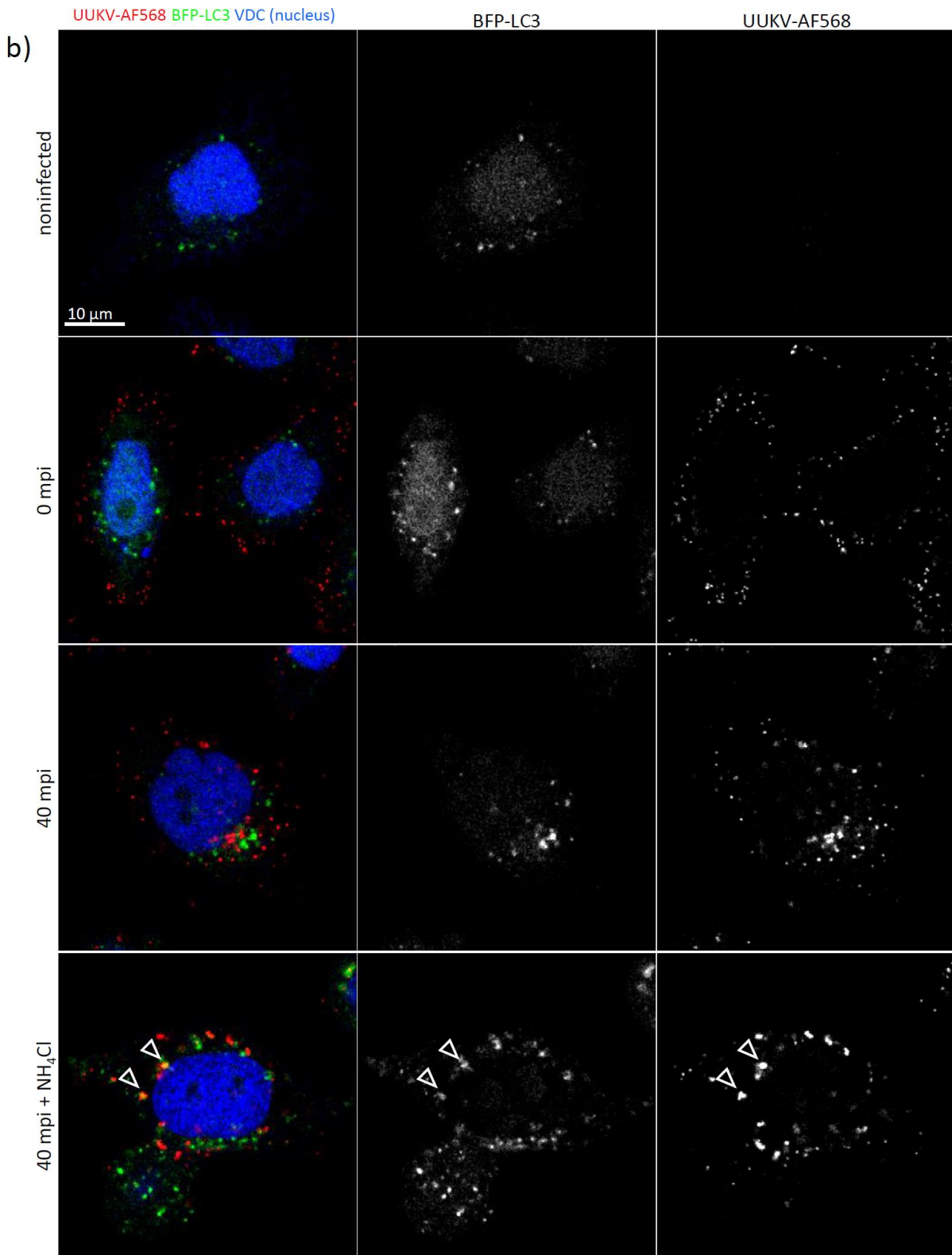
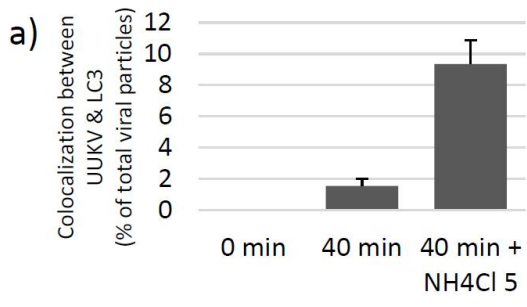
HeLa BFP-LC3 C2 cells were transfected with 10 nM siRNAs targeting *ATG7*. (a) After 72 h of incubation, cells were fixed or (b) treated for 4 h with 100 nM bafilomycin A<sub>1</sub> before fixation. (c) The cells were exposed for 16 h to UUKV at a MOI of 0.25. After fixation, cells were imaged with a confocal microscope and the number of puncta per cell was quantified with the ImageJ analyze particles plugin (after noise reduction with the Gaussian Blur function and separation of overlapping objects with the Watershed function), n = 13-23 cells per sample. Data represent mean ± SD, n = 6 (mock), n = 2 (bafilomycin A<sub>1</sub>), n = 3 (UUKV), two-tailed unpaired t-test, \*\*\*p ≤ 0.001, \*\*p ≤ 0.01, \*p ≤ 0.05, ns stands for nonsignificant.

### **10.5.3 UUKV rarely enters autophagosomes 40 mpi**

Thus far we could demonstrate that Rab11a, a protein associated with REs and autophagy, and *Atg7*, an autophagosome elongating protein, were involved in UUKV entry. Hence, we were wondering whether autophagosomes played a role in UUKV entry. To assess a potential association between viral particles and autophagosomes, UUKV-AF568 was bound to HeLa BFP-LC3 C2 cells on ice and infection was permitted at 37°C. Upon binding on ice (0 mpi), viral particles remained bound to the plasma membrane and did not colocalize with BFP-LC3 (**Figure 36a-b**). 40 minutes after the shift to 37°C, viral particles were internalized and localized in the nuclear periphery (**Figure 36b**). Only 1.5 % of the viral particles associated with BFP-LC3-decorated vesicles (**Figure 36a**). The percentage of viral particles colocalizing with BFP-LC3 could be increased 6-fold by adding NH<sub>4</sub>Cl. Neutralization of endosomal pH by this weak base thereby inhibits lysosomal proteolysis and leads to an accumulation of autophagosomes

218.

# Results



## Results

**Figure 36: UUKV-AF568 rarely associated with BFP-LC3 puncta 40 mpi**

(a) Colocalization between UUKV-AF568 and BFP-LC3 was quantified in three fields of view per sample as described in *Figure 35*. Data represent mean  $\pm$  SD, n = 2. (b) UUKV-AF568 was bound to HeLa BFP-LC3 C2 cells on ice at a MOI of 2 for 1 h. Internalization was allowed at 37°C for 40 min, NH<sub>4</sub>Cl was added 5 minutes following internalization in one sample. After fixation, nuclei were stained with 100 nM Vybrant Dye Cycle (VDC). Cells were imaged with the confocal microscope.

### 11 Discussion

The subject of this PhD thesis is the tick-borne phlebovirus, UUKV. It is commonly used as a model virus for highly pathogenic RVFV, SFTSV, TOSV and HRTV. UUKV enters mammalian cells by receptor-mediated endocytosis and transits Rab5-positive early endosomes<sup>37</sup>. The viral genome is released into the cytosol from late endosomal or lysosomal compartments with a luminal pH inferior to 5.4<sup>37</sup>. The details of how UUKV particles reach acidic compartments to release their genome into the cytosol, remain elusive. An siRNA screen with two genome-wide siRNA libraries (from Dharmacon and Qiagen) was previously performed in our lab to identify additional host factors for infectious entry and replication of UUKV<sup>80</sup>. The v-SNARE VAMP3 appeared as potential host factor from both siRNA libraries. In-depth characterization revealed VAMP3 as an important factor for late penetration of UUKV. The first discovered function of VAMP3 was a role as fusion protein in recycling endosomes and in constitutive exocytosis of recycling vesicles<sup>100,101</sup>. Recent studies also demonstrated a role in the initiation of autophagy<sup>104</sup> and fusion between MVBs and autophagosomes<sup>105</sup>, supporting previously found convergence of the endosomal and autophagic pathways<sup>106</sup>. We thus aimed to clarify the importance of the autophagic pathway in UUKV infection.

#### 11.1 A subset of autophagy-associated proteins is involved in UUKV infection

Virus replication is highly sensitive to commonly used autophagy inhibitors such as wortmannin, bafilomycin A<sub>1</sub>, siRNAs against the vacuolar H<sup>+</sup> ATPase, NH<sub>4</sub>Cl and chloroquine<sup>37,54</sup>. As these perturbants all block the autophagic and the endocytic pathways, these inhibitors cannot be used to specifically investigate the implication of one of these pathways on UUKV infection. To specifically target the autophagic pathway, we decided to assess the role of several autophagy-associated proteins in UUKV infection.

Autophagy is a catabolic pathway for the degradation of cytoplasmic unwanted constituents in lysosomes. Autophagy can specifically degrade viruses and aid establishing an innate and adaptive immune response counteracting viral infection, as it was reported for the two closely related phleboviruses RVFV and SFTSV<sup>147,158,159</sup>. Through evolutionary competition, however, viruses have evolved mechanisms to circumvent antiviral autophagic mechanisms and

## Discussion

even to utilize parts of the autophagosomal machinery for their own purposes<sup>147</sup>. Thus, autophagy can be pro- or antiviral. We demonstrated a proviral role of the autophagy-associated factors Rab11a and Atg7 in UUKV infection. Further autophagy-associated proteins such as Atg3, Atg5, Atg9L1, Atg14L, Atg16L1, Beclin 1, FIP200, Rab1b and WIPI1 had no clear effect on UUKV infection. These results illustrate that the conventional autophagy pathway was most likely not necessary for viral infection. UUKV rather exploits a subset of autophagy-associated proteins for infection.

Rab11a, Rab1b, WIPI1 and FIP200 appeared as host factor candidates in the siRNA screens<sup>80</sup>. The suggested function of Rab11a and Rab1b as host factors for UUKV infection could be confirmed. But despite a good silencing efficiency, Rab1b played a minor role in infection. In contrast, a role of FIP200 and WIPI1 in UUKV infection could not be confirmed. Because we did not assess siRNA-mediated silencing efficiency of FIP200 and WIPI1, no firm conclusion could be drawn on their involvement in infection. Deviating results in the siRNA screen and my experiments could have occurred due to the use of different siRNAs, resulting in inefficient silencing or unspecific off-target effects.

The presence of Atg7 and Rab11a facilitated UUKV infection in different cell lines, expressing or not the virus entry receptor DC-SIGN<sup>54</sup>. Hence, a tissue-specific effect can be excluded and the role of both proteins is not linked to viral particle internalization through DC-SIGN. We specifically addressed the involvement of Atg7 and Rab11a in different steps of the virus life cycle. We found both proteins to play a role in endosomal trafficking of viral particles. They had no effect on plasma membrane binding of viral particles or genome replication.

### **11.2 Rab11 facilitates intracellular trafficking of UUKV particles to acidic compartments for fusion**

Small GTPases of the Rab family regulate intracellular membrane trafficking events. Bound to GTP, Rab proteins recruit specific effectors to regulate vesicle transport and promote tethering and fusion<sup>219</sup>. Rab11a is a small GTPase that regulates recycling endosome trafficking and secretory pathways from the TGN to the plasma membrane<sup>108</sup>. Additionally, Rab11a is proposed to regulate initiation of autophagy<sup>129</sup> and autophagosome-endosome fusion<sup>200</sup>.

The viral receptor DC-SIGN is internalized upon ligand-binding and recycled back to the plasma membrane after dissociation from its cargo<sup>220</sup>. In the case of UUKV internalization,

## Discussion

DC-SIGN dissociates from UUKV in early endosomes to be recycled back to the cell surface<sup>54</sup>. Rab11a and Rab11b are typical regulators for recycling of different receptors such as the transferrin receptor<sup>185,186,189</sup> and mediate recycling from endosomal compartments, through REs to the plasma membrane<sup>194</sup>. We illustrated that expression of DC-SIGN on the plasma membrane did not rely on Rab11a or Rab11b, suggesting that DC-SIGN is recycled independent of these small GTPases. This suggestion is in line with the report, that DC-SIGN did not colocalize with Rab11a during internalization and recycling in monocyte-derived dendritic cells<sup>221</sup>. As an alternative to the late (slow) Rab11a-dependent recycling pathway<sup>194</sup>, an early Rab4-dependent recycling pathway is described<sup>193</sup>. Rab4 regulates a fast recycling from EEs directly to the cell surface<sup>193</sup>. DC-SIGN could be recycled by this Rab4-dependent pathway.

An involvement of Rab11a in viral infection was described previously<sup>222–224</sup>. Rab11a is involved in various steps of the virus life cycle from prefusion steps to replication, viral particle assembly, exocytosis and release. We demonstrated, that Rab11a promoted endosomal trafficking of UUKV particles before viral RNA was released into the cytoplasm. A role of Rab11a in viral entry is also suggested for the mosquito-borne Japanese encephalitis virus (JEV) and the classical swine fever virus (CSFV), both belonging to the family of *Flaviviridae*<sup>225,226</sup>. It has to be mentioned here, that both studies did not directly assess a function of Rab11a in virus entry, instead viral genome replication was used as a readout for functional approaches. Their conclusion that Rab11a is important for viral entry, relies on an inhibition of the viral genome replication after Rab11a silencing or dominant negative mutant expression in combination with virus particle-Rab11a colocalization events during early infection<sup>225,226</sup>. Interestingly, the two arboviruses UUKV and JEV transit Rab5-positive early endosomes, rely on Rab11a and do not require active Rab7 for productive infection<sup>37,225</sup>. These results suggest that the two arboviruses utilize partially similar Rab11a-dependent and Rab7-independent entry pathways. Rab7 is a late endosomal marker, required for maturation of EEs to LEs<sup>227,228</sup> and fusion of LEs with LYSs<sup>229</sup>. To study the role of Rab7 in viral infection, Rab7 mutants were overexpressed or silenced with specific siRNAs. Based on studies using Rab7 and Rab11a perturbants, several viruses are proposed to rely on one of the two proteins for infectious entry into mammalian cells<sup>225,230,231</sup>.

An interesting finding regarding Rab11a- and Rab7-dependent endosomal trafficking was reported for mosquito-borne DENVs<sup>230</sup>. Acosta and colleagues demonstrate that DENV particles transit Rab5-positive EEs and subsequently enter either Rab11a-positive or Rab7-positive vesicles before penetration<sup>230</sup>. Which of the two pathways is used, depends on the

## Discussion

virus strain<sup>230</sup>. Flaviviruses mostly rely on a mildly acidic pH for fusion, that is present in EEs<sup>232</sup>. DENV has a pH-threshold of 6.2<sup>230</sup>. Viruses that fuse from EEs, typically penetrate 3 – 8 mpi<sup>77</sup>. Nevertheless, different DENV serotypes and strains penetrate 14 – 16 mpi<sup>230</sup>. These penetration kinetics rather correspond to those of viruses fusing from LEs<sup>77</sup>. Thus, the penetration kinetics suggest that DENV particles traffic beyond EEs<sup>230</sup>. A feasible explanation for virus trafficking to Rab7-positive LEs or Rab11a-positive REs is the dependence on specific lipids<sup>233</sup>. Effective DENV fusion to intracellular membranes relies on anionic lipids such as BMP and phosphatidylserine (PS)<sup>233</sup>. Indeed, BMP is found in LEs<sup>234</sup>, while PS is present on RE membranes<sup>235</sup>, suggesting that DENV particles can fuse from Rab11a- or Rab7-positive compartments.

Similar to the flaviviruses JEV and specific DENV strains, the phlebovirus UUKV transits Rab5-positive EEs was not affected by expression of a dominant negative Rab7 mutant<sup>37</sup>. Instead, these arboviruses are suggested to rely on Rab11a for infectious entry<sup>225,230</sup>. Penetration from Rab11a-positive compartments, as it is proposed for certain DENV strains<sup>230</sup>, is most likely not the case for UUKV. In contrast to flaviviruses, UUKV particles rely on a more acidic pH for fusion, around 5.4<sup>37</sup>. But the pH level of REs is less acidic than in EEs, around 6.4<sup>235,236</sup>, thus, not suitable for UUKV penetration. Additionally, the vesicle's lipid composition plays an important role in particle fusion<sup>81</sup>. Lipid mixing to liposomes shows that membranous lipids of REs, such as PS, cholesterol and sphingomyelin (SM)<sup>235</sup> do not promote UUKV fusion<sup>81</sup>. Despite no evident importance of Rab7 for infection<sup>37</sup>, several lines of evidence suggest that UUKV particles fuse from acidic late endosomal compartments. The pH threshold for UUKV fusion is 5.4<sup>37</sup>. Such pH levels are usually found in LEs and LYSs<sup>75</sup>. UUKV fusion relies on the anionic lipid BMP<sup>81</sup>, which is present in late endosomal compartments<sup>235</sup>. Acid-activated fusion occurs 20-40 mpi<sup>54</sup>, a timing corresponding to cargo reaching late endosomal compartments<sup>75</sup>. Additionally, infectious entry relies on temperatures above 25°C. Temperatures below 20°C inhibit LE maturation<sup>237</sup>. I therefore propose that UUKV particles traffic from Rab5-positive EEs to acidic late endosomal compartments in a Rab11a-dependent manner. I propose that taking this Rab11a-dependent route allows viral particles to enter acidic compartments in a Rab7-independent manner. A similar entry route could be taken by the poxvirus Vaccinia (VV). VV transits Rab11a-positive REs, and not Rab7-positive LEs, before the virus capsid is released into the cytosol<sup>231</sup>. VV envelope can fuse with the host vesicular membrane at a pH around 5.2<sup>238</sup>, which is typical for LEs<sup>75</sup>. Interestingly, UUKV and VV do not require Rab7 for trafficking, nevertheless a small fraction of UUKV and VV particles colocalizes with Rab7<sup>37,231</sup>. This could be explained by the proposed Rab11a-

## Discussion

dependent and Rab7-independent trafficking to acidic late endosomal compartments. Rab7-positive late endosomal compartments and Rab11a-positive REs form big vesicles in the nuclear periphery<sup>194</sup>. This location to the same cellular compartment allows to speculate about an interplay between the endocytic degradation pathway and the exocytosis pathway, possibly leading to virus particle association with Rab7, a typical marker of LEs<sup>77</sup>. Why UUKV is associated with Rab7-positive vesicles, whereas Rab7 is not required for trafficking, remains to be elucidated. To investigate this, UUKV appears as a precious tool.

In addition to UUKV, we also assessed the role of the vacuolar H<sup>+</sup> ATPase and Rab11a in SFV, RVFV and IAV infection. Just like UUKV, the membrane fusion of SFV, RVFV and IAV is reported to rely on endosomal acidification<sup>239</sup>. This was reflected by our findings that these viruses depended on the vacuolar H<sup>+</sup> ATPase (ATP6V1A) for viral replication. Silencing of Rab11a had no major impact on replication of SFV (early penetrating virus) and IAV (late penetrating virus)<sup>239,240</sup>. Overall this indicates that Rab11a silencing did not result in a block of the general endocytic machinery but was rather restricted to Rab11-mediated vesicular trafficking. SFV is suggested to penetrate from Rab5-positive EEs and does not rely on active Rab7<sup>37,241,242</sup>. The pH threshold for fusion is above 6, and viral particles penetrate around 5 mpi<sup>242</sup>. We demonstrated that Rab11a was not involved in SFV replication, suggesting that this early penetration mechanism does not rely on Rab11a. Similar to UUKV, IAV particles transit Rab5-positive EEs<sup>243</sup>. They reach (CD63-positive) LEs 40 mpi and fusion relies on a pH threshold around 5.1<sup>239,243</sup>. It is well accepted that IAV penetrates from late endosomal compartments. VAMP3 and Rab11a were demonstrated to be involved in UUKV replication but not in IAV replication<sup>80</sup>, indicating that the entry pathways of these two late penetrating viruses diverge. Early entry steps of both viruses rely on Rab5-positive EEs<sup>37,243</sup>. Like VAMP3, Rab11a thus might play a role during late endocytosis. A role of Rab11a in IAV infection was studied previously. Rab11a transports progeny genome to the assembly site and is also involved in assembly of viral particles<sup>244</sup>. In this study we only assessed earlier steps of the IAV life cycle up to and including replication. Hence, our demonstration that Rab11a did not play a role in IAV replication is not contradictory to previous reports, demonstrating an importance of Rab11a in postreplication steps of IAV infection. The infectivity of the late-penetrating phlebovirus RVFV was slightly reduced upon Rab11a silencing. This effect was less pronounced than for UUKV, suggesting that UUKV exhibited entry properties different from the closely related RVFV. Further phleboviruses will have to be tested to find out whether Rab11a is a host factor specific for UUKV or several genus members.

## Discussion

An additional important player in intracellular trafficking of UUKV to late endosomal compartments is the v-SNARE protein VAMP3<sup>80</sup>. VAMP3 is a fusion protein in REs and involved in constitutive exocytosis<sup>100,101</sup>. Yamazaki and colleagues illustrate that silencing VAMP3 inhibits the formation of Rab11a-positive compartments<sup>245</sup>, raising the possibility of a connective function of Rab11a and VAMP3 in UUKV infection. The importance of both proteins in recycling endosome trafficking points towards a potential involvement of these compartments in UUKV intracellular trafficking. Moreover, a role of Rab11a in virus particle entry is not restricted to UUKV. Rab11a also promotes entry of JEV, DENV and VV into mammalian cells<sup>225,230,231</sup>. Thus, I propose to use UUKV as cargo to better understand the role of recycling endosomes in late endosomal trafficking, a function that remains elusive and is potentially subverted by a number of related and unrelated viruses. UUKV transits Rab5-positive EEs, and VAMP3-positive compartments during late endocytosis for productive entry<sup>37,80</sup>. Some viral particles also associate with Rab7 and more than 50 % with LAMP1-positive vesicles during late entry steps<sup>37</sup>. HeLa cells stably expressing eGFP-Rab5, eGFP-VAMP3, eGFP-Rab7 or eGFP-LAMP1 could be established and used to follow trafficking of AF-labeled viral particles to these specific compartments in the presence or absence of Rab11a. Coimmunoprecipitation could identify Rab11a interaction partners and thereby specify the function of Rab11a in UUKV infection. Several Rab11a effectors that regulate activation of other Rab proteins, mediate vesicle transport along the cytoskeleton or fusion with the target membrane have been identified<sup>108,224</sup>. Together this would help to more precisely define in which step of intracellular membrane trafficking Rab11a is involved.

Besides their role in recycling endosome trafficking, Rab11a and VAMP3 are both proposed to be involved in the initiation of autophagy<sup>104,110,129</sup>, pointing towards a potential involvement of the autophagic pathway in UUKV infection. We demonstrated that a number of key autophagy proteins were not important for infection, suggesting an autophagy-independent function of the two proteins in UUKV infection.

To investigate whether UUKV associated with Rab11a-positive vesicles, we assessed colocalization between eGFP-Rab11a and UUKV-AF568. Already after binding on ice, 5 % viral particles colocalized with Rab11a or LAMP1. Rab11a could be close to the plasma membrane because it interacts with the exocytosis complex to fuse REs with the plasma membrane<sup>190</sup> and thus colocalize with membrane-bound viral particles. Newly synthesized LAMP1 is mainly delivered from the Golgi apparatus directly to LEs and then LYSs<sup>246</sup>. However, a small fraction traffics to the plasma membrane before endocytosis and delivery to

## Discussion

LYSs<sup>246</sup>. This fraction could be accountable for the colocalization with membrane-bound viral particles. Due to the presence of Rab11a and LAMP1 on or close to the plasma membrane, we considered the colocalization events upon viral particle binding on ice as background and removed them from all other samples.

UUKV localization to Rab11a-decorated compartments in HeLa cells increased 5 mpi and reached a plateau 10 mpi. The level of 10 % colocalization was maintained until 30 mpi, the last time point investigated. UUKV was previously reported to start entering Rab5-positive early endosomes 5 mpi and to reach a maximum 10 mpi in A549 cells, until no longer detectable 30 mpi<sup>37</sup>. In the meantime, movement to Rab7-positive late endosomes occurred, reaching a maximum 30 – 40 mpi<sup>37</sup>. In case of a direct role of Rab11a-decorated compartments in UUKV trafficking, this timing would argue for a role of Rab11a starting with early endosomal trafficking and proceeding to late endosomal trafficking. To exclude a misinterpretation due to differing entry kinetics in HeLa and A549 cells, endosomal trafficking of UUKV particles should be assessed in HeLa cells. Nevertheless, entry in these two cell lines should be comparable because functional Rab5 is important in both cell lines and internalization and penetration kinetics are comparable<sup>37,54</sup>. Interestingly, colocalization of the Rab11a-dependent JEV, DENV and VV with Rab11a was also observed after colocalization with Rab5, further underlining parallels in UUKV, JEV, DENV and VV entry<sup>225,230,231</sup>.

Our results illustrated, that 10 % of bound or internalized UUKV particles entered Rab11a-positive vesicles. But only a fraction of viral particles will productively infect a cell. Colocalization of such a small fraction therefore raises the question, whether these Rab11a-colocalizing viral particles productively infect the cell. Or, if these Rab11a-colocalizing particles represent noninfectious viral particles and Rab11a indirectly promotes UUKV intracellular trafficking. Rab11a regulates slow recycling from endosomal compartments through REs back to the plasma membrane<sup>194</sup>. With this function, viral particles could be recycled to the plasma membrane. Thus Rab11a-UUKV colocalization would represent a transport that does not result in productive infection. Perturbing Rab11a could interfere with the maturation of late REs and/or the fusion between REs and specific populations of endosomes. Under this assumption, perturbing Rab11a could indirectly impair the maturation of LEs that are important for UUKV entry. Otherwise, Rab11a could directly promote infectious entry by transporting viral particles from Rab5-positive EEs to Rab7- or LAMP1-positive, acidic late endosomal compartments.

## Discussion

### 11.3 Atg7 promotes endosomal trafficking of UUKV

Atg7 is an essential factor with E1-like enzymatic activity for the Atg12 and the LC3 ubiquitin-like conjugation systems of the core autophagic machinery<sup>113</sup>. Atg7 catalyzes the initial step for the formation of the Atg12-Atg5-Atg16L1 complex<sup>113</sup> and activates LC3<sup>247</sup>. After Atg7-mediated LC3 activation, Atg3 and the Atg12-Atg5-Atg16L1 complex catalyze LC3-conjugation to the phospholipid PE on the phagophore membrane<sup>248,249</sup>. LC3 then recruits specific substrates to the phagophore<sup>132,133</sup> and mediates fusion of the autophagosome with the lysosome<sup>135</sup>. Summarizing, Atg7 is an important factor for recruitment of LC3 to the phagophore membrane. By expression of fluorescently labeled LC3, its recruitment to autophagosomes (from a diffuse cytosolic expression to puncta formation) can be followed by fluorescence microscopy. We established HeLa cells stably expressing BFP-LC3. LC3-puncta formation could be induced with the autophagy inducer rapamycin and the autophagic flux inhibitor bafilomycin A<sub>1</sub> and LC3-puncta formation could be inhibited with the autophagosome formation inhibitor wortmannin, together indicating that LC3-decorated structures represent autophagosomes. Hence, HeLa cells stably expressing BFP-LC3 could be used to follow autophagosome formation. Of note, we also detected a high level of LC3-positive vesicles in nonstimulated cells. This is in accordance with literature, describing a high basal autophagic activity in HeLa cells<sup>250</sup>. We demonstrated that three nonoverlapping siRNAs targeting *ATG7* efficiently silenced Atg7. si*ATG7\_2* reduced the number of LC3 puncta per cell. This reduction in LC3 puncta formation reflects the importance of Atg7 in LC3-lipidation<sup>247</sup>. Surprisingly, si*ATG7\_1* and si*ATG7\_3* had no effect on autophagosome formation. Maybe, the remaining Atg7 expression after silencing with these two siRNAs was sufficient to sustain autophagic activity. Despite differential effects on autophagosome formation, all three siRNAs reduced UUKV infection by around 50 %. These results indicated that the role of Atg7 in UUKV infection was not related to autophagy, because no matter if autophagosome formation was obstructed or not, Atg7-silencing reduced infection to a similar extent. Atg3 and Atg7 are consecutively involved in the same step of the autophagic pathway. The enzymatic activity of both proteins is required for lipidation of the autophagy marker LC3<sup>130</sup>. We demonstrated, that only Atg7 played a role in UUKV infection, while knockdown or knockout of Atg3 did not affect infection. An involvement of Atg7 and not of Atg3 further supports the suggestion of an autophagy-independent role of Atg7 in UUKV infection. To my knowledge, a proviral function of Atg7 in viral infection that is not related to autophagy, has not been reported thus far. Autophagy-independent functions of Atg7 are the secretion of lysosomal contents in osteoclasts<sup>251</sup> or interaction with p53 upon nutrient deprivation, that leads to a cell cycle arrest<sup>252</sup>. But

## Discussion

neither would directly explain how Atg7 could function in UUKV endosomal trafficking – thus leaving UUKV as an interesting tool to study autophagy-independent cell biological functions of Atg7 and a likely role in endocytic trafficking.

After autophagy inhibition with wortmannin, some LC3-puncta were present in HeLa BFP-LC3 cells. We could alternatively explain why siATG7\_2 reduced the number of LC3 puncta per cell and siATG7\_1 and siATG7\_3 did not by speculating that these unspecific aggregates form due to overexpression of BFP-LC3. With this hypothesis siATG7\_2 would (in addition to silencing Atg7) unspecifically silence a host factor that blocks BFP-LC3 expression and thereby prevent aggregate formation. To circumvent this uncertainty, I propose to select a HeLa BFP-LC3 clone that expresses a lower level of BFP-LC3 to prevent unspecific aggregation. Another option would be to assess LC3 distribution in HeLa cells with an antibody, binding endogenous LC3.

To assess, whether UUKV particles entered autophagosomes, HeLa cells stably expressing BFP-LC3 were used. UUKV did not associate with LC3-decorated autophagic vesicles 40 mpi in nontreated cells. NH<sub>4</sub>Cl-mediated accumulation of autophagosomes led to 9 % UUKV-autophagosome colocalization. Lysosomotropic weak bases such as NH<sub>4</sub>Cl do not affect LE generation or transport of cargo to LYSs<sup>253-255</sup>. NH<sub>4</sub>Cl elevates the endosomal pH and thereby inhibits lysosomal proteolysis<sup>218</sup> and blocks UUKV penetration into the cytosol<sup>37</sup>. Consequently, in the presence of NH<sub>4</sub>Cl viral particles accumulate in compartments from which they usually fuse. Endosomes can fuse with autophagosomes to form amphisomes, thereby bridging the endosomal and the autophagosomal pathway<sup>106</sup>. If UUKV fusion-competent compartments fuse with LC3-decorated autophagosomes, UUKV could colocalize with LC3, even if viral particles do not require LC3-positive compartments for infectious entry. For future experiments it will thus be important to assess earlier time points for UUKV-autophagosome colocalization.

The suggestion that UUKV follows the classic endocytic pathway for entry into mammalian cells is contradicted by the following finding: Studies with Rab7 mutants revealed that this GTPase, which is important for EE to LE maturation<sup>227,228</sup> and LE LYS fusion<sup>229</sup>, is most likely not involved in infection<sup>37</sup>. How viral particles reach acidic endosomal compartments for fusion remains elusive. We showed that Atg7 was involved in endosomal trafficking of UUKV particles and propose an autophagy-independent function. Such unconventional functions of Atg7 are scarcely studied. Mauthe and colleagues demonstrated that autophagy-related proteins have numerous unconventional functions, which remain to be identified<sup>256,257</sup>. Therefore we hypothesize a role of Atg7 in UUKV intracellular trafficking to reach acidic

## Discussion

endosomal compartments. To characterize this potential role of Atg7 in endosomal trafficking, I propose to assess the distribution of the EE marker Rab5 and the RE marker Rab11a in presence and absence of Atg7. A potential perturbation of endosomal distribution could point to an Atg7-mediated function.

*ATG7* knockout in Huh7 cells reduced UUKV replication by 50 %. Thus, UUKV infection was reduced but ongoing in absence of Atg7. These results could be explained in two different ways. One is that functionally redundant proteins substitute the function of Atg7. Since isoforms of Atg7 are not identified and we do not know the precise function of Atg7 in UUKV infection, I cannot judge whether a functionally redundant protein can substitute Atg7. The partial dependence on Atg7 could also signify that UUKV used distinct entry pathways within one cell line. The use of diverse endocytic pathways was demonstrated previously. A small fraction of UUKV particles is internalized clathrin-dependently while additional clathrin-independent uptake mechanisms exist <sup>37</sup>. It is thus imaginable that UUKV particles can follow distinct endocytic pathways to traffic towards acidic endosomal compartments for fusion.

Similarly, Rab11a knockdown, also allowed UUKV replication. In the case of silencing, a residual protein expression could be sufficient for viral replication. Since a residual protein expression was detected after siRNA-mediated silencing by WB this is a reasonable explanation. As explained above, UUKV could enter mammalian cells by using distinct entry pathways. Apart from that, proteins with a similar function could substitute Rab11a. Indeed, two isoforms are identified, Rab11b or Rab25 (Rab11c), which have overlapping functions with Rab11a in the control of trafficking through REs <sup>185-187</sup>. Despite its expression, which is restricted to brain, heart and testes <sup>183</sup>, a low level of *RAB11B* mRNA could be detected in HeLa cells <sup>80</sup>. Comparable to Rab11a, Rab11b silencing reduced UUKV infection by at least 45 %. Thus Rab11b is likely involved in UUKV infection and could indeed substitute the function of Rab11a. Knockdown of Rab11b with siRNAs remains to be assessed by WB. Interestingly, silencing the two isoforms simultaneously neither enhanced nor weakened the inhibitory effect on UUKV infection. In this case, Rab25 should also be included in the study as it could substitute the function of Rab11a and Rab11b.

### 11.4 Perspectives

This study opens up perspectives for investigations into different directions. The first more fundamental research-based perspective would be to identify the specific function of Rab11a

## Discussion

and Atg7 in UUKV infection. The thesis in hand already gives us an interesting insight into Atg7 function. Mainly known as a key autophagy protein, its function in UUKV infection seems to be independent of autophagosome formation. UUKV thereby represents a suitable and powerful cargo to study a potentially unknown mechanism of action of Atg7 in endosomal trafficking. Rab11a is proposed to promote entry of RNA viruses (UUKV, JEV, DENV) and a DNA virus (VV) into mammalian cells<sup>225,230,231</sup>. This role for infection with diverse acid-dependent viruses suggests a more general function of Rab11a in endocytosis that deserves to be defined more precisely. (Assays are proposed in the discussion above.)

Our findings should contribute to a better understanding of phlebovirus infection and consequently, to the development of new antiviral strategies. In the future, it would therefore be interesting to shed light on the entry pathway of highly pathogenic phleboviruses by extending the model that we have established for UUKV to TOSV, HRTV and SFTSV. The here identified host factors for UUKV infection, Rab11a and Rab11b can indeed be targeted with small molecules and therefore represent an interesting drug target<sup>258</sup>. Investigations in this study are limited to the cell culture adapted human adenocarcinoma cell line HeLa, the human hepatocellular carcinoma cell line Huh7 and the human embryonic kidney cell line HEK 293, all representing an artificial system. Natural infection occurs via an arthropod bite that results in the injection of the virus into the dermis. Dermal DCs are present in this anatomical site of infection and possibly rank among the first encountered cells<sup>40</sup>. It was demonstrated that UUKV and RVFV replicate in immature DCs<sup>54</sup>. Utilizing primary DCs to study virus entry could give a clue whether our findings are applicable to more relevant cells. The degree of complexity in the regulation of endocytic processes increases in polarized cells as compared to nonpolarized cells that were used in this project<sup>259,260</sup>. In addition, endocytic trafficking is differentially regulated in two- and three-dimensional tissue culture<sup>261</sup>. Such distinctions most likely impact virus entry as well. To recapitulate architectural features of the intact tissue, it would thus be interesting to study infection in polarized three-dimensional cell culture. Moreover, it was demonstrated in our lab that glycosylation patterns of mammalian-derived UUKV particles are different from tick cell-derived particles<sup>38</sup>. In this study, exclusively mammalian-derived virus stocks were used. As different glycosylation patterns could well influence receptor recognition and the initial infection, I propose to additionally assess vector-derived virus stocks.

## 12 Publications and Contributions

### 12.1 Peer-reviewed publications

Albornoz, A., Hoffmann, A. B., Lozach, P.-Y. & Tischler, N. D. Early Bunyavirus-Host Cell Interactions. *Viruses* **8**, (2016).

Hoffmann, A. B., Mazelier, M., Léger, P. & Lozach, P.-Y. Deciphering Virus Entry with Fluorescently Labeled Viral Particles. *Methods Mol. Biol.* **1836**, 159–183 (2018).

### 12.2 Conference Contributions

Hoffmann A. B.

Oral presentation: Early bunyavirus-host cell interactions using Uukuniemi virus as a model  
14<sup>th</sup> Workshop “Cell Biology of Viral Infections” of the German Society for Virology,  
Schöntal, Germany, 2015

Hoffmann A. B., Fleckenstein H., Lang V., Brady N., Lozach PY.

Poster presentation: Early phlebovirus host cell interactions using Uukuniemi virus as a model  
26<sup>th</sup> Annual Meeting of the German Society for Virology, Münster, Germany, 2016

Hoffmann A. B., Fleckenstein H., Simon M., Blobner S., Lang V., Brady N., Lozach PY.

Oral presentation: The Autophagic Pathway in Uukuniemi Virus Infection

Keystone symposium on Autophagy Network Integration in Health and Disease, Copper  
Mountain, USA, 2017

Hoffmann A. B., Fleckenstein H., Simon M., Blobner S., Lang V., Brady N., Lozach PY.

Oral presentation: The Autophagic Pathway in Uukuniemi Virus Infection

27<sup>th</sup> Annual Meeting of the German Society for Virology, Marburg, Germany, 2017

Hoffmann A. B., Fleckenstein H., Simon M., Blobner S., Lozach PY.

Poster presentation: Early phlebovirus host cell interactions using Uukuniemi virus as a model  
16<sup>th</sup> Workshop “Cell Biology of Viral Infections” of the German Society for Virology,  
Schöntal, Germany, 2017

### 12.3 Contributions to this thesis

All data shown in this thesis were acquired and analyzed by me, if not stated here otherwise.

**Michelle Yee** performed UUKV infection assays, bypass assays, binding assays and internalization assays and with Huh7 knockout cell lines (Figure 14, Figure 26, Figure 28, Figure 29).

**Ann-Kathrin Mehnert** performed the drug-addition time course with UUKV (Figure 21).

**Hannah Fleckenstein** developed the analysis method for LC3 puncta quantification with ImageJ and **Jana Koch** assessed Atg7 expression and quantified puncta in siATG7 transfected HeLa cells (Figure 34, Figure 35).

**Malte Simon** performed part of the UUKV infection assays with siFIP200 and siWIPI1 (Figure 11b).

**Sven Blobner** performed part of the UUKV infection assays with siRAB11A and siRAB1B (Figure 11a).

**Dr. Keisuke Tabata** produced Huh7 knockout cell lines.

**Dr. Verena Lang** transduced HeLa DC-SIGN cells with the BFP-LC3 encoding construct.

**Dr. Monika Langlotz** sorted the HeLa DC-SIGN BFP-LC3 cell lines.

**Dr. Susann Kummer** produced Influenza A virus.

**Nicole Cordes** produced RVFV  $\Delta$ NSs-eGFP.

## References

### 13 References

1. World Health Organization. WHO | Disease outbreaks. WHO. <https://www.who.int/emergencies/diseases/en/>. Published 2018. Accessed December 22, 2018.
2. Rotenberg D, Jacobson AL, Schneweis DJ, Whitfield AE. Thrips transmission of tospoviruses. *Curr Opin Virol*. 2015;15:80-89. doi:10.1016/j.coviro.2015.08.003
3. Vasilakis N, Gubler DJ, Blitvich B. Arboviruses: Molecular Biology, Evolution and Control. *Am J Trop Med Hyg*. 2016;95(2):488-489. doi:10.4269/ajtmh.16-0281
4. Barzon L. Ongoing and emerging arbovirus threats in Europe. *J Clin Virol*. 2018;107:38-47. doi:10.1016/j.jcv.2018.08.007
5. Negredo A, de la Calle-Prieto F, Palencia-Herrejón E, et al. Autochthonous Crimean–Congo Hemorrhagic Fever in Spain. *N Engl J Med*. 2017;377(2):154-161. doi:10.1056/NEJMoa1615162
6. Stewart RD, Bryant SN, Sheffield JS. West Nile virus infection in pregnancy. *Case Rep Infect Dis*. 2013;2013:351872. doi:10.1155/2013/351872
7. Pealer LN, Marfin AA, Petersen LR, et al. Transmission of West Nile Virus through Blood Transfusion in the United States in 2002. *N Engl J Med*. 2003;349(13):1236-1245. doi:10.1056/NEJMoa030969
8. Iwamoto M, Jernigan DB, Guasch A, et al. Transmission of West Nile Virus from an Organ Donor to Four Transplant Recipients. *N Engl J Med*. 2003;348(22):2196-2203. doi:10.1056/NEJMoa022987
9. Miller WS, Demchak P, Rosenberger CR, Dominik JW, Bradshaw JL. Stability and infectivity of airborne Yellow fever and Rift Valley fever viruses. *Am J Epidemiol*. 1963;77(1):114-121. doi:10.1093/oxfordjournals.aje.a120289
10. Pepin M, Bouloy M, Bird BH, Kemp A, Paweska J. Rift Valley fever virus(Bunyaviridae: Phlebovirus): an update on pathogenesis, molecular epidemiology, vectors, diagnostics and prevention. *Vet Res*. 2010;41(6):61. doi:10.1051/VETRES/2010033
11. Gould E, Pettersson J, Higgs S, Charrel R, de Lamballerie X. Emerging arboviruses: Why today? *One Heal (Amsterdam, Netherlands)*. 2017;4:1-13. doi:10.1016/j.onehlt.2017.06.001
12. World Health Organization. WHO | Disease Outbreak News (DONs). WHO. <https://www.who.int/csr/don/en/>. Published 2018. Accessed December 22, 2018.
13. Sun Y, Li J, Gao GF, Tien P, Liu W. Bunyavirales ribonucleoproteins: the viral replication and transcription machinery. *Crit Rev Microbiol*. March 2018:1-19. doi:10.1080/1040841X.2018.1446901
14. Bhatt S, Gething PW, Brady OJ, et al. The global distribution and burden of dengue. *Nature*. 2013;496(7446):504-507. doi:10.1038/nature12060
15. Van Bortel W, Dorleans F, Rosine J, et al. Chikungunya outbreak in the Caribbean region, December 2013 to March 2014, and the significance for Europe. *Eurosurveillance*. 2014;19(13):20759. doi:10.2807/1560-7917.ES2014.19.13.20759
16. Faria NR, Azevedo R do S da S, Kraemer MUG, et al. Zika virus in the Americas: Early epidemiological and genetic findings. *Science*. 2016;352(6283):345-349.

## References

- doi:10.1126/science.aaf5036
17. Shayan S, Bokaeian M, Shahrivar MR, Chinikar S. Crimean-Congo Hemorrhagic Fever. *Lab Med*. 2015;46(3):180-189. doi:10.1309/LMN1P2FRZ7BKZSCO
  18. WHO | Crimean-Congo haemorrhagic fever (CCHF). WHO. 2018. <https://www.who.int/emergencies/diseases/crimean-congo-haemorrhagic-fever/en/>. Accessed February 9, 2019.
  19. Mehand MS, Al-Shorbaji F, Millett P, Murgue B. The WHO R&D Blueprint: 2018 review of emerging infectious diseases requiring urgent research and development efforts. *Antiviral Res*. 2018;159:63-67. doi:10.1016/j.antiviral.2018.09.009
  20. Adams MJ, Lefkowitz EJ, King AMQ, et al. Changes to taxonomy and the International Code of Virus Classification and Nomenclature ratified by the International Committee on Taxonomy of Viruses (2017). *Arch Virol*. 2017;162(8):2505-2538. doi:10.1007/s00705-017-3358-5
  21. Briese T, Alkhovsky S, Beer M, Calisher CH, Charrel RN, Ebihara H. Create a new order, Bunyavirales, to accommodate nine families (eight new, one renamed) comprising thirteen genera (2016.030a-vM). *International Committee on Taxonomy of Viruses*. [https://talk.ictvonline.org/taxonomy/p/taxonomy-history?taxnode\\_id=20170001](https://talk.ictvonline.org/taxonomy/p/taxonomy-history?taxnode_id=20170001). Published 2016. Accessed October 10, 2018.
  22. Fields BN, Knipe DM (David M, Howley PM. *Fields Virology*. Philadelphia : Wolters Kluwer Health/Lippincott Williams & Wilkins; 2007. <http://www.worldcat.org/title/fields-virology/oclc/71812790>. Accessed October 11, 2018.
  23. International Committee on Taxonomy of Viruses (ICTV). International Committee on Taxonomy of Viruses (ICTV). <https://talk.ictvonline.org/taxonomy/>. Published 2019. Accessed March 11, 2019.
  24. Maes P, Adkins S, Alkhovsky S V., et al. Taxonomy of the order Bunyavirales: second update 2018. *Arch Virol*. January 2019. doi:10.1007/s00705-018-04127-3
  25. Maes P, Alkhovsky S V, Bào Y, et al. Taxonomy of the family Arenaviridae and the order Bunyavirales: update 2018. *Arch Virol*. April 2018. doi:10.1007/s00705-018-3843-5
  26. LaBeaud AD, Pfeil S, Muiruri S, et al. Factors associated with severe human Rift Valley fever in Sangailu, Garissa County, Kenya. Williams M, ed. *PLoS Negl Trop Dis*. 2015;9(3):e0003548. doi:10.1371/journal.pntd.0003548
  27. Madani TA, Al-Mazrou YY, Al-Jeffri MH, et al. Rift Valley fever epidemic in Saudi Arabia: epidemiological, clinical, and laboratory characteristics. *Clin Infect Dis*. 2003;37(8):1084-1092. doi:10.1086/378747
  28. Zhan J, Wang Q, Cheng J, et al. Current status of severe fever with thrombocytopenia syndrome in China. *Virol Sin*. 2017;32(1):51-62. doi:10.1007/s12250-016-3931-1
  29. Liu S, Chai C, Wang C, et al. Systematic review of severe fever with thrombocytopenia syndrome: virology, epidemiology, and clinical characteristics. *Rev Med Virol*. 2014;24(2):90-102. doi:10.1002/rmv.1776
  30. Yu X-J, Liang M-F, Zhang S-Y, et al. Fever with thrombocytopenia associated with a novel bunyavirus in China. *N Engl J Med*. 2011;364(16):1523-1532. doi:10.1056/NEJMoa1010095
  31. Burkhalter KL, Harmon JR, Ashley DC, et al. First Detection of Heartland Virus (Bunyaviridae: Phlebovirus) from Field Collected Arthropods. *Am J Trop Med Hyg*. 2013;89(3):445-452.

## References

- doi:10.4269/ajtmh.13-0209
32. Brault A, Savage H, Duggal N, Eisen R, Staples J. Heartland Virus Epidemiology, Vector Association, and Disease Potential. *Viruses*. 2018;10(9):498. doi:10.3390/v10090498
  33. Cusi MG, Savellini GG, Zanelli G. Toscana virus epidemiology: from Italy to beyond. *Open Virol J*. 2010;4(2):22-28. doi:10.2174/1874357901004020022
  34. Salimi H, Cain MD, Klein RS. Encephalitic Arboviruses: Emergence, Clinical Presentation, and Neuropathogenesis. *Neurotherapeutics*. 2016;13(3):514-534. doi:10.1007/s13311-016-0443-5
  35. Saikku P, Brummer-Korvenkontio M. Arboviruses in Finland. II. Isolation and characterization of Uukuniemi virus, a virus associated with ticks and birds. *Am J Trop Med Hyg*. 1973;22(3):390-399. <http://www.ncbi.nlm.nih.gov/pubmed/4122382>. Accessed September 15, 2015.
  36. Saikku P. Arboviruses in Finland. 3. Uukuniemi virus antibodies in human, cattle, and reindeer sera. *Am J Trop Med Hyg*. 1973;22(3):400-403. <http://www.ncbi.nlm.nih.gov/pubmed/4735908>. Accessed January 13, 2015.
  37. Lozach P-Y, Mancini R, Bitto D, et al. Entry of bunyaviruses into mammalian cells. *Cell Host Microbe*. 2010;7(6):488-499. doi:10.1016/j.chom.2010.05.007
  38. Mazelier M, Rouxel RN, Zumstein M, Mancini R, Bell-Sakyi L, Lozach P-Y. Uukuniemi virus as a tick-borne virus model. *J Virol*. May 2016. doi:10.1128/JVI.00095-16
  39. Mazelier M. Uukuniemi virus as a tick-borne virus model to characterize the vector-host switch in vitro. 2017.
  40. Léger P, Lozach P-Y. Bunyaviruses: from transmission by arthropods to virus entry into the mammalian-host first-target cells. 2015.
  41. Overby AK, Pettersson RF, Grünewald K, Huiskonen JT. Insights into bunyavirus architecture from electron cryotomography of Uukuniemi virus. *Proc Natl Acad Sci U S A*. 2008;105(7):2375-2379. doi:10.1073/pnas.0708738105
  42. Jupille H, Vega-Rua A, Rougeon F, Failloux A-B. Arboviruses: variations on an ancient theme. *Future Virol*. 2014;9(8):733-751. doi:10.2217/fvl.14.62
  43. Albornoz A, Hoffmann AB, Lozach P-Y, Tischler ND. Early Bunyavirus-Host Cell Interactions. *Viruses*. 2016;8(5). doi:10.3390/v8050143
  44. Eifan S, Schnettler E, Dietrich I, Kohl A, Blomström A-L. Non-structural proteins of arthropod-borne bunyaviruses: roles and functions. *Viruses*. 2013;5(10):2447-2468. doi:10.3390/v5102447
  45. Won S, Ikegami T, Peters CJ, Makino S. NSm Protein of Rift Valley Fever Virus Suppresses Virus-Induced Apoptosis. *J Virol*. 2007;81(24):13335-13345. doi:10.1128/JVI.01238-07
  46. Gerrard SR, Bird BH, Albariño CG, Nichol ST. The NSm proteins of Rift Valley fever virus are dispensable for maturation, replication and infection. *Virology*. 2007;359(2):459-465. doi:10.1016/j.virol.2006.09.035
  47. Elliott RM, Brennan B. Emerging phleboviruses. *Curr Opin Virol*. 2014;5:50-57. doi:10.1016/j.coviro.2014.01.011
  48. Spiegel M, Plegge T, Pöhlmann S. The Role of Phlebovirus Glycoproteins in Viral Entry, Assembly and Release. *Viruses*. 2016;8(7):202. doi:10.3390/v8070202

## References

49. Boulant S, Stanifer M, Lozach P-Y. Dynamics of virus-receptor interactions in virus binding, signal-ing, and endocytosis. *Viruses*. 2015.
50. Pietrantoni A, Fortuna C, Remoli ME, Ciufolini MG, Superti F. Bovine lactoferrin inhibits Toscana virus infection by binding to heparan sulphate. *Viruses*. 2015;7(2):480-495. doi:10.3390/v7020480
51. Riblett AM, Blomen VA, Jae LT, et al. A Haploid Genetic Screen Identifies Heparan Sulfate Proteoglycans Supporting Rift Valley Fever Virus Infection. Dermody TS, ed. *J Virol*. 2016;90(3):1414-1423. doi:10.1128/JVI.02055-15
52. de Boer SM, Kortekaas J, de Haan CAM, Rottier PJM, Moormann RJM, Bosch BJ. Heparan sulfate facilitates Rift Valley fever virus entry into the cell. *J Virol*. 2012;86(24):13767-13771. doi:10.1128/JVI.01364-12
53. Sun Y, Qi Y, Liu C, et al. Nonmuscle myosin heavy chain IIA is a critical factor contributing to the efficiency of early infection of severe fever with thrombocytopenia syndrome virus. *J Virol*. 2014;88(1):237-248. doi:10.1128/JVI.02141-13
54. Lozach P-Y, Kühbacher A, Meier R, et al. DC-SIGN as a receptor for phleboviruses. *Cell Host Microbe*. 2011;10(1):75-88. doi:10.1016/j.chom.2011.06.007
55. Hofmann H, Li X, Zhang X, et al. Severe fever with thrombocytopenia virus glycoproteins are targeted by neutralizing antibodies and can use DC-SIGN as a receptor for pH-dependent entry into human and animal cell lines. *J Virol*. 2013;87(8):4384-4394. doi:10.1128/JVI.02628-12
56. van Kooyk Y. C-type lectins on dendritic cells: key modulators for the induction of immune responses. *Biochem Soc Trans*. 2008;36(Pt 6):1478-1481. doi:10.1042/BST0361478
57. Svajger U, Anderlüh M, Jeras M, Obermajer N. C-type lectin DC-SIGN: an adhesion, signalling and antigen-uptake molecule that guides dendritic cells in immunity. *Cell Signal*. 2010;22(10):1397-1405. doi:10.1016/j.cellsig.2010.03.018
58. Guo Y, Feinberg H, Conroy E, et al. Structural basis for distinct ligand-binding and targeting properties of the receptors DC-SIGN and DC-SIGNR. *Nat Struct Mol Biol*. 2004;11(7):591-598. doi:10.1038/nsmb784
59. Léger P, Tetard M, Youness B, et al. Differential Use of the C-Type Lectins L-SIGN and DC-SIGN for Phlebovirus Endocytosis. *Traffic*. 2016;17(6):639-656. doi:10.1111/tra.12393
60. Tani H, Shimojima M, Fukushi S, et al. Characterization of Glycoprotein-Mediated Entry of Severe Fever with Thrombocytopenia Syndrome Virus. Lyles DS, ed. *J Virol*. 2016;90(11):5292-5301. doi:10.1128/JVI.00110-16
61. Dominguez-Soto A, Aragonese-Fenoll L, Martin-Gayo E, et al. The DC-SIGN-related lectin LSECtin mediates antigen capture and pathogen binding by human myeloid cells. *Blood*. 2007;109(12):5337-5345. doi:10.1182/blood-2006-09-048058
62. Liu W, Tang L, Zhang G, et al. Characterization of a Novel C-type Lectin-like Gene, LSECtin. *J Biol Chem*. 2004;279(18):18748-18758. doi:10.1074/jbc.M311227200
63. Zhang F, Ren S, Zuo Y. DC-SIGN, DC-SIGNR and LSECtin: C-type lectins for infection. *Int Rev Immunol*. 2014;33(1):54-66. doi:10.3109/08830185.2013.834897
64. Azad AK, Torrelles JB, Schlesinger LS. Mutation in the DC-SIGN cytoplasmic triacidic cluster motif markedly attenuates receptor activity for phagocytosis and endocytosis of mannose-containing ligands by human myeloid cells. *J Leukoc Biol*. 2008;84(6):1594-1603.

## References

- doi:10.1189/jlb.0308192
65. Rapoport I, Chen YC, Cupers P, et al. Dileucine-based sorting signals bind to the beta chain of AP-1 at a site distinct and regulated differently from the tyrosine-based motif-binding site. *EMBO J.* 1998;17(8):2148-2155. doi:10.1093/emboj/17.8.2148
  66. Cambi A, de Lange F, van Maarseveen NM, et al. Microdomains of the C-type lectin DC-SIGN are portals for virus entry into dendritic cells. *J Cell Biol.* 2004;164(1):145-155. doi:10.1083/jcb.200306112
  67. Cambi A, Beeren I, Joosten B, Fransen JA, Figdor CG. The C-type lectin DC-SIGN internalizes soluble antigens and HIV-1 virions via a clathrin-dependent mechanism. *Eur J Immunol.* 2009;39(7):1923-1928. doi:10.1002/eji.200939351
  68. Gringhuis SI, den Dunnen J, Litjens M, van Het Hof B, van Kooyk Y, Geijtenbeek TBH. C-type lectin DC-SIGN modulates Toll-like receptor signaling via Raf-1 kinase-dependent acetylation of transcription factor NF-kappaB. *Immunity.* 2007;26(5):605-616. doi:10.1016/j.immuni.2007.03.012
  69. Gringhuis SI, den Dunnen J, Litjens M, van der Vlist M, Geijtenbeek TBH. Carbohydrate-specific signaling through the DC-SIGN signalosome tailors immunity to Mycobacterium tuberculosis, HIV-1 and Helicobacter pylori. *Nat Immunol.* 2009;10(10):1081-1088. doi:10.1038/ni.1778
  70. Liu J, Xu M, Tang B, et al. Single-Particle Tracking Reveals the Sequential Entry Process of the Bunyavirus Severe Fever with Thrombocytopenia Syndrome Virus. *Small.* December 2018:1803788. doi:10.1002/smll.201803788
  71. de Boer SM, Kortekaas J, Spel L, Rottier PJM, Moormann RJM, Bosch BJ. Acid-activated structural reorganization of the Rift Valley fever virus Gc fusion protein. *J Virol.* 2012;86(24):13642-13652. doi:10.1128/JVI.01973-12
  72. Filone CM, Hanna SL, Caino MC, Bambina S, Doms RW, Cherry S. Rift valley fever virus infection of human cells and insect hosts is promoted by protein kinase C epsilon. *PLoS One.* 2010;5(11):e15483. doi:10.1371/journal.pone.0015483
  73. Harmon B, Schudel BR, Maar D, et al. Rift Valley fever virus strain MP-12 enters mammalian host cells via caveola-mediated endocytosis. *J Virol.* 2012;86(23):12954-12970. doi:10.1128/JVI.02242-12
  74. Hackett BA, Yasunaga A, Panda D, et al. RNASEK is required for internalization of diverse acid-dependent viruses. *Proc Natl Acad Sci U S A.* 2015;112(25):7797-7802. doi:10.1073/pnas.1424098112
  75. Huotari J, Helenius A. Endosome maturation. *EMBO J.* 2011;30(17):3481-3500. doi:10.1038/emboj.2011.286
  76. Drake MJ, Brennan B, Briley K, et al. A role for glycolipid biosynthesis in severe fever with thrombocytopenia syndrome virus entry. Whelan SPJ, ed. *PLoS Pathog.* 2017;13(4):e1006316. doi:10.1371/journal.ppat.1006316
  77. Lozach P-Y, Huotari J, Helenius A. Late-penetrating viruses. *Curr Opin Virol.* 2011;1(1):35-43. doi:10.1016/j.coviro.2011.05.004
  78. Mercer J, Schelhaas M, Helenius A. Virus Entry by Endocytosis. *Annu Rev Biochem.* 2010;79(1):803-833. doi:10.1146/annurev-biochem-060208-104626

## References

79. Yamauchi Y, Boukari H, Banerjee I, Sbalzarini IF, Horvath P, Helenius A. Histone Deacetylase 8 Is Required for Centrosome Cohesion and Influenza A Virus Entry. Pecosz A, ed. *PLoS Pathog.* 2011;7(10):e1002316. doi:10.1371/journal.ppat.1002316
80. Meier R, Franceschini A, Horvath P, et al. Genome-wide small interfering RNA screens reveal VAMP3 as a novel host factor required for Uukuniemi virus late penetration. *J Virol.* 2014;88(15):8565-8578. doi:10.1128/JVI.00388-14
81. Bitto D, Halldorsson S, Caputo A, Huiskonen JT. Low pH and Anionic Lipid Dependent Fusion of Uukuniemi Phlebovirus to Liposomes. *J Biol Chem.* January 2016. doi:10.1074/jbc.M115.691113
82. White JM, Whittaker GR. Fusion of Enveloped Viruses in Endosomes. *Traffic.* March 2016. doi:10.1111/tra.12389
83. Halldorsson S, Li S, Li M, Harlos K, Bowden TA, Huiskonen JT. Shielding and activation of a viral membrane fusion protein. *Nat Commun.* 2018;9(1):349. doi:10.1038/s41467-017-02789-2
84. Gallala HD, Sandhoff K. Biological function of the cellular lipid BMP-BMP as a key activator for cholesterol sorting and membrane digestion. *Neurochem Res.* 2011;36(9):1594-1600. doi:10.1007/s11064-010-0337-6
85. Ichikawa S, Hirabayashi Y. Glucosylceramide synthase and glycosphingolipid synthesis. *Trends Cell Biol.* 1998;8(5):198-202. <http://www.ncbi.nlm.nih.gov/pubmed/9695839>. Accessed February 11, 2019.
86. Kielian M. Mechanisms of Virus Membrane Fusion Proteins. *Annu Rev Virol.* 2014;1(1):171-189. doi:10.1146/annurev-virology-031413-085521
87. Harrison SC. Viral membrane fusion. *Virology.* 2015;479-480:498-507. doi:10.1016/j.virol.2015.03.043
88. Halldorsson S, Behrens A-J, Harlos K, et al. Structure of a phleboviral envelope glycoprotein reveals a consolidated model of membrane fusion. *Proc Natl Acad Sci.* 2016;113(26):7154-7159. doi:10.1073/pnas.1603827113
89. Dessau M, Modis Y. Crystal structure of glycoprotein C from Rift Valley fever virus. *Proc Natl Acad Sci.* 2013;110(5):1696-1701. doi:10.1073/pnas.1217780110
90. Mudhasani R, Tran JP, Retterer C, et al. IFITM-2 and IFITM-3 but Not IFITM-1 Restrict Rift Valley Fever Virus. *J Virol.* 2013;87(15):8451-8464. doi:10.1128/JVI.03382-12
91. Wu Y, Zhu Y, Gao F, et al. Structures of phlebovirus glycoprotein Gn and identification of a neutralizing antibody epitope. *Proc Natl Acad Sci.* 2017;114(36):E7564-E7573. doi:10.1073/pnas.1705176114
92. Kielian M, Chanel-Vos C, Liao M. Alphavirus Entry and Membrane Fusion. *Viruses.* 2010;2(4):796-825. doi:10.3390/v2040796
93. Modis Y, Nayak V. Molecular Mechanisms of Flaviviral Membrane Fusion. In: *West Nile Encephalitis Virus Infection.* New York, NY: Springer New York; 2009:265-286. doi:10.1007/978-0-387-79840-0\_12
94. Reguera J, Weber F, Cusack S. Bunyaviridae RNA Polymerases (L-Protein) Have an N-Terminal, Influenza-Like Endonuclease Domain, Essential for Viral Cap-Dependent Transcription. Rey FA, ed. *PLoS Pathog.* 2010;6(9):e1001101. doi:10.1371/journal.ppat.1001101

## References

95. Jin H, Elliott RM. Non-viral sequences at the 5' ends of Dugbe nairovirus S mRNAs. *J Gen Virol.* 1993;74 ( Pt 10)(10):2293-2297. doi:10.1099/0022-1317-74-10-2293
96. Prehaud C, Lopez N, Blok MJ, Obry V, Bouloy M. Analysis of the 3' Terminal Sequence Recognized by the Rift Valley Fever Virus Transcription Complex in Its Ambisense S Segment. *Virology.* 1997;227(1):189-197. doi:10.1006/viro.1996.8324
97. Emery VC, Bishop DH. Characterization of Punta Toro S mRNA species and identification of an inverted complementary sequence in the intergenic region of Punta Toro phlebovirus ambisense S RNA that is involved in mRNA transcription termination. *Virology.* 1987;156(1):1-11. <http://www.ncbi.nlm.nih.gov/pubmed/18644551>. Accessed January 7, 2019.
98. Jääntti J, Hildén P, Rönkä H, Mäkiranta V, Keränen S, Kuismanen E. Immunocytochemical analysis of Uukuniemi virus budding compartments: role of the intermediate compartment and the Golgi stack in virus maturation. *J Virol.* 1997;71(2):1162-1172. <http://www.ncbi.nlm.nih.gov/pubmed/8995638>. Accessed February 11, 2019.
99. Lozach P-Y, Burleigh L, Staropoli I, et al. Dendritic cell-specific intercellular adhesion molecule 3-grabbing non-integrin (DC-SIGN)-mediated enhancement of dengue virus infection is independent of DC-SIGN internalization signals. *J Biol Chem.* 2005;280(25):23698-23708. doi:10.1074/jbc.M504337200
100. Galli T, Chilcote T, Mundigl O, Binz T, Niemann H, De Camilli P. Tetanus toxin-mediated cleavage of cellubrevin impairs exocytosis of transferrin receptor-containing vesicles in CHO cells. *J Cell Biol.* 1994;125(5):1015-1024. <http://www.pubmedcentral.nih.gov/articlerender.fcgi?artid=2120045&tool=pmcentrez&rendertype=abstract>. Accessed January 10, 2015.
101. McMahon HT, Ushkaryov YA, Edelman L, et al. Cellubrevin is a ubiquitous tetanus-toxin substrate homologous to a putative synaptic vesicle fusion protein. *Nature.* 1993;364(6435):346-349. doi:10.1038/364346a0
102. Mallard F, Tang BL, Galli T, et al. Early/recycling endosomes-to-TGN transport involves two SNARE complexes and a Rab6 isoform. *J Cell Biol.* 2002;156(4):653-664. doi:10.1083/jcb.200110081
103. Klionsky DJ, Abdalla FC, Abeliovich H, et al. Guidelines for the use and interpretation of assays for monitoring autophagy. *Autophagy.* 2012;8(4):445-544. <http://www.pubmedcentral.nih.gov/articlerender.fcgi?artid=3404883&tool=pmcentrez&rendertype=abstract>. Accessed July 10, 2014.
104. Puri C, Renna M, Bento CF, Moreau K, Rubinsztein DC. Diverse Autophagosomal Membrane Sources Coalesce in Recycling Endosomes. *Cell.* 2013;154(6):1285-1299. doi:10.1016/j.cell.2013.08.044
105. Fader CM, Sánchez DG, Mestre MB, Colombo MI. TI-VAMP/VAMP7 and VAMP3/cellubrevin: two v-SNARE proteins involved in specific steps of the autophagy/multivesicular body pathways. *Biochim Biophys Acta.* 2009;1793(12):1901-1916. doi:10.1016/j.bbamcr.2009.09.011
106. Gordon PB, Seglen PO. Prelysosomal convergence of autophagic and endocytic pathways. *Biochem Biophys Res Commun.* 1988;151(1):40-47. <http://www.ncbi.nlm.nih.gov/pubmed/3126737>. Accessed January 12, 2015.
107. García IA, Martínez HE, Alvarez C. Rab1b regulates COPI and COPII dynamics in mammalian cells. *Cell Logist.* 2011;1(4):159-163. doi:10.4161/cl.1.4.18221

## References

108. Welz T, Wellbourne-Wood J, Kerkhoff E. Orchestration of cell surface proteins by Rab11. *Trends Cell Biol.* 2014;24(7):407-415. doi:10.1016/j.tcb.2014.02.004
109. Zoppino FCM, Militello RD, Slavin I, Alvarez C, Colombo MI. Autophagosome formation depends on the small GTPase Rab1 and functional ER exit sites. *Traffic.* 2010;11(9):1246-1261. doi:10.1111/j.1600-0854.2010.01086.x
110. Longatti A, Lamb CA, Razi M, Yoshimura S, Barr FA, Tooze SA. TBC1D14 regulates autophagosome formation via Rab11- and ULK1-positive recycling endosomes. *J Cell Biol.* 2012;197(5):659-675. doi:10.1083/jcb.201111079
111. De Duve C. The lysosome. *Sci Am.* 1963;208:64-72. <http://www.ncbi.nlm.nih.gov/pubmed/14025755>. Accessed January 7, 2019.
112. Tsukada M, Ohsumi Y. Isolation and characterization of autophagy-defective mutants of *Saccharomyces cerevisiae*. *FEBS Lett.* 1993;333(1-2):169-174. doi:10.1016/0014-5793(93)80398-E
113. Mizushima N, Noda T, Yoshimori T, et al. A protein conjugation system essential for autophagy. *Nature.* 1998;395(6700):395-398. doi:10.1038/26506
114. Tooze SA, Dikic I. Autophagy Captures the Nobel Prize. *Cell.* 2016;167(6):1433-1435. doi:10.1016/j.cell.2016.11.023
115. Catarino S, Pereira P, Girão H. Molecular control of chaperone-mediated autophagy. *Essays Biochem.* 2017;61(6):663-674. doi:10.1042/EBC20170057
116. Santambrogio L, Cuervo AM. Chasing the elusive mammalian microautophagy. *Autophagy.* 2011;7(6):652-654. <http://www.ncbi.nlm.nih.gov/pubmed/21460618>. Accessed January 16, 2019.
117. Kim J, Kundu M, Viollet B, Guan K-L. AMPK and mTOR regulate autophagy through direct phosphorylation of Ulk1. *Nat Cell Biol.* 2011;13(2):132-141. doi:10.1038/ncb2152
118. Hosokawa N, Hara T, Kaizuka T, et al. Nutrient-dependent mTORC1 Association with the ULK1–Atg13–FIP200 Complex Required for Autophagy. Schmid SL, ed. *Mol Biol Cell.* 2009;20(7):1981-1991. doi:10.1091/mbc.e08-12-1248
119. Dunlop EA, Hunt DK, Acosta-Jaquez HA, Fingar DC, Tee AR. ULK1 inhibits mTORC1 signaling, promotes multisite Raptor phosphorylation and hinders substrate binding. *Autophagy.* 2011;7(7):737-747. <http://www.ncbi.nlm.nih.gov/pubmed/21460630>. Accessed January 9, 2019.
120. Ganley IG, Lam DH, Wang J, Ding X, Chen S, Jiang X. ULK1.ATG13.FIP200 complex mediates mTOR signaling and is essential for autophagy. *J Biol Chem.* 2009;284(18):12297-12305. doi:10.1074/jbc.M900573200
121. Hamasaki M, Furuta N, Matsuda A, et al. Autophagosomes form at ER–mitochondria contact sites. *Nature.* 2013;495(7441):389-393. doi:10.1038/nature11910
122. Karanasios E, Walker SA, Okkenhaug H, et al. Autophagy initiation by ULK complex assembly on ER tubulovesicular regions marked by ATG9 vesicles. *Nat Commun.* 2016;7(1):12420. doi:10.1038/ncomms12420
123. Karanasios E, Stapleton E, Manifava M, et al. Dynamic association of the ULK1 complex with omegasomes during autophagy induction. *J Cell Sci.* 2013;126(Pt 22):5224-5238. doi:10.1242/jcs.132415

## References

124. Di Bartolomeo S, Corazzari M, Nazio F, et al. The dynamic interaction of AMBRA1 with the dynein motor complex regulates mammalian autophagy. *J Cell Biol.* 2010;191(1):155-168. doi:10.1083/jcb.201002100
125. Russell RC, Tian Y, Yuan H, et al. ULK1 induces autophagy by phosphorylating Beclin-1 and activating VPS34 lipid kinase. *Nat Cell Biol.* 2013;15(7):741-750. doi:10.1038/ncb2757
126. Polson HEJ, de Lartigue J, Rigden DJ, et al. Mammalian Atg18 (WIPI2) localizes to omegasome-anchored phagophores and positively regulates LC3 lipidation. *Autophagy.* 2010;6(4):506-522. doi:10.4161/auto.6.4.11863
127. Bakula D, Müller AJ, Zuleger T, et al. WIPI3 and WIPI4  $\beta$ -propellers are scaffolds for LKB1-AMPK-TSC signalling circuits in the control of autophagy. *Nat Commun.* 2017;8:15637. doi:10.1038/ncomms15637
128. Axe EL, Walker SA, Manifava M, et al. Autophagosome formation from membrane compartments enriched in phosphatidylinositol 3-phosphate and dynamically connected to the endoplasmic reticulum. *J Cell Biol.* 2008;182(4):685-701. doi:10.1083/jcb.200803137
129. Puri C, Vicinanza M, Ashkenazi A, et al. The RAB11A-Positive Compartment Is a Primary Platform for Autophagosome Assembly Mediated by WIPI2 Recognition of PI3P-RAB11A. *Dev Cell.* 2018;45(1):114-131.e8. doi:10.1016/j.devcel.2018.03.008
130. Tanida I, Ueno T, Kominami E. LC3 conjugation system in mammalian autophagy. *Int J Biochem Cell Biol.* 2004;36(12):2503-2518. doi:10.1016/j.biocel.2004.05.009
131. Mizushima N, Yoshimori T, Levine B. Methods in mammalian autophagy research. *Cell.* 2010;140(3):313-326. doi:10.1016/j.cell.2010.01.028
132. Pankiv S, Clausen TH, Lamark T, et al. p62/SQSTM1 binds directly to Atg8/LC3 to facilitate degradation of ubiquitinated protein aggregates by autophagy. *J Biol Chem.* 2007;282(33):24131-24145. doi:10.1074/jbc.M702824200
133. Kirkin V, Lamark T, Sou Y-S, et al. A role for NBR1 in autophagosomal degradation of ubiquitinated substrates. *Mol Cell.* 2009;33(4):505-516. doi:10.1016/j.molcel.2009.01.020
134. Verlhac P, Grégoire IP, Azocar O, et al. Autophagy Receptor NDP52 Regulates Pathogen-Containing Autophagosome Maturation. *Cell Host Microbe.* 2015;17(4):515-525. doi:10.1016/J.CHOM.2015.02.008
135. McEwan DG, Popovic D, Gubas A, et al. PLEKHM1 Regulates Autophagosome-Lysosome Fusion through HOPS Complex and LC3/GABARAP Proteins. *Mol Cell.* 2015;57(1):39-54. doi:10.1016/J.MOLCEL.2014.11.006
136. Hayashi-Nishino M, Fujita N, Noda T, Yamaguchi A, Yoshimori T, Yamamoto A. A subdomain of the endoplasmic reticulum forms a cradle for autophagosome formation. *Nat Cell Biol.* 2009;11(12):1433-1437. doi:10.1038/ncb1991
137. Ravikumar B, Moreau K, Jahreiss L, Puri C, Rubinsztein DC. Plasma membrane contributes to the formation of pre-autophagosomal structures. *Nat Cell Biol.* 2010;12(8):747-757. doi:10.1038/ncb2078
138. Nishimura T, Tamura N, Kono N, et al. Autophagosome formation is initiated at phosphatidylinositol synthase-enriched ER subdomains. *EMBO J.* 2017;36(12):1719-1735. doi:10.15252/embj.201695189
139. Ge L, Melville D, Zhang M, Schekman R. The ER-Golgi intermediate compartment is a key

## References

- membrane source for the LC3 lipidation step of autophagosome biogenesis. *Elife*. 2013;2:e00947. doi:10.7554/eLife.00947
140. Hailey DW, Rambold AS, Satpute-Krishnan P, et al. Mitochondria supply membranes for autophagosome biogenesis during starvation. *Cell*. 2010;141(4):656-667. doi:10.1016/j.cell.2010.04.009
  141. Kakuta S, Yamaguchi J, Suzuki C, Sasaki M, Kazuno S, Uchiyama Y. Small GTPase Rab1B is associated with ATG9A vesicles and regulates autophagosome formation. *FASEB J*. 2017;31(9):3757-3773. doi:10.1096/fj.201601052R
  142. Orsi A, Razi M, Dooley HC, et al. Dynamic and transient interactions of Atg9 with autophagosomes, but not membrane integration, are required for autophagy. Klumperman J, ed. *Mol Biol Cell*. 2012;23(10):1860-1873. doi:10.1091/mbc.e11-09-0746
  143. Velikkakath AKG, Nishimura T, Oita E, Ishihara N, Mizushima N. Mammalian Atg2 proteins are essential for autophagosome formation and important for regulation of size and distribution of lipid droplets. Yoshimori T, ed. *Mol Biol Cell*. 2012;23(5):896-909. doi:10.1091/mbc.e11-09-0785
  144. Itakura E, Kishi C, Inoue K, Mizushima N. Beclin 1 Forms Two Distinct Phosphatidylinositol 3-Kinase Complexes with Mammalian Atg14 and UVRAG. Subramani S, ed. *Mol Biol Cell*. 2008;19(12):5360-5372. doi:10.1091/mbc.e08-01-0080
  145. Jiang P, Nishimura T, Sakamaki Y, et al. The HOPS complex mediates autophagosome-lysosome fusion through interaction with syntaxin 17. *Mol Biol Cell*. 2014;25(8):1327-1337. doi:10.1091/mbc.E13-08-0447
  146. Itakura E, Kishi-Itakura C, Mizushima N. The Hairpin-type Tail-Anchored SNARE Syntaxin 17 Targets to Autophagosomes for Fusion with Endosomes/Lysosomes. *Cell*. 2012;151(6):1256-1269. doi:10.1016/j.cell.2012.11.001
  147. Choi Y, Bowman JW, Jung JU. Autophagy during viral infection - a double-edged sword. *Nat Rev Microbiol*. March 2018. doi:10.1038/s41579-018-0003-6
  148. Bauckman KA, Owusu-Boaitey N, Mysorekar IU. Selective autophagy: Xenophagy. *Methods*. 2015;75:120-127. doi:10.1016/j.ymeth.2014.12.005
  149. Deretic V, Saitoh T, Akira S. Autophagy in infection, inflammation and immunity. *Nat Rev Immunol*. 2013;13(10):722-737. doi:10.1038/nri3532
  150. Abdoli A, Alirezaei M, Mehrbod P, Forouzanfar F. Autophagy: The multi-purpose bridge in viral infections and host cells. *Rev Med Virol*. April 2018:e1973. doi:10.1002/rmv.1973
  151. Ahmad L, Mostowy S, Sancho-Shimizu V. Autophagy-Virus Interplay: From Cell Biology to Human Disease. *Front Cell Dev Biol*. 2018;6:155. doi:10.3389/fcell.2018.00155
  152. Viret C, Rozières A, Faure M. Autophagy during Early Virus-Host Cell Interactions. *J Mol Biol*. April 2018. doi:10.1016/j.jmb.2018.04.018
  153. Ke P-Y. The Multifaceted Roles of Autophagy in Flavivirus-Host Interactions. *Int J Mol Sci*. 2018;19(12):3940. doi:10.3390/ijms19123940
  154. Pleet ML, Branscome H, DeMarino C, et al. Autophagy, EVs, and Infections: A Perfect Question for a Perfect Time. *Front Cell Infect Microbiol*. 2018;8:362. doi:10.3389/fcimb.2018.00362
  155. Yordy B, Tal MC, Hayashi K, Arojo O, Iwasaki A. Autophagy and selective deployment of Atg

## References

- proteins in antiviral defense. *Int Immunol*. 2013;25(1):1-10. doi:10.1093/intimm/dxs101
156. Lee HK, Lund JM, Ramanathan B, Mizushima N, Iwasaki A. Autophagy-Dependent Viral Recognition by Plasmacytoid Dendritic Cells. *Science* (80- ). 2007;315(5817):1398-1401. doi:10.1126/science.1136880
157. Yang Q, Liu T-T, Lin H, et al. TRIM32-TAX1BP1-dependent selective autophagic degradation of TRIF negatively regulates TLR3/4-mediated innate immune responses. Philpott DJ, ed. *PLoS Pathog*. 2017;13(9):e1006600. doi:10.1371/journal.ppat.1006600
158. Moy RH, Gold B, Molleston JM, et al. Antiviral autophagy restricts Rift Valley fever virus infection and is conserved from flies to mammals. *Immunity*. 2014;40(1):51-65. doi:10.1016/j.immuni.2013.10.020
159. Sun Y, Liu M, Lei X, Yu X. SFTS phlebovirus promotes LC3-II accumulation and nonstructural protein of SFTS phlebovirus co-localizes with autophagy proteins. *Sci Rep*. 2018;8(1):5287. doi:10.1038/s41598-018-23610-0
160. Thurston TLM, Wandel MP, von Muhlinen N, Foeglein Á, Randow F. Galectin 8 targets damaged vesicles for autophagy to defend cells against bacterial invasion. *Nature*. 2012;482(7385):414-418. doi:10.1038/nature10744
161. Staring J, von Castelmur E, Blomen VA, et al. PLA2G16 represents a switch between entry and clearance of Picornaviridae. *Nature*. 2017;541(7637):412-416. doi:10.1038/nature21032
162. Heckmann BL, Boada-Romero E, Cunha LD, Magne J, Green DR. LC3-Associated Phagocytosis and Inflammation. *J Mol Biol*. 2017;429(23):3561-3576. doi:10.1016/j.jmb.2017.08.012
163. Dengjel J, Schoor O, Fischer R, et al. Autophagy promotes MHC class II presentation of peptides from intracellular source proteins. *Proc Natl Acad Sci*. 2005;102(22):7922-7927. doi:10.1073/pnas.0501190102
164. Chaumorcel M, Lussignol M, Mouna L, et al. The Human Cytomegalovirus Protein TRS1 Inhibits Autophagy via Its Interaction with Beclin 1. *J Virol*. 2012;86(5):2571-2584. doi:10.1128/JVI.05746-11
165. Orvedahl A, Alexander D, Tallóczy Z, et al. HSV-1 ICP34.5 Confers Neurovirulence by Targeting the Beclin 1 Autophagy Protein. *Cell Host Microbe*. 2007;1(1):23-35. doi:10.1016/j.chom.2006.12.001
166. Lee J-S, Li Q, Lee J-Y, et al. FLIP-mediated autophagy regulation in cell death control. *Nat Cell Biol*. 2009;11(11):1355-1362. doi:10.1038/ncb1980
167. Nanbo A, Imai M, Watanabe S, et al. Ebola virus is internalized into host cells via macropinocytosis in a viral glycoprotein-dependent manner. Rey FA, ed. *PLoS Pathog*. 2010;6(9):e1001121. doi:10.1371/journal.ppat.1001121
168. Shtanko O, Reyes AN, Jackson WT, Davey RA. Autophagy-Associated Proteins Control Ebola Virus Internalization Into Host Cells. *J Infect Dis*. 2018;218(suppl\_5):S346-S354. doi:10.1093/infdis/jiy294
169. Pirooz SD, He S, Zhang T, et al. UVRAG is required for virus entry through combinatorial interaction with the class C-Vps complex and SNAREs. *Proc Natl Acad Sci U S A*. 2014;111(7):2716-2721. doi:10.1073/pnas.1320629111
170. Lee Y-R, Lei H-Y, Liu M-T, et al. Autophagic machinery activated by dengue virus enhances

## References

- virus replication. *Virology*. 2008;374(2):240-248. doi:10.1016/j.virol.2008.02.016
171. Panyasrivanit M, Khakpoor A, Wikan N, Smith DR. Co-localization of constituents of the dengue virus translation and replication machinery with amphisomes. *J Gen Virol*. 2009;90(Pt 2):448-456. doi:10.1099/vir.0.005355-0
172. Zhang J, Lan Y, Li MY, et al. Flaviviruses Exploit the Lipid Droplet Protein AUP1 to Trigger Lipophagy and Drive Virus Production. *Cell Host Microbe*. 2018;23(6):819-831.e5. doi:10.1016/j.chom.2018.05.005
173. Heaton NS, Randall G. Dengue virus-induced autophagy regulates lipid metabolism. *Cell Host Microbe*. 2010;8(5):422-432. doi:10.1016/j.chom.2010.10.006
174. Buckingham EM, Jarosinski KW, Jackson W, Carpenter JE, Grose C. Exocytosis of Varicella-Zoster Virus Virions Involves a Convergence of Endosomal and Autophagy Pathways. Longnecker RM, ed. *J Virol*. 2016;90(19):8673-8685. doi:10.1128/JVI.00915-16
175. Hervé JC, Bourmeyster N. Rab GTPases, master controllers of eukaryotic trafficking. *Small GTPases*. 2018;9(1-2):1-4. doi:10.1080/21541248.2018.1428853
176. Müller MP, Goody RS. Molecular control of Rab activity by GEFs, GAPs and GDI. *Small GTPases*. 2018;9(1-2):5-21. doi:10.1080/21541248.2016.1276999
177. Martinez H, García IA, Sampieri L, Alvarez C. Spatial-Temporal Study of Rab1b Dynamics and Function at the ER-Golgi Interface. Jackson CL, ed. *PLoS One*. 2016;11(8):e0160838. doi:10.1371/journal.pone.0160838
178. Zhao X, Claude A, Chun J, Shields DJ, Presley JF, Melançon P. GBF1, a cis-Golgi and VTCs-localized ARF-GEF, is implicated in ER-to-Golgi protein traffic. *J Cell Sci*. 2006;119(18):3743-3753. doi:10.1242/jcs.03173
179. Kawamoto K, Yoshida Y, Tamaki H, et al. GBF1, a guanine nucleotide exchange factor for ADP-ribosylation factors, is localized to the cis-Golgi and involved in membrane association of the COPI coat. *Traffic*. 2002;3(7):483-495. <http://www.ncbi.nlm.nih.gov/pubmed/12047556>. Accessed January 14, 2019.
180. García-Mata R, Szul T, Alvarez C, Sztul E. ADP-ribosylation factor/COPI-dependent events at the endoplasmic reticulum-Golgi interface are regulated by the guanine nucleotide exchange factor GBF1. *Mol Biol Cell*. 2003;14(6):2250-2261. doi:10.1091/mbc.E02-11-0730
181. Szul T, Sztul E. COPII and COPI Traffic at the ER-Golgi Interface. *Physiology*. 2011;26(5):348-364. doi:10.1152/physiol.00017.2011
182. Goldenring JR, Soroka CJ, Shen KR, et al. Enrichment of rab11, a small GTP-binding protein, in gastric parietal cells. *Am J Physiol*. 1994;267(2 Pt 1):G187-94. doi:10.1152/ajpgi.1994.267.2.G187
183. Lai F, Stubbs L, Artzt K. Molecular Analysis of Mouse Rab11b: A New Type of Mammalian YPT/Rab Protein. *Genomics*. 1994;22(3):610-616. doi:10.1006/geno.1994.1434
184. Goldenring JR, Shen KR, Vaughan HD, Modlin IM. Identification of a small GTP-binding protein, Rab25, expressed in the gastrointestinal mucosa, kidney, and lung. *J Biol Chem*. 1993;268(25):18419-18422. <http://www.ncbi.nlm.nih.gov/pubmed/8360141>. Accessed February 14, 2019.
185. Ullrich O, Reinsch S, Urbé S, Zerial M, Parton RG. Rab11 regulates recycling through the pericentriolar recycling endosome. *J Cell Biol*. 1996;135(4):913-924.

## References

- doi:10.1083/JCB.135.4.913
186. Schlierf B, Fey GH, Hauber J, Hocke GM, Rosorius O. Rab11b Is Essential for Recycling of Transferrin to the Plasma Membrane. *Exp Cell Res.* 2000;259(1):257-265. doi:10.1006/excr.2000.4947
  187. Casanova JE, Wang X, Kumar R, et al. Association of Rab25 and Rab11a with the apical recycling system of polarized Madin-Darby canine kidney cells. *Mol Biol Cell.* 1999;10(1):47-61. <http://www.ncbi.nlm.nih.gov/pubmed/9880326>. Accessed February 14, 2019.
  188. Campa CC, Hirsch E. Rab11 and phosphoinositides: A synergy of signal transducers in the control of vesicular trafficking. *Adv Biol Regul.* 2017;63:132-139. doi:10.1016/j.jbior.2016.09.002
  189. Ren M, Xu G, Zeng J, De Lemos-Chiarandini C, Adesnik M, Sabatini DD. Hydrolysis of GTP on rab11 is required for the direct delivery of transferrin from the pericentriolar recycling compartment to the cell surface but not from sorting endosomes. *Proc Natl Acad Sci U S A.* 1998;95(11):6187-6192. <http://www.ncbi.nlm.nih.gov/pubmed/9600939>. Accessed January 15, 2019.
  190. Takahashi S, Kubo K, Waguri S, et al. Rab11 regulates exocytosis of recycling vesicles at the plasma membrane. *J Cell Sci.* 2012;125(Pt 17):4049-4057. doi:10.1242/jcs.102913
  191. Grimsey NJ, Coronel LJ, Cordova IC, Trejo J. Recycling and Endosomal Sorting of Protease-activated Receptor-1 Is Distinctly Regulated by Rab11A and Rab11B Proteins. *J Biol Chem.* 2016;291(5):2223-2236. doi:10.1074/jbc.M115.702993
  192. Lapierre LA, Dorn MC, Zimmerman CF, Navarre J, Burnette JO, Goldenring JR. Rab11b resides in a vesicular compartment distinct from Rab11a in parietal cells and other epithelial cells. *Exp Cell Res.* 2003;290(2):322-331. <http://www.ncbi.nlm.nih.gov/pubmed/14567990>. Accessed February 14, 2019.
  193. Sheff DR, Daro EA, Hull M, Mellman I. The receptor recycling pathway contains two distinct populations of early endosomes with different sorting functions. *J Cell Biol.* 1999;145(1):123-139. <http://www.ncbi.nlm.nih.gov/pubmed/10189373>. Accessed September 15, 2017.
  194. Wang F, Chen X, Zhang X, Ma L. Phosphorylation State of  $\mu$ -Opioid Receptor Determines the Alternative Recycling of Receptor via Rab4 or Rab11 Pathway. *Mol Endocrinol.* 2008;22(8):1881-1892. doi:10.1210/me.2007-0496
  195. Urbé S, Huber LA, Zerial M, Tooze SA, Parton RG. Rab11, a small GTPase associated with both constitutive and regulated secretory pathways in PC12 cells. *FEBS Lett.* 1993;334(2):175-182. <http://www.ncbi.nlm.nih.gov/pubmed/8224244>. Accessed January 22, 2018.
  196. Chen W, Feng Y, Chen D, Wandinger-Ness A. Rab11 Is Required for Trans-Golgi Network-to-Plasma Membrane Transport and a Preferential Target for GDP Dissociation Inhibitor. Pfeffer SR, ed. *Mol Biol Cell.* 1998;9(11):3241-3257. doi:10.1091/mbc.9.11.3241
  197. Horgan CP, Hanscom SR, Jolly RS, Futter CE, McCaffrey MW. Rab11-FIP3 links the Rab11 GTPase and cytoplasmic dynein to mediate transport to the endosomal-recycling compartment. *J Cell Sci.* 2010;123(Pt 2):181-191. doi:10.1242/jcs.052670
  198. Schonteich E, Wilson GM, Burden J, et al. The Rip11/Rab11-FIP5 and kinesin II complex regulates endocytic protein recycling. *J Cell Sci.* 2008;121(22):3824-3833. doi:10.1242/JCS.032441
  199. Savina A, Fader CM, Damiani MT, Colombo MI. Rab11 promotes docking and fusion of

## References

- multivesicular bodies in a calcium-dependent manner. *Traffic*. 2005;6(2):131-143. doi:10.1111/j.1600-0854.2004.00257.x
200. Fader CM, Sánchez D, Furlán M, Colombo MI. Induction of autophagy promotes fusion of multivesicular bodies with autophagic vacuoles in k562 cells. *Traffic*. 2008;9(2):230-250. doi:10.1111/j.1600-0854.2007.00677.x
201. Knævelsrud H, Sjøreng K, Raiborg C, et al. Membrane remodeling by the PX-BAR protein SNX18 promotes autophagosome formation. *J Cell Biol*. 2013;202(2):331-349. doi:10.1083/jcb.201205129
202. Razi M, Chan EYW, Tooze SA. Early endosomes and endosomal coatome are required for autophagy. *J Cell Biol*. 2009;185(2):305-321. doi:10.1083/jcb.200810098
203. Rusten TE, Stenmark H. How do ESCRT proteins control autophagy? *J Cell Sci*. 2009;122(13):2179-2183. doi:10.1242/jcs.050021
204. Zennou V, Petit C, Guetard D, Nerhbass U, Montagnier L, Charneau P. HIV-1 Genome Nuclear Import Is Mediated by a Central DNA Flap. *Cell*. 2000;101(2):173-185. doi:10.1016/S0092-8674(00)80828-4
205. Oker-Blom N, Salminen A, Brummer-Korvenkonito M, Kaeaeriaeinen L, Weckstroem P. Isolation of some viruses other than typical tick-borne encephalitis viruses from Ixodes ricinus ticks in Finland. *Ann Med Exp Biol Fenn*. 1964;42:109-112. <http://www.ncbi.nlm.nih.gov/pubmed/14229542>. Accessed January 31, 2019.
206. Hoffmann AB, Mazelier M, Léger P, Lozach P-Y. Deciphering Virus Entry with Fluorescently Labeled Viral Particles. *Methods Mol Biol*. 2018;1836:159-183. doi:10.1007/978-1-4939-8678-1\_8
207. de Chaumont F, Dallongeville S, Chenouard N, et al. Icy: an open bioimage informatics platform for extended reproducible research. *Nat Methods*. 2012;9(7):690-696. doi:10.1038/nmeth.2075
208. Mercer TJ, Gubas A, Tooze SA. A molecular perspective of mammalian autophagosome biogenesis. *J Biol Chem*. 2018;293(15):5386-5395. doi:10.1074/jbc.R117.810366
209. Olivo-Marin J-C. Extraction of spots in biological images using multiscale products. *Pattern Recognit*. 2002;35(9):1989-1996. doi:10.1016/S0031-3203(01)00127-3
210. Ly HJ, Ikegami T. Rift Valley fever virus NSs protein functions and the similarity to other bunyavirus NSs proteins. *Virol J*. 2016;13:118. doi:10.1186/s12985-016-0573-8
211. White J, Helenius A. pH-dependent fusion between the Semliki Forest virus membrane and liposomes. *Proc Natl Acad Sci U S A*. 1980;77(6):3273-3277. <http://www.ncbi.nlm.nih.gov/pubmed/6997876>. Accessed December 16, 2018.
212. Ramalho-Santos J, Nir S, Düzgünes N, de Carvalho AP, de Lima M da C. A common mechanism for influenza virus fusion activity and inactivation. *Biochemistry*. 1993;32(11):2771-2779. <http://www.ncbi.nlm.nih.gov/pubmed/8457544>. Accessed December 16, 2018.
213. Mizushima N, Yoshimori T, Ohsumi Y. The role of Atg proteins in autophagosome formation. *Annu Rev Cell Dev Biol*. 2011;27:107-132. doi:10.1146/annurev-cellbio-092910-154005
214. Ravikumar B, Vacher C, Berger Z, et al. Inhibition of mTOR induces autophagy and reduces toxicity of polyglutamine expansions in fly and mouse models of Huntington disease. *Nat Genet*. 2004;36(6):585-595. doi:10.1038/ng1362

## References

215. Yoshimori T, Yamamoto A, Moriyama Y, Futai M, Tashiro Y. Bafilomycin A1, a specific inhibitor of vacuolar-type H(+)-ATPase, inhibits acidification and protein degradation in lysosomes of cultured cells. *J Biol Chem.* 1991;266(26):17707-17712. <http://www.ncbi.nlm.nih.gov/pubmed/1832676>. Accessed December 16, 2018.
216. Yamamoto A, Tagawa Y, Yoshimori T, Moriyama Y, Masaki R, Tashiro Y. Bafilomycin A1 prevents maturation of autophagic vacuoles by inhibiting fusion between autophagosomes and lysosomes in rat hepatoma cell line, H-4-II-E cells. *Cell Struct Funct.* 1998;23(1):33-42. <http://www.ncbi.nlm.nih.gov/pubmed/9639028>. Accessed December 16, 2018.
217. Powis G, Bonjouklian R, Berggren MM, et al. Wortmannin, a potent and selective inhibitor of phosphatidylinositol-3-kinase. *Cancer Res.* 1994;54(9):2419-2423. <http://www.ncbi.nlm.nih.gov/pubmed/8162590>. Accessed August 3, 2018.
218. Amenta JS, Hlivko TJ, McBee AG, Shinozuka H, Brocher S. Specific inhibition by NH<sub>4</sub>Cl of autophagy-associated proteolysis in cultured fibroblasts. *Exp Cell Res.* 1978;115(2):357-366. <http://www.ncbi.nlm.nih.gov/pubmed/689091>. Accessed December 16, 2018.
219. Stenmark H. Rab GTPases as coordinators of vesicle traffic. *Nat Rev Mol Cell Biol.* 2009;10(8):513-525. doi:10.1038/nrm2728
220. Engering A, Geijtenbeek TBH, van Vliet SJ, et al. The dendritic cell-specific adhesion receptor DC-SIGN internalizes antigen for presentation to T cells. *J Immunol.* 2002;168(5):2118-2126. <http://www.ncbi.nlm.nih.gov/pubmed/11859097>. Accessed January 14, 2015.
221. Horrevorts SK, Duinkerken S, Bloem K, et al. Toll-Like Receptor 4 Triggering Promotes Cytosolic Routing of DC-SIGN-Targeted Antigens for Presentation on MHC Class I. *Front Immunol.* 2018;9:1231. doi:10.3389/fimmu.2018.01231
222. Bruce EA, Stuart A, McCaffrey MW, Digard P. Role of the Rab11 pathway in negative-strand virus assembly. *Biochem Soc Trans.* 2012;40(6):1409-1415. doi:10.1042/BST20120166
223. Guichard A, Nizet V, Bier E. RAB11-mediated trafficking in host-pathogen interactions. *Nat Rev Microbiol.* 2014;12(9):624-634. doi:10.1038/nrmicro3325
224. Vale-Costa S, Amorim M. Recycling Endosomes and Viral Infection. *Viruses.* 2016;8(3):64. doi:10.3390/v8030064
225. Liu C-C, Zhang Y-N, Li Z-Y, et al. Rab5 and Rab11 Are Required for Clathrin-Dependent Endocytosis of Japanese Encephalitis Virus in BHK-21 Cells. *J Virol.* 2017;91(19). doi:10.1128/JVI.01113-17
226. Zhang Y-N, Liu Y-Y, Xiao F-C, et al. Rab5, Rab7, and Rab11 are required for caveolae-dependent endocytosis of classic swine fever virus in porcine alveolar macrophages. *J Virol.* May 2018;JVI.00797-18. doi:10.1128/JVI.00797-18
227. Feng Y, Press B, Wandinger-Ness A. Rab 7: an important regulator of late endocytic membrane traffic. *J Cell Biol.* 1995;131(6 Pt 1):1435-1452. <http://www.ncbi.nlm.nih.gov/pubmed/8522602>. Accessed March 5, 2019.
228. Press B, Feng Y, Hoflack B, Wandinger-Ness A. Mutant Rab7 causes the accumulation of cathepsin D and cation-independent mannose 6-phosphate receptor in an early endocytic compartment. *J Cell Biol.* 1998;140(5):1075-1089. <http://www.ncbi.nlm.nih.gov/pubmed/9490721>. Accessed March 5, 2019.
229. Bucci C, Thomsen P, Nicoziani P, McCarthy J, van Deurs B. Rab7: A Key to Lysosome Biogenesis. Pfeffer SR, ed. *Mol Biol Cell.* 2000;11(2):467-480. doi:10.1091/mbc.11.2.467

## References

230. Acosta EG, Castilla V, Damonte EB. Differential Requirements in Endocytic Trafficking for Penetration of Dengue Virus. Salinas S, ed. *PLoS One*. 2012;7(9):e44835. doi:10.1371/journal.pone.0044835
231. Hsiao J-C, Chu L-W, Lo Y-T, et al. Intracellular Transport of Vaccinia Virus in HeLa Cells Requires WASH-VPEF/FAM21-Retromer Complexes and Recycling Molecules Rab11 and Rab22. McFadden G, ed. *J Virol*. 2015;89(16):8365-8382. doi:10.1128/JVI.00209-15
232. Smit JM, Moesker B, Rodenhuis-Zybert I, Wilschut J. Flavivirus cell entry and membrane fusion. *Viruses*. 2011;3(2):160-171. doi:10.3390/v3020160
233. Zaitseva E, Yang S-T, Melikov K, Pourmal S, Chernomordik L V. Dengue Virus Ensures Its Fusion in Late Endosomes Using Compartment-Specific Lipids. Diamond MS, ed. *PLoS Pathog*. 2010;6(10):e1001131. doi:10.1371/journal.ppat.1001131
234. Kobayashi T, Beuchat M-H, Chevallier J, et al. Separation and Characterization of Late Endosomal Membrane Domains. *J Biol Chem*. 2002;277(35):32157-32164. doi:10.1074/jbc.M202838200
235. Gagescu R, Demaurex N, Parton RG, Hunziker W, Huber LA, Gruenberg J. The Recycling Endosome of Madin-Darby Canine Kidney Cells Is a Mildly Acidic Compartment Rich in Raft Components. Kaiser C, ed. *Mol Biol Cell*. 2000;11(8):2775-2791. doi:10.1091/mbc.11.8.2775
236. van IJzendoorn SCD. Recycling endosomes. *J Cell Sci*. 2006;119(9):1679-1681. doi:10.1242/jcs.02948
237. Dunn WA, Hubbard AL, Aronson NN. Low temperature selectively inhibits fusion between pinocytotic vesicles and lysosomes during heterophagy of 125I-asialofetuin by the perfused rat liver. *J Biol Chem*. 1980;255(12):5971-5978. <http://www.ncbi.nlm.nih.gov/pubmed/6155379>. Accessed March 1, 2019.
238. Gong S, Lai C, Esteban M. Vaccinia virus induces cell fusion at acid pH and this activity is mediated by the N-terminus of the 14-kDa virus envelope protein. *Virology*. 1990;178(1):81-91. doi:10.1016/0042-6822(90)90381-Z
239. White J, Matlin K, Helenius A. Cell fusion by Semliki Forest, influenza, and vesicular stomatitis viruses. *J Cell Biol*. 1981;89(3):674-679. doi:10.1083/JCB.89.3.674
240. Helenius A, Kartenbeck J, Simons K, Fries E. On the entry of Semliki forest virus into BHK-21 cells. *J Cell Biol*. 1980;84(2):404-420. <http://www.ncbi.nlm.nih.gov/pubmed/6991511>. Accessed November 7, 2017.
241. Kielian MC, Marsh M, Helenius A. Kinetics of endosome acidification detected by mutant and wild-type Semliki Forest virus. *EMBO J*. 1986;5(12):3103-3109. doi:10.1002/j.1460-2075.1986.tb04616.x
242. Quirin K, Eschli B, Scheu I, Poort L, Kartenbeck J, Helenius A. Lymphocytic choriomeningitis virus uses a novel endocytic pathway for infectious entry via late endosomes. *Virology*. 2008;378(1):21-33. doi:10.1016/j.virol.2008.04.046
243. Sieczkarski SB, Whittaker GR. Differential Requirements of Rab5 and Rab7 for Endocytosis of Influenza and Other Enveloped Viruses. *Traffic*. 2003;4(5):333-343. doi:10.1034/j.1600-0854.2003.00090.x
244. Amorim MJ. A Comprehensive Review on the Interaction Between the Host GTPase Rab11 and Influenza A Virus. *Front Cell Dev Biol*. 2019;6:176. doi:10.3389/fcell.2018.00176

## References

245. Yamazaki Y, Schönherr C, Varshney GK, Dogru M, Hallberg B, Palmer RH. Goliath family E3 ligases regulate the recycling endosome pathway via VAMP3 ubiquitylation. *EMBO J*. 2013;32(4):524-537. doi:10.1038/emboj.2013.1
246. Carlsson SR, Fukuda M. The lysosomal membrane glycoprotein lamp-1 is transported to lysosomes by two alternative pathways. *Arch Biochem Biophys*. 1992;296(2):630-639. <http://www.ncbi.nlm.nih.gov/pubmed/1632650>. Accessed March 6, 2019.
247. Tanida I, Tanida-Miyake E, Ueno T, Kominami E. The Human Homolog of *Saccharomyces cerevisiae* Apg7p Is a Protein-activating Enzyme for Multiple Substrates Including Human Apg12p, GATE-16, GABARAP, and MAP-LC3. *J Biol Chem*. 2001;276(3):1701-1706. doi:10.1074/jbc.C000752200
248. Tanida I, Tanida-Miyake E, Komatsu M, Ueno T, Kominami E. Human Apg3p/Aut1p Homologue Is an Authentic E2 Enzyme for Multiple Substrates, GATE-16, GABARAP, and MAP-LC3, and Facilitates the Conjugation of hApg12p to hApg5p. *J Biol Chem*. 2002;277(16):13739-13744. doi:10.1074/jbc.M200385200
249. Otomo C, Metlagel Z, Takaesu G, Otomo T. Structure of the human ATG12~ATG5 conjugate required for LC3 lipidation in autophagy. *Nat Struct Mol Biol*. 2013;20(1):59-66. doi:10.1038/nsmb.2431
250. Tanida I, Minematsu-Ikeguchi N, Ueno T, Kominami E. Lysosomal turnover, but not a cellular level, of endogenous LC3 is a marker for autophagy. *Autophagy*. 2005;1(2):84-91. <http://www.ncbi.nlm.nih.gov/pubmed/16874052>. Accessed July 25, 2018.
251. DeSelm CJ, Miller BC, Zou W, et al. Autophagy Proteins Regulate the Secretory Component of Osteoclastic Bone Resorption. *Dev Cell*. 2011;21(5):966-974. doi:10.1016/j.devcel.2011.08.016
252. Lee IH, Kawai Y, Fergusson MM, et al. Atg7 modulates p53 activity to regulate cell cycle and survival during metabolic stress. *Science*. 2012;336(6078):225-228. doi:10.1126/science.1218395
253. Ascoli M. Lysosomal accumulation of the hormone-receptor complex during receptor-mediated endocytosis of human choriogonadotropin. *J Cell Biol*. 1984;99(4 Pt 1):1242-1250. <http://www.ncbi.nlm.nih.gov/pubmed/6090468>. Accessed February 20, 2019.
254. Ukkonen P, Lewis V, Marsh M, Helenius A, Mellman I. Transport of macrophage Fc receptors and Fc receptor-bound ligands to lysosomes. *J Exp Med*. 1986;163(4):952-971. <http://www.ncbi.nlm.nih.gov/pubmed/3950548>. Accessed February 20, 2019.
255. Clague MJ, Urbé S, Aniento F, Gruenberg J. Vacuolar ATPase activity is required for endosomal carrier vesicle formation. *J Biol Chem*. 1994;269(1):21-24. <http://www.ncbi.nlm.nih.gov/pubmed/8276796>. Accessed February 20, 2019.
256. Mauthe M, Langereis M, Jung J, et al. An siRNA screen for ATG protein depletion reveals the extent of the unconventional functions of the autophagy proteome in virus replication. *J Cell Biol*. 2016;214(5):619-635. doi:10.1083/jcb.201602046
257. Mauthe M, Reggiori F. ATG proteins: Are we always looking at autophagy? *Autophagy*. 2016;12(12):2502-2503. doi:10.1080/15548627.2016.1236878
258. Kumar AP, Lukman S. Allosteric binding sites in Rab11 for potential drug candidates. Gasset M, ed. *PLoS One*. 2018;13(6):e0198632. doi:10.1371/journal.pone.0198632
259. Mostov K, Su T, ter Beest M. Polarized epithelial membrane traffic: conservation and plasticity. *Nat Cell Biol*. 2003;5(4):287-293. doi:10.1038/ncb0403-287

## References

260. Fölsch H, Mattila PE, Weisz OA. Taking the scenic route: biosynthetic traffic to the plasma membrane in polarized epithelial cells. *Traffic*. 2009;10(8):972-981. doi:10.1111/j.1600-0854.2009.00927.x
261. Mrozowska PS, Fukuda M. Regulation of podocalyxin trafficking by Rab small GTPases in 2D and 3D epithelial cell cultures. *J Cell Biol*. 2016;213(3):355-369. doi:10.1083/jcb.201512024